CHAPTER 10: Fetal Imaging

After discovery of the Roentgen ray and the demonstration of the various uses to which it might be put, it was thought possible that it might also afford a valuable method of investigating the shape and size of the pelvis.

—J. Whitridge Williams (1903)

INTRODUCTION

X-ray techniques were just on the horizon when the first edition of this textbook was published. The first application focused on the maternal pelvis without attention to the fetus. Thus, congenital abnormalities were routinely not discovered until birth. Subsequent radiographic efforts to evaluate the fetus were later replaced by ultrasonography and more recently by magnetic resonance (MR) imaging, techniques which have become increasingly sophisticated. The subspecialty of fetal medicine has developed only because of these advances, and today's practitioner can hardly imagine obstetrical care without them.

SONOGRAPHY IN OBSTETRICS

Prenatal sonography can be used to accurately assess gestational age, fetal number, viability, and placental location, and it can aid diagnosis of many fetal abnormalities. With improvements in resolution and image display, anomalies are increasingly detected in the first trimester, and Doppler is used to manage pregnancies complicated by growth impairment or anemia. The American College of Obstetricians and Gynecologists (2016) recommends that prenatal sonography be performed in all pregnancies and considers it an important part of obstetrical care in the United States.

Technology and Safety

The real-time image on the ultrasound screen is produced by sound waves that are reflected back from fluid and tissue interfaces of the fetus, amnionic fluid, and placenta. Sector array transducers contain groups of piezoelectric crystals working simultaneously in arrays. These crystals convert electrical energy into sound waves, which are emitted in synchronized pulses. Sound waves pass through tissue layers and are reflected back to the transducer when they encounter an interface between tissues of different densities. Dense tissue such as bone produces high-velocity reflected waves, which are displayed as bright echoes on the screen. Conversely, fluid generates few reflected waves and appears dark. Digital images generated at 50 to more than 100 frames per second undergo postprocessing that yields the appearance of real-time imaging.

Ultrasound refers to sound waves traveling at a frequency above 20,000 hertz (cycles per second). Higher-frequency transducers yield better image resolution, whereas lower frequencies penetrate tissue more effectively. Transducers use wide-bandwidth technology to perform within a range of frequencies. In early pregnancy, a 5- to 10-megahertz (MHz) transvaginal transducer usually provides excellent resolution, because the early fetus is close to the transducer. And, in the first and second trimesters, a 4- to 6-MHz transabdominal transducer is similarly close enough to the fetus to yield precise images. By the third trimester, however, a lower frequency 2- to 5-MHz transducer may be needed for tissue penetration—particularly in obese patients—and this can lead to compromised resolution.

Fetal Safety

Sonography should be performed only for a valid medical indication, using the lowest possible exposure setting to gain necessary information—the *ALARA* principle—*a*s *l*ow *a*s *r*easonably *a*chievable. Examinations are performed only by those trained to recognize fetal abnormalities and artifacts that may mimic pathology, using techniques to avoid ultrasound exposure beyond what is considered safe for the fetus (American College of Obstetricians and Gynecologists, 2016; American Institute of Ultrasound in Medicine, 2013b). No causal relationship has been demonstrated between diagnostic ultrasound and any recognized adverse effect in human pregnancy. The International Society of Ultrasound in Obstetrics and Gynecology (2016) further concludes that there is no scientifically proven association between ultrasound exposure in the first or second trimesters and autism

spectrum disorder or its severity.

All sonography machines are required to display two indices: the *thermal index* and the *mechanical index*. The thermal index is a measure of the relative probability that the examination may raise the temperature, potentially high enough to induce injury. That said, fetal damage resulting from commercially available ultrasound equipment in routine practice is extremely unlikely. The potential for temperature elevation is higher with longer examination time and is greater near bone than in soft tissue. Theoretical risks are higher during organogenesis than later in gestation. The thermal index for soft tissue, *Tis*, is used before 10 weeks' gestation, and that for bone, *Tib*, is used at or beyond 10 weeks' (American Institute of Ultrasound in Medicine, 2013b). The thermal index is higher with pulsed Doppler applications than with routine B-mode scanning (Doppler). In the first trimester, if pulsed Doppler is clinically indicated, the thermal index should be ≤0.7, and the exposure time should be as brief as possible (American Institute of Ultrasound in Medicine, 2016). To document the embryonic or fetal heart rate, motion-mode (M-mode) imaging is used instead of pulsed Doppler imaging.

The mechanical index is a measure of the likelihood of adverse effects related to rarefactional pressure, such as cavitation—which is relevant only in tissues that contain air. Microbubble ultrasound contrast agents are not used in pregnancy for this reason. In mammalian tissues that do not contain gas bodies, no adverse effects have been reported over the range of diagnostically relevant exposures. Because fetuses cannot contain gas bodies, they are not considered at risk.

The use of sonography for any nonmedical purpose, such as "keepsake fetal imaging," is considered *contrary to responsible medical practice* and is not condoned by the Food and Drug Administration (2014), the American Institute of Ultrasound in Medicine (2012, 2013b), or the American College of Obstetricians and Gynecologists (2016).

Operator Safety

The reported prevalence of work-related musculoskeletal discomfort or injury among sonographers approximates 70 percent (Janga, 2012; Roll, 2012). The main risk factors for injury during transabdominal ultrasound examinations are awkward posture, sustained static forces, and various pinch grips used while maneuvering the transducer (Centers for Disease Control and Prevention, 2006). Maternal habitus can be contributory because more force is often employed when imaging obese patients.

The following guidelines may help avert injury:

1. Position the patient close to you on the examination table. As a result, your elbow is close to your body, shoulder abduction is less than 30 degrees, and your thumb is facing up.
2. Adjust the table or chair height so that your forearm is parallel to the floor.
3. If seated, use a chair with back support, support your feet, and keep ankles in neutral position. Do not lean toward the patient or monitor.
4. Face the monitor squarely and position it so that it is viewed at a neutral angle, such as 15 degrees downward.
5. Avoid reaching, bending, or twisting while scanning.
6. Frequent breaks may prevent muscle strain. Stretching and strengthening exercises can be helpful.

Gestational Age Assessment

The earlier that sonography is performed, the more accurate the gestational age assessment. Specific criteria for "re-dating" a pregnancy, that is, reassigning the gestational age and estimated date of delivery using initial sonogram findings, are shown in Table 10-1. The only exception to revising the gestational age based on early sonography is if the pregnancy resulted from assisted reproductive technology, in which case accuracy of gestational age assessment is presumed.

TABLE 10-1

Sonographic Gestational Age Assessment

Gestational Age	Parameter(s)	Threshold to Revise[a]
<9 wks	CRL	>5 d
9 to <14 wks	CRL	>7 d
14 to <16 wks	BPD, HC, AC, FL	>7 d
16 to <22 wks	BPD, HC, AC, FL	>10 d
22 to <28 wks	BPD, HC, AC, FL	>14 d
≥28 weeks	BPD, HC, AC, FL	>21 d

[a]Sonographic gestational age should be used when the LMP-derived gestational age differs from that obtained with sonography by the threshold value.

AC = abdominal circumference; BPD = biparietal diameter; CRL = crown-rump length; FL = femur length; HC = head circumference; LMP = last menstrual period.

Modified from American College of Obstetricians and Gynecologists, 2017b.

Sonographic measurement of the crown-rump length (CRL) is the most accurate method to establish or confirm gestational age (Appendix, Fetal Sonographic Measurements). As noted, transvaginal imaging typically yields higher resolution images. The CRL is measured in the midsagittal plane with the embryo or fetus in a neutral, nonflexed position so that its length can be measured in a straight line (Fig. 10-1). The measurement should include neither the yolk sac nor a limb bud. The mean of three discrete measurements is used. Until $13^{6/7}$ weeks' gestation, the CRL is accurate to within 5 to 7 days (American College of Obstetricians and Gynecologists, 2017b).

FIGURE 10-1

The measured crown-rump length in this 12-week 3-day fetus approximates 6 cm.

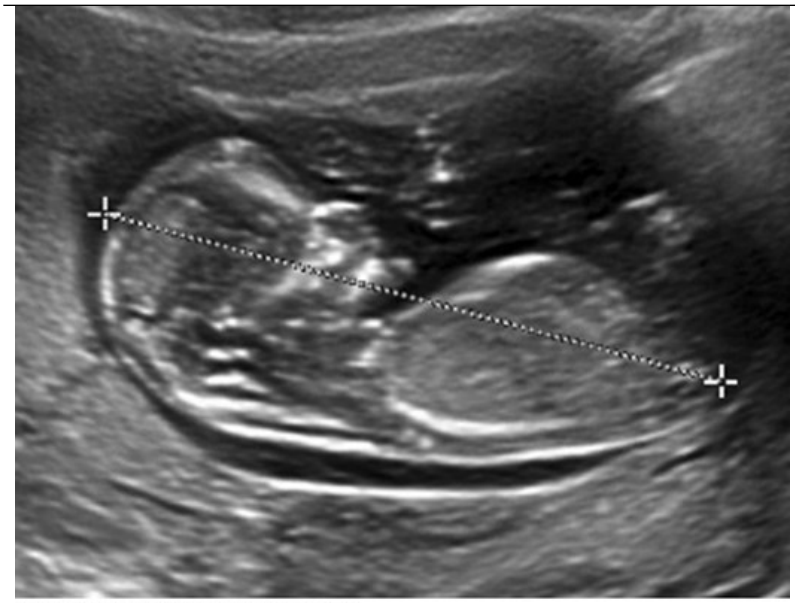

Starting at $14^{0/7}$ weeks, equipment software formulas calculate estimated gestational age and fetal weight from measurements of the biparietal diameter, head and abdominal circumference, and femur length (Fig. 10-2). The estimates are most accurate when multiple parameters are used but may over- or underestimate fetal weight by up to 20 percent (American College of Obstetricians and Gynecologists, 2016). Various nomograms for other fetal structures, including the cerebellar diameter, ear length, ocular distances, thoracic circumference, and lengths of kidney, long bones, and feet, may be used to address specific questions regarding organ system abnormalities or syndromes (Appendix, Fetal Sonographic Measurements).

FIGURE 10-2

Fetal biometry. **A.** Transthalamic view. A transverse (axial) image of the head is obtained at the level of the cavum septum pellucidum (*arrows*) and thalami (*asterisks*). The biparietal diameter is measured perpendicular to the sagittal midline, from the outer edge of the skull in the near field to the inner edge of the skull in the far field. By convention, the near field is that which is closer to the sonographic transducer. The head circumference is measured circumferentially around the outer border of the skull. **B.** Femur length. The femur is measured perpendicular to the femoral shaft, from each diaphyseal end, excluding the epiphysis. **C.** Abdominal circumference. This is a transverse measurement at the level of the stomach (*S*). The J-shaped structure (*arrowheads*) indicates the confluence of the umbilical vein and the right portal vein. Ideally, only one rib is visible on each side of the abdomen, indicating that the image was not taken at an oblique angle.

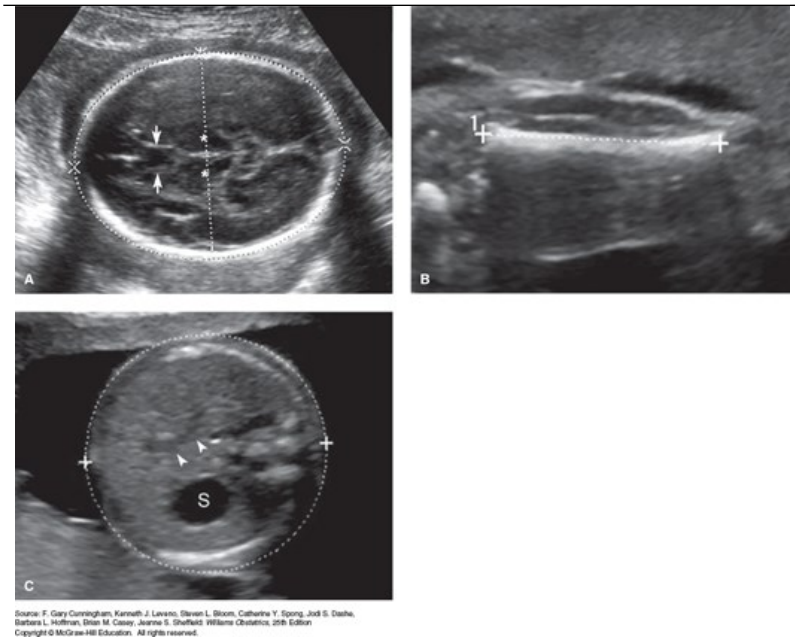

Source: F. Gary Cunningham, Kenneth J. Leveno, Steven L. Bloom, Catherine Y. Spong, Jodi S. Dashe, Barbara L. Hoffman, Brian M. Casey, Jeanne S. Sheffield: Williams Obstetrics, 25th Edition

The biparietal diameter (BPD) most accurately reflects gestational age, with a variation of 7 to 10 days in the second trimester. The BPD is measured perpendicular to the midline falx in the *transthalamic view*, at the level of the thalami and cavum septum pellucidum (CSP) (see Fig. 10-2A). Calipers are placed from the outer edge of the skull in the near field to the inner edge of the skull in the far field. The head circumference (HC) is also measured in the transthalamic view. An ellipse is placed around the outer edge of the skull or the circumference is calculated using BPD and occipital-frontal diameter (OFD) values. The *cephalic index*, which is the BPD divided by the OFD, is normally 70 to 86 percent.

If the head shape is flattened—*dolichocephaly,* or rounded—*brachycephaly,* the HC is more reliable than the BPD. These head shape variants may be normal or can be secondary to fetal position or oligohydramnios. But, dolichocephaly can occur with neural-tube defects, and brachycephaly may be seen in fetuses with Down syndrome. Also, with abnormal skull shape, *craniosynostosis* and other craniofacial abnormalities are a consideration.

The femur length (FL) correlates well with both BPD and gestational age. It is measured with the beam perpendicular to the long axis of the shaft. Calipers are placed at each end of the calcified diaphysis and exclude the epiphysis. For gestational age estimation, it has a variation of 7 to 11 days in the second trimester (see Fig. 10-2B). A femur measurement that is <2.5th percentile for gestational age or that is shortened to ≤90 percent of that expected based on the measured BPD is a minor marker for Down syndrome (Chap. 14, Second-Trimester Markers—"Soft Signs"). The normal range for the FL to abdominal circumference (AC) ratio is generally 20 to 24 percent. A dramatically foreshortened FL or a FL-to-AC ratio below 18 percent prompts evaluation for a skeletal dysplasia (Skeletal Abnormalities).

Of biometric parameters, AC is most affected by fetal growth. Thus, for gestational age estimation, AC has the greatest variation, which can reach 2 to 3 weeks in the second trimester. To measure the AC, a circle is placed outside the fetal skin in a transverse image that contains the stomach and the confluence of the umbilical vein with the portal sinus (see Fig. 10-2C). The image should appear as round as possible and ideally contains no more than 1 rib on each side of the abdomen. The kidneys should not be visible in the image.

Variability of the sonographic gestational age estimate increases with advancing gestation. Accordingly, pregnancies not imaged prior to 22 weeks to confirm or revise gestational age are considered *suboptimally dated* (American College of Obstetricians and Gynecologists, 2017a). Although the estimate is improved by averaging multiple parameters, if one parameter differs significantly from the others, consideration should be given to excluding it from the calculation. The outlier may result from poor visibility, but it could also indicate a fetal abnormality or growth problem. Reference tables such as the one in the Appendix (Fetal Sonographic Measurements) may be used to estimate fetal weight percentiles.

First-Trimester Sonography

Indications for sonography before 14 weeks' gestation are listed in Table 10-2. Early pregnancy can be evaluated using transabdominal or transvaginal sonography, or both. The components listed in Table 10-3 should be assessed. First-trimester sonography can reliably diagnose anembryonic gestation, embryonic demise, ectopic pregnancy, and gestational trophoblastic disease. The first trimester is also the ideal time to evaluate the uterus,

adnexa, and cul-de-sac. Determination of chorionicity in a multifetal gestation is most accurate in the first trimester (Chap. 45, Sonographic Determination).

TABLE 10-2

Some Indications for First-Trimester Ultrasound Examination

Confirm an intrauterine pregnancy
Evaluate a suspected ectopic pregnancy
Define the cause of vaginal bleeding
Evaluate pelvic pain
Estimate gestational age
Diagnose or evaluate multifetal gestations
Confirm cardiac activity
Assist chorionic villus sampling, embryo transfer, and localization and removal of an intrauterine device
Assess for certain fetal anomalies, such as anencephaly, in high-risk patients
Evaluate maternal pelvic masses and/or uterine abnormalities
Measure nuchal translucency when part of a screening program for fetal aneuploidy
Evaluate suspected gestational trophoblastic disease

Modified from the American Institute of Ultrasound in Medicine, 2013a.

TABLE 10-3

Components of Standard Ultrasound Examination by Trimester

First Trimester	Second and Third Trimester
Gestational sac size, location, and number	Fetal number, including amnionicity and chorionicity of multifetal gestations
Embryo and/or yolk sac identification	Fetal cardiac activity
Crown-rump length	Fetal presentation
Fetal number, including amnionicity and chorionicity of multifetal gestations	Placental location, appearance, and relationship to the internal cervical os, with documentation of placental cord insertion site when technically possible
Embryonic/fetal cardiac activity	Amnionic fluid volume
Assessment of embryonic/fetal anatomy appropriate for the first trimester	Gestational age assessment
Evaluation of the maternal uterus, adnexa, and cul-de-sac	Fetal weight estimation
Evaluation of the fetal nuchal region, with consideration of fetal nuchal translucency assessment	Fetal anatomical survey, including documentation of technical limitations
	Evaluation of the maternal uterus, adnexa, and cervix when appropriate

Modified from the American Institute of Ultrasound in Medicine, 2013a.

An intrauterine gestational sac is reliably visualized with transvaginal sonography by 5 weeks, and an embryo with cardiac activity by 6 weeks (Fig. 10-3). The embryo should be visible transvaginally once the mean sac diameter has reached 25 mm—otherwise the gestation is *anembryonic*. Cardiac motion is usually visible with transvaginal imaging when the embryo length reaches 5 mm. In embryos <7 mm without cardiac activity, subsequent examination may be needed to determine viability (American College of Obstetricians and Gynecologists, 2016). At Parkland hospital, first-trimester demise is diagnosed if the embryo has reached 10 mm and lacks cardiac motion. Other criteria for this diagnosis are found in Chapter 18 (Table 18-3).

FIGURE 10-3

A. The measured crown-rump length is approximately 7 mm in this 6-week embryo. **B.** M-mode demonstrates embryonic cardiac activity and a heart rate of 124 beats per minute.

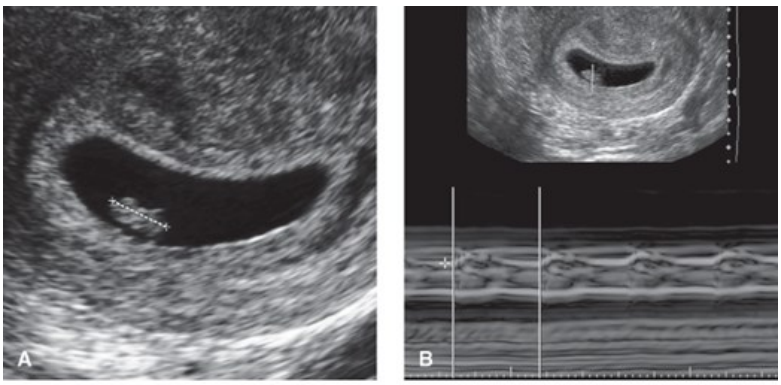

Source: F. Gary Cunningham, Kenneth J. Leveno, Steven L. Bloom, Catherine Y. Spong, Jodi S. Dashe, Barbara L. Hoffman, Brian M. Casey, Jeanne S. Sheffield: *Williams Obstetrics*, 25th Edition

Nuchal Translucency

Nuchal translucency (NT) evaluation is a component of first-trimester aneuploidy screening, discussed in Chapter 14 (Traditional Aneuploidy Screening Tests). It represents the maximum thickness of the subcutaneous translucent area between the skin and soft tissue overlying the fetal spine at the back of the neck. NT is measured in the sagittal plane between 11 and 14 weeks' gestation using precise criteria (Table 10-4). When the NT measurement is increased, the risk for fetal aneuploidy and various structural anomalies—in particular heart defects—is significantly elevated.

TABLE 10-4

Guidelines for Nuchal Translucency (NT) Measurement

The margins of NT edges must be clear enough for proper caliper placement
The fetus must be in the midsagittal plane
The image must be magnified so that it is filled by the fetal head, neck, and upper thorax
The fetal neck must be in a neutral position, not flexed and not hyperextended
The amnion must be seen as separate from the NT line
Electronic calipers must be used to perform the measurement
The + calipers must be placed on the inner borders of the nuchal space with none of the horizontal crossbar itself protruding into the space
The calipers must be placed perpendicular to the long axis of the fetus
The measurement must be obtained at the widest space of the NT

From the American Institute of Ultrasound in Medicine, 2013a, with permission.

Fetal Anomaly Detection

Assessment for selected fetal abnormalities in an at-risk pregnancy is done with first-trimester sonography (see Table 10-2). Research in this area has focused on anatomy visible at 11 to 14 weeks' gestation, to coincide with sonography performed as part of aneuploidy screening. *With current technology, it is not realistic to expect that all major abnormalities detectable in the second trimester may be visualized in the first trimester.* Thus, first-trimester scanning should not replace second-trimester anatomical evaluation (American College of Obstetricians and Gynecologists, 2016).

As examples, in one study of more than 40,000 pregnancies undergoing sonographic aneuploidy screening between 11 and 14 weeks, basic anatomical evaluation yielded a detection rate of approximately 40 percent for structural abnormalities (Syngelaki, 2011). Bromley and colleagues (2014) similarly found that late first-trimester sonography identified major abnormalities in 0.5 percent of pregnancies, representing approximately 40 percent of pregnancies with anomalies detected prenatally. Detection rates are very high for anencephaly, alobar holoprosencephaly, and ventral wall defects.

But, in one analysis of more than 60,000 pregnancies with these early scans, only a third of major cardiac anomalies were identified, and *no* cases of microcephaly, agenesis of the corpus callosum, cerebellar abnormalities, congenital pulmonary airway malformations, or bowel obstruction were detected (Syngelaki, 2011). In another study of low-risk or unselected pregnancies, 32 percent of anomalies were detected, whereas in pregnancies described as high-risk, anomaly detection exceeded 60 percent (Karim, 2017).

Second- and Third-Trimester Sonography

It is recommended that sonography be routinely offered to all pregnant women between 18 and 22 weeks' gestation (American College of Obstetricians and Gynecologists, 2016). This time interval permits accurate assessment of gestational age, fetal anatomy, placental location, and cervical length. Recognizing that the gestational age at which abnormalities are identified may affect pregnancy management options, providers may opt to perform the examination prior to 20 weeks. The many additional indications for second- and third-trimester sonography are listed in Table 10-5. The three examination types are *standard*, *specialized*—which includes targeted sonography, and *limited*.

TABLE 10-5

Some Indications for Second- or Third-Trimester Ultrasound Examination

Maternal Indications
Vaginal bleeding
Abdominal/pelvic pain
Pelvic mass
Suspected uterine abnormality
Suspected ectopic pregnancy
Suspected molar pregnancy
Suspected placenta previa and subsequent surveillance
Suspected placental abruption
Preterm premature rupture of membranes and/or preterm labor
Cervical insufficiency
Adjunct to cervical cerclage
Adjunct to amniocentesis or other procedure
Adjunct to external cephalic version
Fetal Indications
Gestational age estimation
Fetal-growth evaluation
Significant uterine size/clinical date discrepancy
Suspected multifetal gestation
Fetal anatomical evaluation
Fetal anomaly screening
Assessment for findings that raise the aneuploidy risk
Abnormal biochemical markers
Fetal presentation determination
Suspected hydramnios or oligohydramnios
Fetal well-being evaluation
Follow-up evaluation of a fetal anomaly
History of congenital anomaly in prior pregnancy
Suspected fetal death
Fetal condition evaluation in late registrants for prenatal care

Adapted from the American Institute of Ultrasound in Medicine, 2013a.

The standard sonogram includes evaluation of fetal number and presentation, cardiac activity, amnionic fluid volume, placental position, fetal biometry, and fetal anatomy (American Institute of Ultrasound in Medicine, 2013b). When technically feasible, the maternal cervix and adnexa are examined as clinically appropriate. Components are found in Table 10-3, and the fetal anatomical structures that should be evaluated are listed in Table 10-6. With twins or other multiples, documentation also includes the number of chorions and amnions, comparison of fetal sizes, estimation of amnionic fluid volume within each sac, and fetal sex determination (Chap. 45, Sonographic Determination).

TABLE 10-6

Components of Standard and Targeted Fetal Anatomic Surveys

Standard Sonogram	Additional Targeted (Detailed) Sonogram Components

Head, face, and neck Lateral cerebral ventricles Choroid plexus Midline falx Cavum septum pellucidum Cerebellum Cisterna magna Upper lip Consideration of nuchal skin fold measurement at 15–20 weeks	**Head, face, and neck** Integrity and shape of cranium Third ventricle[a] Fourth ventricle[a] Corpus callosum[a] Cerebellar lobes, vermis Brain parenchyma Profile Coronal nose, lips, lens[a] Palate[a], maxilla, mandible, and tongue[a] Ear position and size[a] Orbits[a] Neck
Chest Cardiac activity Four-chamber view of the heart Left ventricular outflow tract Right ventricular outflow tract	**Chest** Aortic arch Superior/inferior venae cavae 3-vessel view 3-vessel and trachea view Lungs Integrity of diaphragm Ribs[a]
Abdomen Stomach: presence, size, and situs Kidneys Urinary bladder Umbilical cord insertion into fetal abdomen Umbilical cord vessel number	**Abdomen** Small and large bowel[a] Adrenal glands[a] Gallbladder[a] Liver Renal arteries[a] Spleen[a] Integrity of abdominal wall
Spine Cervical, thoracic, lumbar, and sacral spine	**Spine** Shape and curvature Integrity of spine and overlying soft tissue
Extremities Legs and arms	**Extremities** Architecture, position, number Hands Feet Digits[a]: number, position
Fetal sex In multifetal gestations and when medically indicated	

[a]When medically indicated (determined on case-by-case basis).

Modified from the American Institute of Ultrasound in Medicine, 2013a; Wax, 2014.

The *targeted* sonogram is a type of *specialized* examination. It is performed when the risk for a fetal anatomical or genetic abnormality is elevated because of history, screening test result, or abnormal finding during standard examination (Table 10-7). Targeted sonograms include a detailed anatomical survey, the components of which are shown in Table 10-6. Because it carries the CPT code 76811, this sonogram is colloquially called the "76811 examination." It is intended to be indication-driven and should not be repeated later in the absence of an extenuating circumstance. Physicians who perform or interpret targeted sonograms should have expertise in fetal imaging, through both training and ongoing experience (Wax, 2014). For many of the targeted examination components, the physician determines on a case-by-case basis whether assessment is needed (American College of Obstetricians and Gynecologists, 2016). Other types of specialized examinations include fetal echocardiography, Doppler evaluation, and the biophysical profile, which is described in Chapter 17 (Acoustic Stimulation Tests).

TABLE 10-7

Indications for Targeted Fetal Anatomical Ultrasound Examination

Prior fetus or neonate with a structural or genetic/chromosomal abnormality
Current pregnancy with known or suspected fetal abnormality or confirmed growth abnormality
Increased risk for fetal structural anomaly in current pregnancy
Maternal diabetes diagnosed before 24 weeks' gestation
Assisted reproductive technology to achieve conception
Maternal prepregnancy body mass index >30 kg/m^2
Multifetal gestation (Chap. 45, Mechanisms of Multifetal Gestations)
Abnormal serum alpha-fetoprotein or estriol levels
Teratogen exposure
Nuchal translucency measurement ≥3.0 mm
Increased risk for fetal genetic/chromosomal abnormality in current pregnancy
Parental carriage of genetic/chromosomal abnormality
Maternal age ≥35 at delivery
Abnormal aneuploidy screening test result
Minor aneuploidy marker (on standard sonogram)
Nuchal translucency measurement ≥3.0 mm
Other condition affecting the fetus
Congenital infection (Chaps. 64 and 65)
Drug dependence
Alloimmunization (Chap. 15, Red Cell Alloimmunization)
Amnionic fluid abnormality (Chap. 11, Hydramnios)

Modified from Wax, 2014, 2015.

A *limited* sonogram is performed to address a specific clinical question. Examples include evaluation of fetal presentation, viability, amnionic fluid volume, or placental location. In the absence of an emergency, a limited examination is only performed if a standard sonogram has already been completed. Otherwise, provided that the gestational age is at least 18 weeks, a standard sonogram is recommended.

Fetal Anomaly Detection

With current advances in imaging technology, approximately 50 percent of major fetal abnormalities overall are detected with standard sonography (Rydberg, 2017). The sensitivity of sonography for detecting fetal anomalies varies according to factors such as gestational age, maternal habitus, fetal position, equipment features, examination type, operator skill, and the specific abnormality in question. For example, maternal obesity has been associated with a 20-percent reduction in the anomaly detection rate (Dashe, 2009).

Detection also varies considerably according to the abnormality. For example, population-based data from 18 registries comprise the EUROCAT

network. Between 2011 and 2015, EUROCAT (2017) prenatal detection rates for selected fetal anomalies—excluding genetic conditions—were as follows: anencephaly, 99 percent; spina bifida, 89 percent; hydrocephaly, 78 percent; cleft lip/palate, 68 percent; hypoplastic left heart, 87 percent; transposition of the great vessels, 64 percent; diaphragmatic hernia, 74 percent; gastroschisis, 94 percent; omphalocele, 92 percent; bilateral renal agenesis, 94 percent; posterior urethral valves, 79 percent; limb-reduction defects, 57 percent; and clubfoot, 57 percent.

Importantly, however, the overall anomaly detection rate, excluding aneuploidy, was *below 40 percent.* This reflects inclusion of anomalies with minimal or no sonographic detection in the second trimester, such as microcephaly, choanal atresia, cleft palate, Hirschsprung disease, anal atresia, and congenital skin disorders. These are mentioned because clinicians tend to focus on abnormalities amenable to sonographic detection, whereas those not readily detectable may be equally devastating to families. *Therefore, every sonographic examination should include a frank discussion of examination limitations.*

Most anomalous neonates are born to women whose pregnancies are otherwise considered low-risk, that is, without an indication for targeted sonography. Thus, for standard sonographic examinations, accurate documentation and quality assurance are essential to optimize detection rates. Practice guidelines and standards established by organizations such as the American Institute of Ultrasound in Medicine (2013b) and the International Society of Ultrasound in Obstetrics and Gynecology (Salomon, 2011) have undoubtedly contributed to improvements in anomaly detection rates. Ultrasound practice accreditation is a process offered by the American Institute of Ultrasound in Medicine and the American College of Radiology that was developed to improve imaging quality and adherence to guidelines. It includes review of images and their storage, ultrasound equipment, report generation, and the qualifications of physicians and sonographers. The Society for Maternal-Fetal Medicine (2013) recommends that whenever possible, obstetrical ultrasound examinations by maternal-fetal medicine subspecialists be performed by accredited practices.

Amnionic Fluid Volume

Evaluation of amnionic fluid volume is a component of every second- or third-trimester sonogram, and volumes vary with gestational age. *Oligohydramnios* indicates an amnionic fluid volume below normal range, and subjective crowding of the fetus is often noted. *Hydramnios*—also called *polyhydramnios*—defines a volume above a given normal threshold. Amnionic fluid volume is usually assessed semiquantitatively. Measurements include either the single deepest vertical fluid pocket or the sum of the deepest vertical pockets from each of four equal uterine quadrants—the *amnionic fluid index* (Phelan, 1987). Reference ranges have been established for both measurements from 16 weeks' gestation onward. The single deepest vertical pocket is normally between 2 and 8 cm, and the amnionic fluid index normally ranges between 8 and 24 cm. A further discussion and images are provided in Chapter 11 (Hydramnios).

Cervical Length Assessment

Evaluation of the relationship between the placenta and the internal cervical os is an essential component of the standard sonogram. Abnormalities of the placenta and umbilical cord are reviewed in Chapter 6 (Normal Placenta). Although the cervix may be imaged transabdominally (Fig. 10-4), this is often limited by technical factors that include maternal habitus, cervical position, or shadowing by the fetal presenting part. In addition, the maternal bladder or pressure from the transducer may artificially elongate the appearance of the cervix. As a result, values from transabdominal or transvaginal measurement of the cervix can differ significantly.

FIGURE 10-4

A. Transabdominal image of the cervix depicting the internal os and external os. **B.** Transvaginal imaging provides a more accurate evaluation of the cervix and should be used for medical decision-making. In this image, arrowheads mark the endocervical canal. (Reproduced with permission from Dr. Emily Adhikari.)

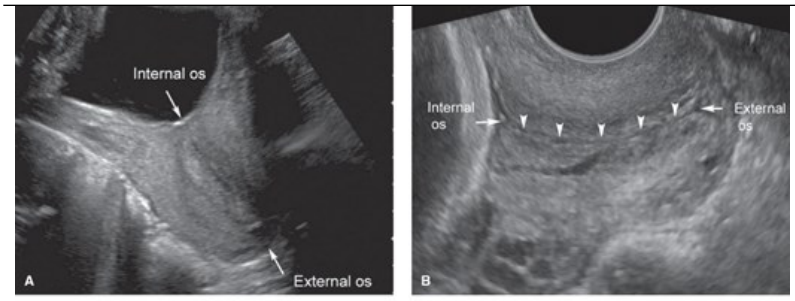

If the cervix appears shortened or if it cannot be adequately visualized during transabdominal evaluation, transvaginal assessment is considered (American Institute of Ultrasound in Medicine, 2013b). Only cervical length measurements obtained transvaginally at or beyond 16 weeks' gestation are considered sufficiently accurate for clinical decision-making (see Fig. 10-4). A foreshortened cervix is associated with an elevated risk for preterm birth, particularly in the setting of prior preterm birth, and the degree of risk rises proportionally with the degree of cervical shortening (Chap. 42, Preterm Birth Prevention).

To measure the cervix transvaginally, the imaging criteria shown in Table 10-8 are followed. The endocervical canal should be visible in its entirety, and images ideally are obtained over several minutes to allow for dynamic change. During examination, visible funneling or debris is sought. Funneling is a protrusion of amnionic membranes into a portion of the endocervical canal that has dilated (Fig. 10-5). Funneling is not an independent predictor of preterm birth, however, it is associated with cervical shortening, and transvaginal assessment is recommended if a funnel is suspected transabdominally. The cervical length is measured distal to the funnel, because the base of the funnel becomes the functional internal os. If the cervix is dilated, as with cervical insufficiency, the membranes may prolapse through the endocervical canal and into the vagina, producing an hourglass appearance. Sludge or debris represents an aggregate of particulate matter within the amnionic sac, close to the internal os. In pregnancies at risk for preterm birth, sludge is associated with a further increased risk.

TABLE 10-8

Criteria for Transvaginal Evaluation of the Cervix

Imaging the Cervix
Maternal bladder should be empty.
Transducer is inserted under real-time observation, identifying midsagittal plane, internal os, and then external os, while keeping the internal os in view.
Internal os, external os, and entire endocervical canal should be visible. The internal os may appear as a small triangular indentation at the junction of the amnionic cavity and endocervical canal.
Image is enlarged so that the cervix fills approximately 75% of the screen.
Anterior and posterior width of the cervix should be approximately equal.
Transducer is pulled back slightly until the image begins to blur, ensuring that pressure is not placed on the cervix, then inserted only enough to restore a clear image.
Images should be obtained with and without fundal or suprapubic pressure, to assess for dynamic change–or shortening on real-time imaging.
Measuring the Cervix
Calipers are placed where anterior and posterior walls of cervix meet.
Endocervical canal appears as a faint, linear echodensity.
If canal has a curved contour, a straight line between the internal and external os will deviate from the path of the endocervical canal.
If midpoint of the line between the internal and external canal deviates by ≥3 mm from the endocervical canal, measure the cervical length in two linear segments.
Funneling, sludge (debris), or dynamic change is noted.
At least three separate images are measured during a period of at least 3 minutes to allow for dynamic change. Visualization of cervical shortening on real-time imaging, with or without fundal or suprapubic pressure, raises preterm birth risks.
Shortest cervical length image that meets all criteria should be used.

Modified from Iams, 2013.

FIGURE 10-5

Transvaginal image depicting a foreshortened cervix with funneling. Funneling is a protrusion of amnionic membranes into a portion of the endocervical canal that has dilated. The distal protruding edge of the funnel becomes the functional internal os (*left arrow*). Thus, the measured cervical length, which lies between the arrows, should not include the funnel. (Reproduced with permission from Dr. Emily Adhikari.)

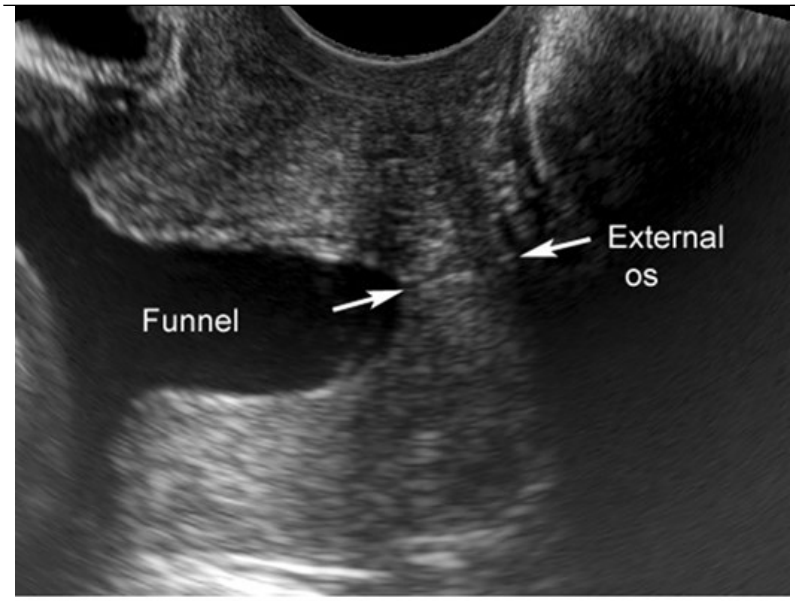

NORMAL AND ABNORMAL FETAL ANATOMY

Many fetal anomalies and syndromes may be characterized with targeted sonography, and selected abnormalities are discussed subsequently. This list is not intended to be comprehensive but covers abnormalities commonly detected with standard sonography and those that are potentially amenable to fetal therapy. Sonographic features of chromosomal abnormalities are reviewed in Chapters 13 and 14, and fetal therapy is discussed in Chapter 16.

Brain and Spine

Standard sonographic evaluation of the fetal brain includes three transverse (axial) views. The *transthalamic view* is used to measure the BPD and HC and includes the midline falx, cavum septum pellucidum (CSP), and thalami (see Fig. 10-1A). The CSP is the space between the two laminae that separate the frontal horns of the lateral ventricles. Inability to visualize a normal CSP may indicate a midline brain abnormality such as agenesis of the corpus callosum, lobar holoprosencephaly, or septo-optic dysplasia (de Morsier syndrome). The *transventricular view* includes the lateral ventricles, which contain the echogenic choroid plexus (Fig. 10-6). The ventricles are measured at their atrium, which is the confluence of the temporal and occipital horns. The *transcerebellar view* is obtained by angling the transducer back through the posterior fossa (Fig. 10-7). In this view, the cerebellum and cisterna magna are measured, and between 15 and about 20 weeks, the nuchal skinfold thickness may also be measured. From 15 until 22 weeks' gestation, the cerebellar diameter in millimeters is roughly equivalent to the gestational age in weeks (Goldstein, 1987). The cisterna magna normally measures between 2 and 10 mm. Effacement of the cisterna magna is present in the *Chiari II malformation*, discussed later (Ventriculomegaly).

FIGURE 10-6

The transventricular view depicts the lateral ventricles, which contain the echogenic choroid plexus (*CP*). The lateral ventricle is measured at the *atrium* (*arrows*), which is the confluence of the temporal and occipital horns. A normal measurement is between 5 and 10 mm throughout the second and third trimesters. The atria measured 6 mm in this 21-week fetus.

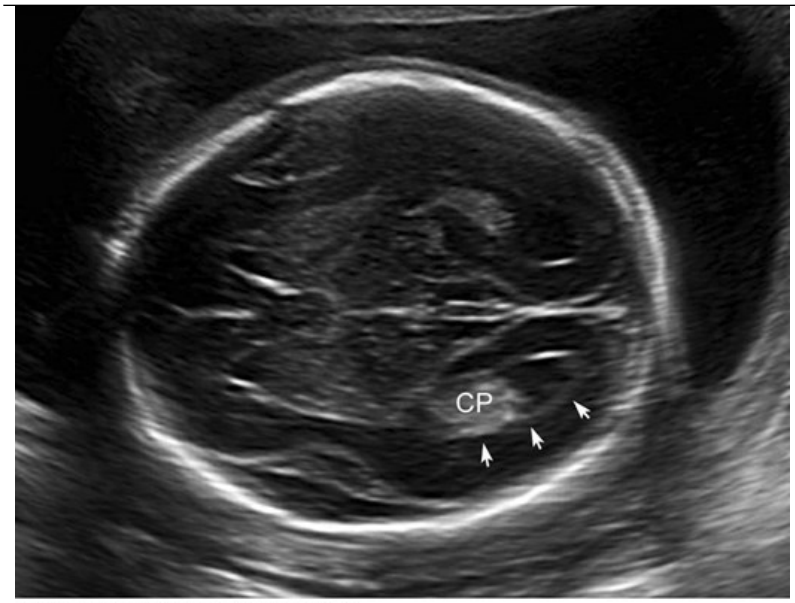

FIGURE 10-7

Transcerebellar view of the posterior fossa, demonstrating measurement of the cerebellum (+), cisterna magna (*x*), and nuchal fold thickness (*bracket*). Care is taken not to angle obliquely down the spine, which may artificially increase the nuchal fold measurement.

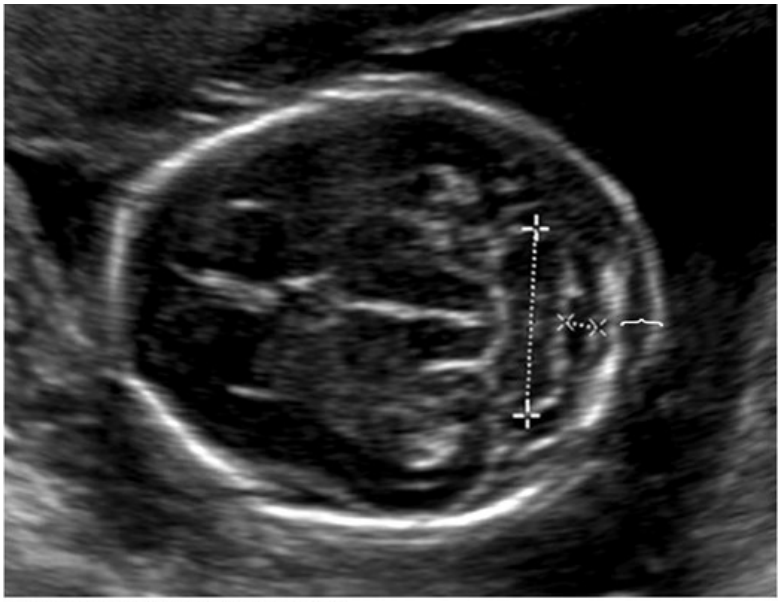

Imaging of the spine includes evaluation of the cervical, thoracic, lumbar, and sacral regions (Fig. 10-8). Representative spinal images for record keeping are often obtained in the sagittal or coronal plane, but real-time imaging of each spinal segment in the transverse plane is more sensitive for anomaly detection. Transverse images demonstrate three ossification centers. The anterior ossification center is the vertebral body, and the posterior paired ossification centers represent the junction of vertebral laminae and pedicles. Ossification of the spine proceeds in a cranial-caudal fashion, such that ossification of the upper sacrum (S_1-S_2) is not generally visible sonographically before 16 weeks' gestation, and ossification of the entire sacrum may not be visible until 21 weeks (De Biasio, 2003). Thus, detection of some spinal abnormalities can be challenging in the early second trimester.

FIGURE 10-8

Normal fetal spine. In this sagittal image of a 21-week fetus, the cervical (*C*), thoracic (*T*), lumbar (*L*), and sacral spine (*S*) are depicted. Arrows denote the parallel rows of paired posterior ossification centers—representing the junction of vertebral lamina and pedicles.

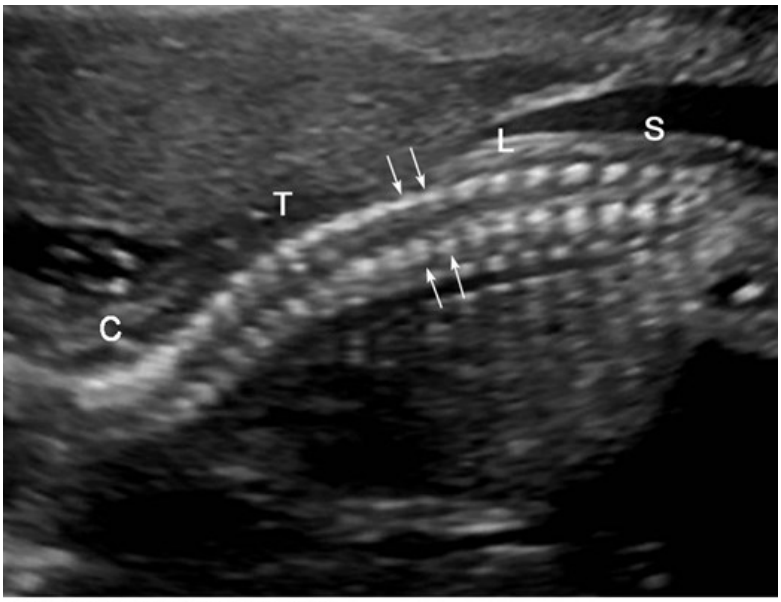

If a brain or spinal abnormality is identified, targeted sonography is indicated. The International Society of Ultrasound in Obstetrics and Gynecology (2007) has published guidelines for a "fetal neurosonogram." Fetal MR imaging may also be helpful (Fetal Anatomical Evaluation).

Neural-Tube Defects

These defects include anencephaly, myelomeningocele (also called spina bifida), cephalocele, and other rare spinal fusion (or *schisis*) abnormalities. They result from incomplete closure of the neural tube by the embryonic age of 26 to 28 days. Their birth prevalence is 0.9 in 1000 in the United States and most of Europe and 1.3 in 1000 in the United Kingdom (Cragan, 2009; Dolk, 2010). Many neural-tube defects can be prevented with folic acid supplementation. When isolated, neural-tube defect inheritance is multifactorial, and the recurrence risk without periconceptional folic acid supplementation is 3 to 5 percent (Chap. 13, Genetic Tests).

Screening for neural-tube defects with maternal serum alpha-fetoprotein (MSAFP) has been offered routinely as part of prenatal care since the 1980s (Chap. 14, Maternal Serum AFP Elevation: Neural-Tube Defect Screening). Women currently have the option of neural-tube defect screening with MSAFP, sonography, or both (American College of Obstetricians and Gynecologists, 2016). Serum screening is generally performed between 15 and 20 weeks' gestation. And, if using an upper threshold of 2.5 multiples of the median (MoM), the anticipated detection rate is at least 90 percent for fetal anencephaly and 80 percent for myelomeningocele. Targeted sonography is the preferred diagnostic test, and in addition to characterizing the neural-tube defect, it may identify other abnormalities or conditions that also result in MSAFP elevation (Table 14-6).

Anencephaly is characterized by absence of the cranium and telencephalic structures above the level of the skull base and orbits (Fig. 10-9). *Acrania* is absence of the cranium with protrusion of disorganized brain tissue. Both are uniformly lethal and are generally considered together, with anencephaly as the final stage of acrania (Bronshtein, 1991). These anomalies are often diagnosed in the late first trimester, and with adequate visualization, virtually all cases may be diagnosed in the second trimester. Inability to image the BPD raises suspicion. The face often appears triangular, and sagittal images readily demonstrate absence of the ossified cranium. Hydramnios from impaired fetal swallowing is common in the third trimester.

FIGURE 10-9

Anencephaly/acrania. **A.** Acrania. This 11-week fetus has absence of the cranium, with protrusion of a disorganized mass of brain tissue that resembles a "shower cap" (*arrows*) and a characteristic triangular facial appearance. **B.** Anencephaly. This sagittal image shows the absence of

forebrain and cranium above the skull base and orbit. The long white arrow points to the fetal orbit, and the short white arrow indicates the nose.

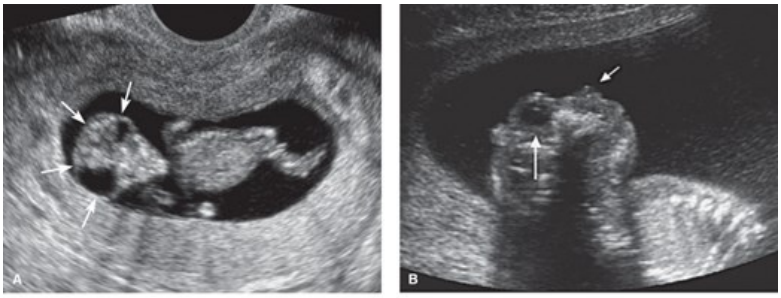

Cephalocele is the herniation of meninges through a cranial defect, typically located in the midline occipital region (Fig. 10-10). When brain tissue herniates through the skull defect, the anomaly is termed an *encephalocele.* Herniation of the cerebellum and other posterior fossa structures constitutes a *Chiari III malformation.* Associated hydrocephalus and microcephaly are common, and survivors have a high incidence of neurological deficits and intellectual disability. Cephalocele is an important feature of the autosomal recessive *Meckel-Gruber syndrome,* which includes cystic renal dysplasia and polydactyly. A cephalocele not located in the occipital midline raises suspicion for *amnionic-band sequence* (Chap. 6, Amniochorion).

FIGURE 10-10

Encephalocele. This transverse image depicts a large defect in the occipital region of the cranium (*arrows*) through which meninges and brain tissue have herniated.

Spina bifida is a defect in the vertebrae, typically the dorsal arches, with exposure of the meninges and spinal cord. The birth prevalence approximates 1 in 2000 (Cragan, 2009; Dolk, 2010). Most cases are *open spina bifida*—the defect includes the skin and soft tissues. Herniation of a meningeal sac containing neural elements is termed a *myelomeningocele* (Fig. 10-11). When only a meningeal sac is present, the defect is a *meningocele.* Although the sac may be easier to image in the sagittal plane, transverse images more readily demonstrate separation or splaying of the lateral processes.

FIGURE 10-11

Myelomeningocele. In this sagittal image of a lumbosacral myelomeningocele, the arrowheads indicate nerve roots within the anechoic herniated sac. The overlying skin is visible above the level of the spinal defect but abruptly stops at the defect (*arrow*).

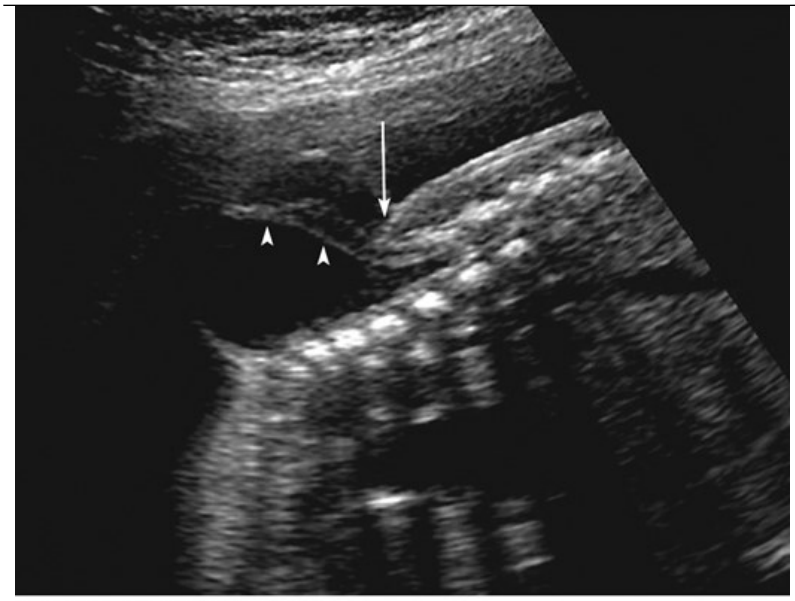

Detection of spina bifida is aided by two characteristic cranial findings (Nicolaides, 1986). Scalloping of the frontal bones is termed the *lemon sign*, and anterior curvature of the cerebellum with effacement of the cisterna magna is the *banana sign* (Fig. 10-12). These findings are manifestations of the Chiari II malformation, also called the *Arnold-Chiari malformation*. This develops when downward displacement of the spinal cord pulls a portion of the cerebellum through the foramen magnum and into the upper cervical canal. *Ventriculomegaly* is another frequent associated sonographic finding, particularly after midgestation. More than 80 percent of infants with open spina bifida require ventriculoperitoneal shunt placement. A small BPD is often present as well. Children with spina bifida require multidisciplinary care to address problems related to the defect, therapeutic shunting, and deficits in swallowing, bladder and bowel function, and ambulation. Fetal myelomeningocele surgery is discussed in Chapter 16 (Open Fetal Surgery).

FIGURE 10-12

Cranial findings in myelomeningocele. **A.** Image of a fetal head at the level of the lateral ventricles demonstrates inward bowing or scalloping of the frontal bones (*arrows*)—the lemon sign. **B.** Image of a fetal head at the level of the posterior fossa shows anterior curvature of the cerebellum (*arrows*) with effacement of the cisterna magna—the banana sign.

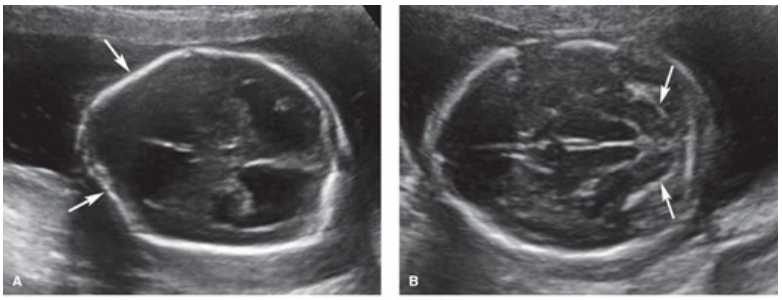

Ventriculomegaly

Characterized by distention of the cerebral ventricles by cerebrospinal fluid (CSF), this finding is a nonspecific marker of abnormal brain development (Pilu, 2011). The atrium normally measures between 5 and 10 mm from 15 weeks' gestation until term (see Fig. 10-6). Mild ventriculomegaly is diagnosed when the atrial width measures 10 to 15 mm (Fig. 10-13), and overt or severe ventriculomegaly when it exceeds 15 mm. The larger the atrium, the greater the likelihood of an abnormal outcome (Gaglioti, 2009; Joó, 2008). CSF is produced within the ventricles by the *choroid plexus*, which is composed of loose connective tissue surrounding an epithelium-lined capillary core. The choroid plexus often appears to *dangle* within the ventricle when severe ventriculomegaly is present.

FIGURE 10-13

Ventriculomegaly. In this transverse view of the cranium, the white line depicts measurement of the atrium of the lateral ventricle, which measured 12 mm, consistent with mild ventriculomegaly.

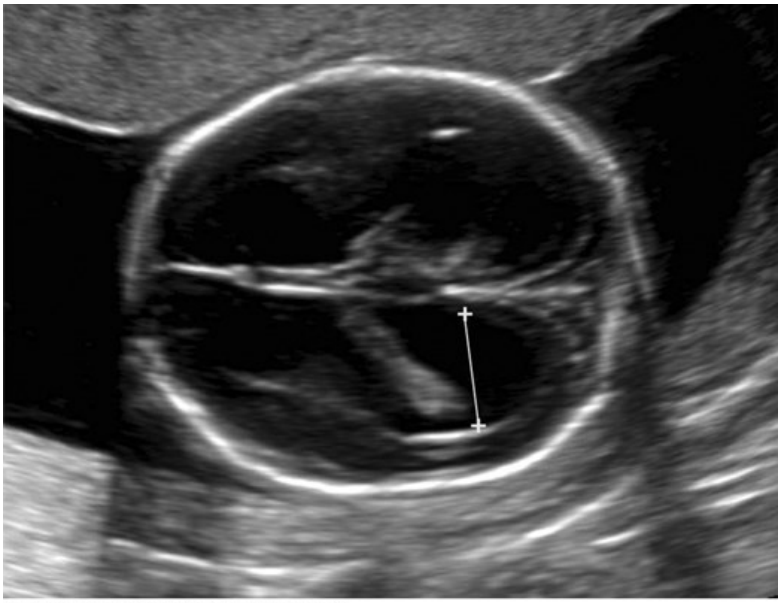

Ventriculomegaly may be caused by various genetic and environmental insults. It may be due to other central nervous system (CNS) abnormalities—such as Dandy-Walker malformation or holoprosencephaly, to an obstructive process—such as aqueductal stenosis, or to a destructive process—such as porencephaly or an intracranial teratoma. Initial evaluation includes a targeted examination of fetal anatomy, testing for congenital infections such as cytomegalovirus and toxoplasmosis, and chromosomal microarray analysis, which is described in Chapter 13 (Chromosomal Microarray Analysis). Fetal MR imaging should be considered to assess for associated abnormalities that may not be detectable sonographically.

Prognosis is generally determined by etiology, severity, and rate of progression. However, even with mild-appearing and isolated ventriculomegaly, prognosis can vary widely. In a systematic review of nearly 1500 mild-to-moderate cases, 1 to 2 percent were associated with congenital infection, 5 percent with aneuploidy, and 12 percent with neurological abnormality (Devaseelan, 2010). A neurological abnormality was significantly more common if ventriculomegaly progressed with advancing gestation.

Agenesis of the Corpus Callosum

The corpus callosum is the major fiber bundle connecting reciprocal regions of the cerebral hemispheres. With complete agenesis of the corpus callosum, a normal cavum septum pellucidum cannot be visualized sonographically. Also, the frontal horns are displaced laterally, and the atria show mild enlargement posteriorly—such that the ventricle has a characteristic “teardrop” appearance (Fig. 10-14). Callosal dysgenesis involves only the caudal portions—the body and splenium—and consequently may be more difficult to detect prenatally.

FIGURE 10-14

Agenesis of the corpus callosum. This image demonstrates a “teardrop” shaped ventricle with mild ventriculomegaly (*dotted line*) and laterally displaced frontal horns (*arrow*). A normal cavum septum pellucidum cannot be visualized.

In population-based studies, agenesis of the corpus callosum has a prevalence of 1 in 5000 births (Glass, 2008; Szabo, 2011). In a review of apparently isolated cases, fetal MR imaging identified additional brain abnormalities in more than 20 percent (Sotiriadis, 2012). If the anomaly was still considered isolated following MR imaging, normal developmental outcome was reported in 75 percent of cases, but severe disability occurred in 12 percent. Agenesis of the corpus callosum is associated with other anomalies, aneuploidy, and more than 200 genetic syndromes. Thus, genetic counseling can be challenging.

Holoprosencephaly

In early normal brain development, the prosencephalon or forebrain divides as it becomes the telencephalon and diencephalon. With holoprosencephaly, the prosencephalon fails to divide completely into two separate cerebral hemispheres and underlying paired diencephalic structures. Main forms of holoprosencephaly are a continuum that contains, with decreasing severity, *alobar*, *semilobar*, and *lobar* types. In the most severe form—*alobar holoprosencephaly*—a single monoventricle, with or without a covering mantle of cortex, surrounds fused central thalami (Fig. 10-15). In *semilobar holoprosencephaly*, partial separation of the hemispheres occurs. *Lobar holoprosencephaly* is characterized by a variable degree of fusion of frontal structures and should be considered when a normal CSP cannot be seen.

FIGURE 10-15

Alobar holoprosencephaly. **A.** Transverse cranial image of a fetus with alobar holoprosencephaly, depicting fused thalami (*Th*) encircled by a monoventricle (*V*) with a covering mantle *(M)* of cortex. The midline falx is absent. (Reproduced with permission from Rafael Levy, RDMS.) **B.** In this profile view of the face, a soft tissue mass—a proboscis (*arrow*), protrudes from the region of the forehead.

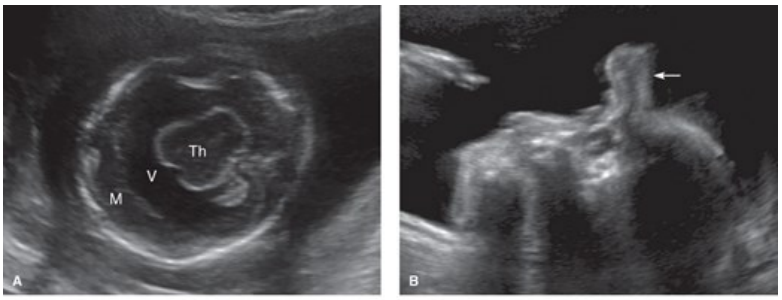

Differentiation into two cerebral hemispheres is induced by prechordal mesenchyme, which is also responsible for differentiation of the midline face. Thus, holoprosencephaly may be associated with anomalies of the orbits and eyes—hypotelorism, cyclopia, or micro-ophthalmia; lips—median cleft;

or nose—ethmocephaly, cebocephaly, or arhinia with proboscis (see Fig. 10-15).

The birth prevalence of holoprosencephaly is only 1 in 10,000 to 15,000. However, the abnormality has been identified in nearly 1 in 250 early abortuses, which attests to the extremely high in-utero lethality (Orioli, 2010; Yamada, 2004). The alobar form accounts for 40 to 75 percent of cases, and 30 to 40 percent have a numerical chromosomal abnormality, particularly trisomy 13 (Orioli, 2010; Solomon, 2010). Conversely, two thirds of trisomy 13 cases are found to have holoprosencephaly. Fetal karyotype or chromosomal microarray analysis should be offered when this anomaly is identified.

Dandy-Walker Malformation—Vermian Agenesis

This posterior fossa abnormality is characterized by agenesis of the cerebellar vermis, posterior fossa enlargement, and elevation of the tentorium. Sonographically, fluid in the enlarged cisterna magna visibly communicates with the fourth ventricle through the cerebellar vermis defect, with visible separation of the cerebellar hemispheres (Fig. 10-16). The birth prevalence approximates 1 in 12,000 (Long, 2006). Associated anomalies and aneuploidy are common. These include ventriculomegaly in 30 to 40 percent, other anomalies in approximately 50 percent, and aneuploidy in 40 percent (Ecker, 2000; Long, 2006). Dandy-Walker malformation is also associated with numerous genetic and sporadic syndromes, congenital viral infections, and teratogen exposure, all of which greatly affect the prognosis. Thus, the initial evaluation mirrors that for ventriculomegaly (Ventriculomegaly).

FIGURE 10-16

Dandy-Walker malformation. This transcerebellar image demonstrates agenesis of the cerebellar vermis. The cerebellar hemispheres (+) are widely separated by a fluid collection that connects the 4th ventricle (*asterisk*) to the enlarged cisterna magna (*CM*).

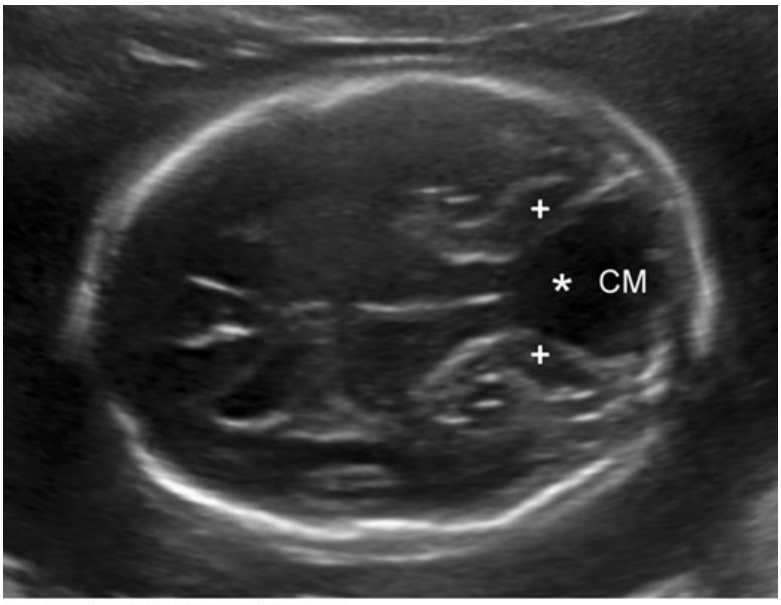

Inferior vermian agenesis, also called *Dandy-Walker variant*, is a term used when only the inferior portion of the vermis is absent. But, even when vermian agenesis appears to be partial and relatively subtle, the prevalence of associated anomalies and aneuploidy is still high, and the prognosis is often poor (Ecker, 2000; Long, 2006).

Schizencephaly and Porencephaly

Schizencephaly is a rare brain abnormality characterized by clefts in one or both cerebral hemispheres, typically involving the perisylvian fissure. The cleft is lined by heterotopic gray matter and communicates with the ventricle, extending through the cortex to the pial surface (Fig. 10-17). Schizencephaly is believed to be an abnormality of neuronal migration, which explains its typically delayed recognition until after midpregnancy (Howe, 2012). It is associated with absence of the cavum septum pellucidum, resulting in the frontal horn communication shown in the image below.

FIGURE 10-17

Schizencephaly. This transverse image of the fetal head shows a large cleft that extends from the right lateral ventricle through the cortex. Because the borders of the cleft are separate, the defect is termed *open-lipped*. (Reproduced with permission from Michael Davidson, RDMS.)

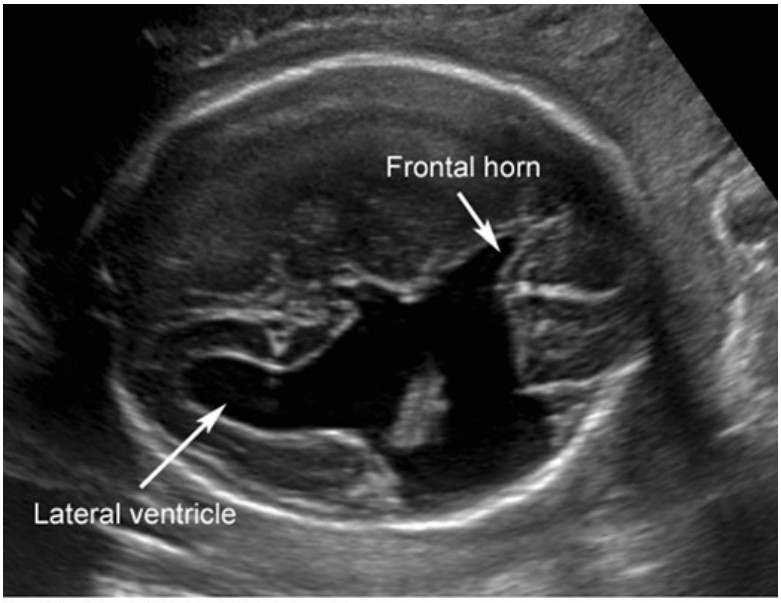

In contrast, porencephaly is a cystic space within the brain that is lined by white matter and may or may not communicate with the ventricular system. It is generally considered to be a destructive lesion and may develop following intracranial hemorrhage in the setting of neonatal alloimmune thrombocytopenia or following death of a monochorionic co-twin (Fig. 45-20). Fetal MR imaging should be considered when either of these CNS anomalies is identified.

Sacrococcygeal Teratoma

This germ cell tumor is one of the most common tumors in neonates, with a birth prevalence of approximately 1 in 28,000 (Derikx, 2006; Swamy, 2008). It is thought to arise from the totipotent cells along Hensen node, anterior to the coccyx. Classification of sacrococcygeal teratoma (SCT) includes four types (Altman, 1974). Type 1 is predominantly external with a minimal presacral component; type 2 is predominantly external but with a significant intrapelvic component; type 3 is predominantly internal but with abdominal extension; and type 4 is entirely internal with no external component. The tumor histological type may be mature, immature, or malignant.

Sonographically, SCT appears as a solid and/or cystic mass that arises from the anterior sacrum and usually extends inferiorly and externally as it grows (Fig. 10-18). Solid components often have varying echogenicity, appear disorganized, and may enlarge rapidly with advancing gestation. Internal pelvic components may be more challenging to visualize, and fetal MR imaging should be considered. Hydramnios is frequent, and hydrops may develop from high-output cardiac failure, either as a consequence of tumor vascularity or secondary to bleeding within the tumor and resultant anemia. Mentioned throughout this chapter, hydrops is more fully described in Chapter 15 (Hydrops Fetalis). Fetuses with tumors >5 cm often require cesarean delivery, and classical hysterotomy may be needed (Gucciardo, 2011). As shown in Figure 16-3, fetal surgery is suitable for some SCT cases.

FIGURE 10-18

Sacrococcygeal teratoma. Sonographically, this tumor appears as a solid and/or cystic mass that arises from the anterior sacrum and tends to extend inferiorly and externally as it grows. In this image, a 7 × 6 cm inhomogeneous solid mass is visible below the normal-appearing sacrum. There is also an internal component to the tumor.

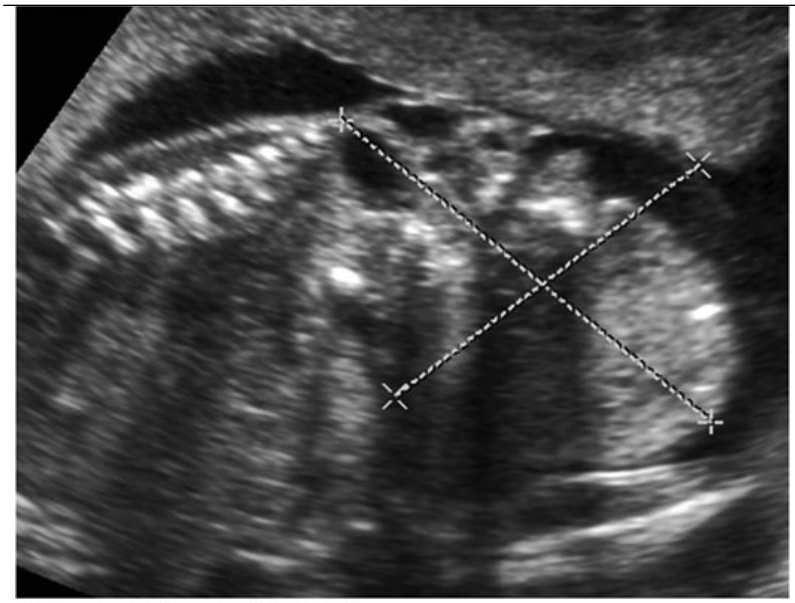

Caudal Regression Sequence—Sacral Agenesis

This rare anomaly is characterized by absence of the sacral spine and often portions of the lumbar spine. It is approximately 25 times more common in diabetic pregnancies (Garne, 2012). Sonographic findings include a spine that appears abnormally short, lacks normal lumbosacral curvature, and terminates abruptly above the level of the iliac wings. Because the sacrum does not lie between the iliac wings, they are abnormally close together and may appear "shield-like." There may also be abnormal positioning of the lower extremities and lack of normal local soft tissue development. Caudal regression should be differentiated from *sirenomelia*, which is a rare anomaly characterized by a single fused lower extremity that occupies the midline.

Face and Neck

Normal fetal lips and nose are shown in Figure 10-19. A fetal profile is not a required component of standard examination but may be helpful in identifying cases of *micrognathia*—an abnormally small jaw (Fig. 10-20). Micrognathia should be considered in the evaluation of hydramnios (Chap. 11, Hydramnios). Use of the *ex-utero intrapartum treatment (EXIT)* procedure for severe micrognathia is discussed in Chapter 16 (Ex-Utero Intrapartum Treatment).

FIGURE 10-19

Midline face. This view demonstrates the integrity of the upper lip.

FIGURE 10-20

Fetal profile. **A.** This image depicts a normal fetal profile. **B.** This fetus has severe micrognathia, which creates a severely recessed chin.

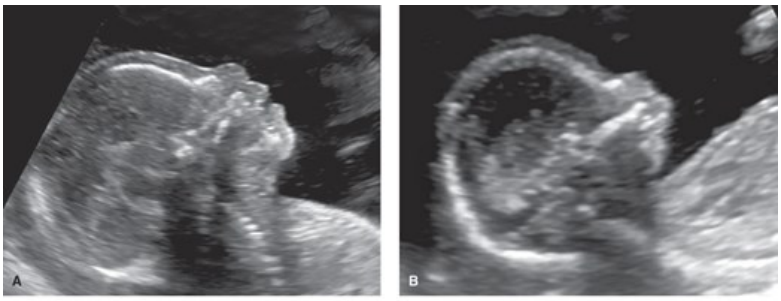

Facial Clefts

There are three main types of clefts. The first type, *cleft lip and palate*, always involves the lip, may also involve the hard palate, can be unilateral or bilateral, and has a birth prevalence that approximates 1 in 1000 (Cragan, 2009; Dolk, 2010). If isolated, the inheritance is multifactorial—with a recurrence risk of 3 to 5 percent for one prior affected child. If a cleft is visible in the upper lip, a transverse image at the level of the alveolar ridge may demonstrate that the defect also involves the primary palate (Fig. 10-21).

FIGURE 10-21

Cleft lip/palate. **A.** This fetus has a prominent unilateral (left-sided) cleft lip. **B.** Transverse view of the palate in the same fetus demonstrates a defect in the alveolar ridge (*arrow*). The tongue (*T*) is also visible.

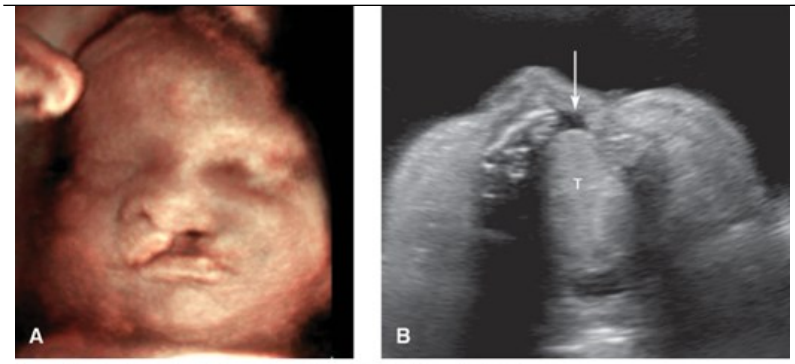

In one systematic review of low-risk pregnancies, cleft lip was identified sonographically in only about half of cases (Maarse, 2010). Approximately 40 percent of those detected in prenatal series are associated with other anomalies or syndromes, and aneuploidy is common (Maarse, 2011; Offerdal, 2008). The rate of associated anomalies is highest for bilateral defects that involve the palate. Using data from the Utah Birth Defect Network, Walker and associates (2001) identified aneuploidy in 1 percent with cleft lip alone, 5 percent with unilateral cleft lip and palate, and 13 percent with bilateral cleft lip and palate. It is reasonable to offer fetal chromosomal microarray analysis when a cleft is identified.

The second type of cleft is *isolated cleft palate.* It begins at the uvula, may involve the soft palate, and occasionally involves the hard palate—but does not involve the lip. The birth prevalence approximates 1 in 2000 (Dolk, 2010). Identification of isolated cleft palate has been described using specialized 2- and 3-dimensional sonography (Ramos, 2010; Wilhelm, 2010). However, it is not expected to be visualized during a standard sonographic examination (Maarse, 2011; Offerdal, 2008).

A third type of cleft is *median cleft lip,* which is found in association with several conditions. These include agenesis of the primary palate, hypotelorism, and holoprosencephaly. Median clefts may also be associated with hypertelorism and frontonasal hyperplasia, formerly called the *median cleft face syndrome.*

Cystic Hygroma

This venolymphatic malformation is characterized by fluid-filled sacs that extend from the posterior neck (Fig. 10-22). Cystic hygromas may be diagnosed as early as the first trimester and vary widely in size. They are believed to develop when lymph from the head fails to drain into the jugular vein and accumulates instead in jugular lymphatic sacs. Their birth prevalence approximates 1 in 5000. But, reflecting the high in-utero lethality of the condition, the first-trimester incidence exceeds 1 in 300 (Malone, 2005).

FIGURE 10-22

Cystic hygromas. **A.** This 9-week fetus with a cystic hygroma (*arrow*) was later found to have Noonan syndrome. **B.** Massive multiseptated hygromas (*arrowheads*) in the setting of hydrops fetalis at 15 weeks' gestation.

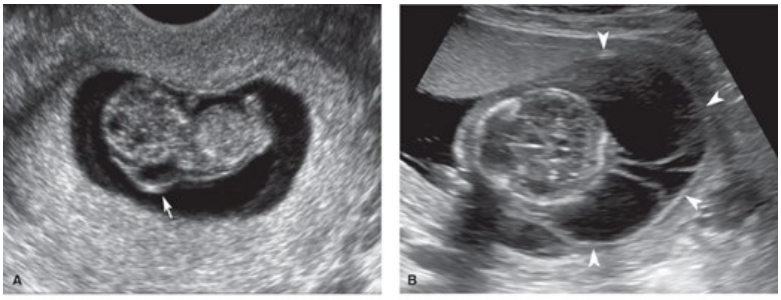

Up to 70 percent of cystic hygromas are associated with aneuploidy. When cystic hygromas are diagnosed in the first trimester, trisomy 21 is the most common aneuploidy, followed by 45,X and trisomy 18 (Kharrat, 2006; Malone, 2005). First-trimester fetuses with cystic hygromas are five times more likely to be aneuploid than fetuses with a thickened nuchal translucency. When cystic hygromas are diagnosed in the second trimester, approximately

75 percent of aneuploid cases are 45,X—*Turner syndrome* (Johnson, 1993; Shulman, 1992).

Even in the absence of aneuploidy, cystic hygromas confer a significantly greater risk for other anomalies, particularly cardiac anomalies that are flow-related. These include hypoplastic left heart and coarctation of the aorta. Cystic hygromas also may be part of a genetic syndrome. One is *Noonan syndrome,* an autosomal dominant disorder that shares several features with Turner syndrome, including short stature, lymphedema, high-arched palate, and often pulmonary valve stenosis.

Large cystic hygromas are usually associated with hydrops fetalis, rarely resolve, and carry a poor prognosis. Small hygromas may undergo spontaneous resolution, and provided that fetal karyotype and echocardiography results are normal, the prognosis *may* be good. The likelihood of a nonanomalous liveborn neonate with normal karyotype following identification of first-trimester hygroma is approximately 1 in 6 (Kharrat, 2006; Malone, 2005).

Thorax

The lungs appear homogeneous and surround the heart. In the four-chamber view of the heart, they comprise approximately two thirds of the area, with the heart occupying the remaining third. The thoracic circumference is measured at the skin line in a transverse plane at the level of the four-chamber view. In cases of suspected pulmonary hypoplasia secondary to a small thorax, such as with severe skeletal dysplasia, comparison with a reference table may be helpful (Appendix, Fetal Sonographic Measurements). Various abnormalities may appear sonographically as cystic or solid space-occupying lesions or as an effusion outlining the heart or lung(s). Fetal therapy for thoracic abnormalities is discussed in Chapter 16 (Percutaneous Procedures).

Congenital Diaphragmatic Hernia

This is a defect in the diaphragm through which abdominal organs herniate into the thorax. It is left-sided in approximately 75 percent of cases, right-sided in 20 percent, and bilateral in 5 percent (Gallot, 2007). The prevalence of congenital diaphragmatic hernia (CDH) is 1 in 3000 to 4000 births (Cragan, 2009; Dolk, 2010). Associated anomalies and aneuploidy are found in 40 percent of cases (Gallot, 2007; Stege, 2003). With suspected CDH, targeted sonography and fetal echocardiography should be performed, and fetal chromosomal microarray analysis should be offered. In population-based series, the presence of an associated abnormality reduces the overall survival rate of neonates with CDH from approximately 50 percent to about 20 percent (Colvin, 2005; Gallot, 2007). If there are no associated abnormalities, the major causes of neonatal mortality are pulmonary hypoplasia and pulmonary hypertension.

Sonographically, left-sided CDH typically shows dextroposition of the heart toward the right side of the thorax and a cardiac axis pointing toward the midline (Fig. 10-23). Associated findings include the stomach bubble or bowel peristalsis in the chest and a wedge-shaped mass—the liver—located anteriorly in the left hemithorax. Liver herniation complicates at least 50 percent of cases and is associated with a 30-percent reduction in the survival rate (Mullassery, 2010). With large lesions, impaired swallowing and mediastinal shift may result in hydramnios and hydrops, respectively.

FIGURE 10-23

Congenital diaphragmatic hernia. In this transverse view of the thorax, the heart is shifted to the far right side of the chest by a left-sided diaphragmatic hernia containing stomach (*S*), liver (*L*), and bowel (*B*).

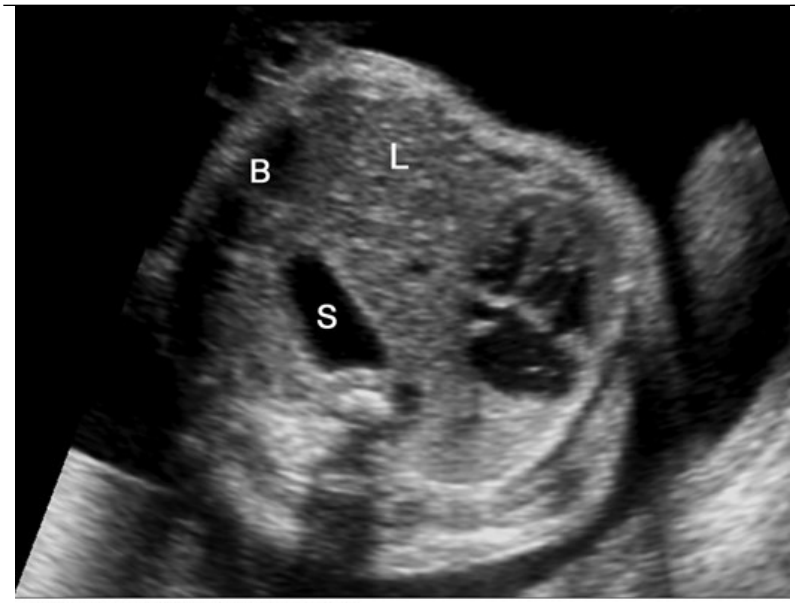

Efforts to reduce neonatal mortality rates and need for extracorporeal membrane oxygenation (ECMO) have focused on indicators such as the sonographic lung-to-head ratio, MR imaging measurements of lung volume, and the degree of liver herniation (Jani, 2012; Oluyomi-Obi, 2016; Worley, 2009). These and fetal therapy for CDH are reviewed in Chapter 16 (Congenital Diaphragmatic Hernia).

Congenital Cystic Adenomatoid Malformation

This abnormality represents a hamartomatous overgrowth of terminal bronchioles that communicates with the tracheobronchial tree. It is also called *congenital pulmonary airway malformation (CPAM),* based on an understanding that not all histopathological types are *cystic* or *adenomatoid* (Azizkhan, 2008; Stocker, 1977, 2002). The estimated prevalence is 1 in 6000 to 8000 births, and this rate is rising because of improved sonographic detection of milder cases (Burge, 2010; Duncombe, 2002).

Sonographically, congenital cystic adenomatoid malformation (CCAM) is a well-circumscribed thoracic mass that may appear solid and echogenic or may have one or multiple variably sized cysts (Fig. 10-24). It usually involves one lobe, has blood supply from the pulmonary artery, and drains into the pulmonary veins. Lesions with cysts ≥5 mm are generally termed *macrocystic*, and lesions with cysts <5 mm are termed *microcystic* (Adzick, 1985).

FIGURE 10-24

Transverse **(A)** and sagittal **(B)** images of a 26-week fetus with a very large left-sided microcystic congenital cystic adenomatoid malformation (CCAM). The mass (*C*) fills the thorax and has shifted the heart to the far right side of the chest, with development of ascites (*asterisks*). Fortunately, the mass did not continue to grow, the ascites resolved, and the neonate was delivered at term and did well following resection.

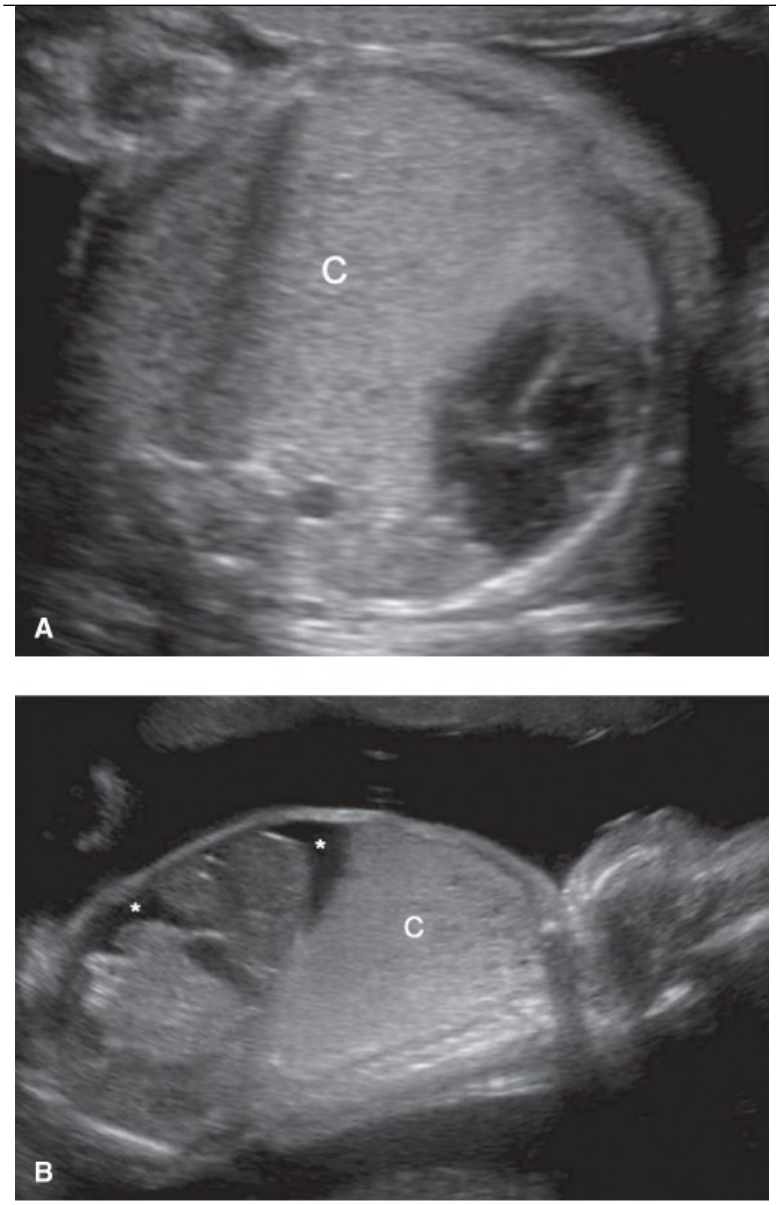

Source: F. Gary Cunningham, Kenneth J. Leveno, Steven L. Bloom, Catherine Y. Spong, Jodi S. Dashe, Barbara L. Hoffman, Brian M. Casey, Jeanne S. Sheffield: *Williams Obstetrics*, 25th Edition

In a review of 645 CCAM cases, the overall survival rate exceeded 95 percent, and 30 percent of cases demonstrated apparent prenatal resolution. The other 5 percent of cases—typically very large lesions with associated mediastinal shift—were complicated by hydrops, and the prognosis was poor (Cavoretto, 2008). CCAMs often become less conspicuous with advancing gestation. However, a subset of CCAMs demonstrates rapid growth between 18 and 26 weeks' gestation. Corticosteroid therapy has been used for large microcystic lesions to forestall growth and potentially ameliorate hydrops (Curran, 2010; Peranteau, 2016). If a large dominant cyst is present, thoracoamnionic shunt placement may lead to hydrops resolution. Fetal therapy for CCAM is discussed in Chapter 16 (Percutaneous Procedures).

Pulmonary Sequestration

Also called a *bronchopulmonary sequestration*, this abnormality is an accessory lung bud "sequestered" from the tracheobronchial tree, that is, a mass of nonfunctioning lung tissue. Most cases diagnosed prenatally are *extralobar,* which means they are enveloped in their own pleura. Overall, however, most sequestrations present in adulthood and are *intralobar*—within the pleura of another lobe. Extralobar pulmonary sequestration is considered significantly less common than CCAM, and no precise prevalence has been reported. Lesions have a left-sided predominance and most often involve the left lower lobe. Of cases, 10 to 20 percent are located below the diaphragm, and associated anomalies have been reported in

approximately 10 percent of cases (Yildirim, 2008).

Sonographically, pulmonary sequestration presents as a homogeneous, echogenic thoracic mass (Fig. 10-25A). Thus, it may resemble a microcystic CCAM. However, the blood supply is from the systemic circulation—from the aorta rather than the pulmonary artery (see Fig. 10-25B). In 5 to 10 percent with pulmonary sequestration, a large ipsilateral pleural effusion develops, and without treatment, this may result in pulmonary hypoplasia or hydrops (see Fig. 10-25C,D). Therapeutic thoracoamnionic shunting of effusions is discussed in Chapter 16 (Percutaneous Procedures). Hydrops may also result from mediastinal shift or high-output cardiac failure due to the left-to-right shunt imposed by the mass. In the absence of a pleural effusion, the reported survival rate exceeds 95 percent, and 40 percent of cases demonstrate apparent prenatal resolution (Cavoretto, 2008).

FIGURE 10-25

Pulmonary sequestration. **A.** This transverse image at the level of the 4-chamber view of the heart depicts a pulmonary sequestration involving the left lower lobe in a 25-week fetus. Mass effect leads to dextroposition of the heart to the right side of the chest. **B.** A sagittal image shows the pulmonary sequestration supplied by a branch of the abdominal aorta. **C.** Over the next 3 weeks, a large ipsilateral pleural effusion develops (*asterisk*), resulting in mediastinal shift and dextroposition of the heart to the far right thorax. **D.** Following placement of a double-pigtail shunt through the chest wall and into the effusion, the effusion drained and the lung significantly reexpanded. Arrows points to coils of the pigtail shunt. (Reproduced with permission from Dr. Elaine Duryea.)

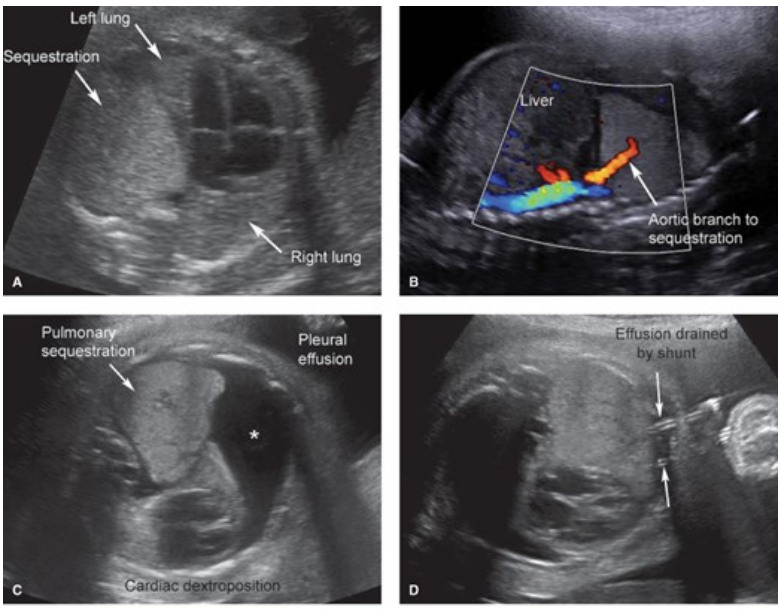

Congenital High Airway Obstruction Sequence

This rare anomaly usually results from laryngeal or tracheal atresia. The normal egress of lung fluid is obstructed, and the tracheobronchial tree and lungs become massively distended. Sonographically, the lungs appear brightly echogenic, the bronchi are dilated, the diaphragm is flattened or everted, and the heart is compressed (Fig. 10-26). Venous return is impaired and ascites develops, typically followed by hydrops. In one review of 118 cases, associated anomalies were identified in more than 50 percent (Sanford, 2012). Congenital high airway obstruction sequence (CHAOS) is a feature of the autosomal recessive *Fraser syndrome* and has been associated with the 22q11.2 deletion syndrome. In some cases, the obstructed airway spontaneously perforates, which potentially confers a better prognosis. The EXIT procedure has significantly improved outcome in selected cases (Chap. 16, Ex-Utero Intrapartum Treatment).

FIGURE 10-26

Congenital high airway obstruction sequence (CHAOS). The lungs appear brightly echogenic, and one is marked by an "L." The bronchi, one of which is noted by an arrow, are dilated with fluid. Flattening and eversion of the diaphragm is common, as is ascites (*asterisks*).

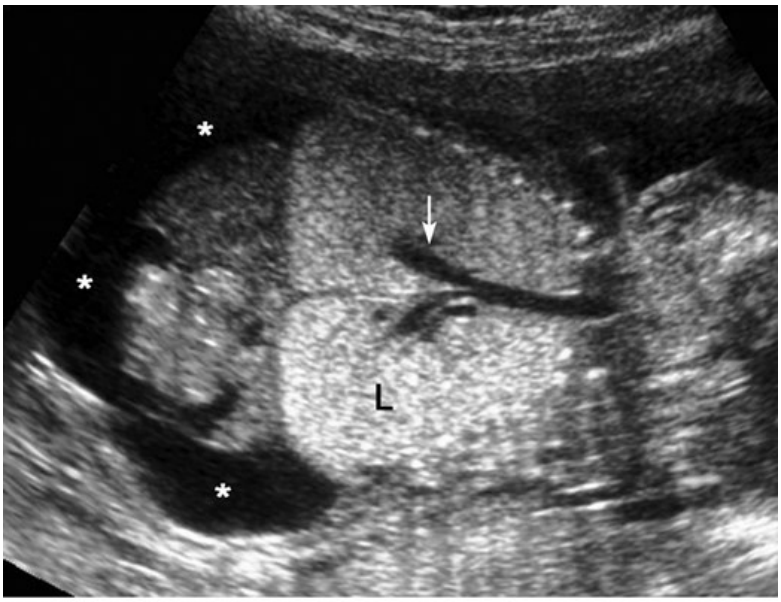

Heart

Cardiac malformations are the most common class of congenital anomalies, and their overall prevalence is 8 in 1000 births (Cragan, 2009). Almost 90 percent of cardiac defects are multifactorial or polygenic in origin, another 1 to 2 percent result from a single-gene disorder or gene-deletion syndrome, and 1 to 2 percent stem from exposure to a teratogen such as isotretinoin, hydantoin, or maternal diabetes. Based on data from population-based registries, approximately 1 in 8 liveborn and stillborn neonates with a congenital heart defect has a chromosomal abnormality (Dolk, 2010; Hartman, 2011). Of chromosomal abnormalities associated with cardiac anomalies, trisomy 21 accounts for more than 50 percent of cases. Others are trisomy 18, 22q11.2 deletion, trisomy 13, and monosomy X (Hartman, 2011). Of these aneuploid fetuses, 50 to 70 percent also have extracardiac anomalies. Chromosomal microarray analysis should be offered when cardiac defects are found.

Traditionally, detection of congenital cardiac anomalies is more challenging than for anomalies of other organ systems. Routine second-trimester sonography identifies approximately 40 percent of those with major cardiac anomalies before 22 weeks' gestation, and specialized sonography may identify 80 percent (Romosan, 2009; Trivedi, 2012). For selected anomalies, prenatal detection may improve neonatal survival. This may be particularly true for *ductal-dependent* lesions—those requiring prostaglandin infusion after birth to keep the ductus arteriosus open (Franklin, 2002; Mahle, 2001; Tworetzky, 2001).

Basic Cardiac Examination

Standard cardiac assessment includes a four-chamber view, evaluation of rate and rhythm, and evaluation of the left and right ventricular outflow tracts (Figs. 10–27 and 10-28A–C). Examination of the cardiac outflow tracts aids detection of abnormalities that might not be appreciated in the four-chamber view. These include tetralogy of Fallot, transposition of the great vessels, and truncus arteriosus.

FIGURE 10-27

The four-chamber view. **A.** Diagram demonstrating measurement of the cardiac axis from the four-chamber view of the fetal heart. **B.** Sonogram of the four-chamber view at 22 weeks' gestation shows the normal symmetry of the atria and ventricles, normal position of the mitral and triscuspid valves, pulmonary veins entering the left atrium, and descending aorta (*Ao*). L = left; LA = left atrium; LV = left ventricle; R = right; RA = right atrium; RV = right ventricle.

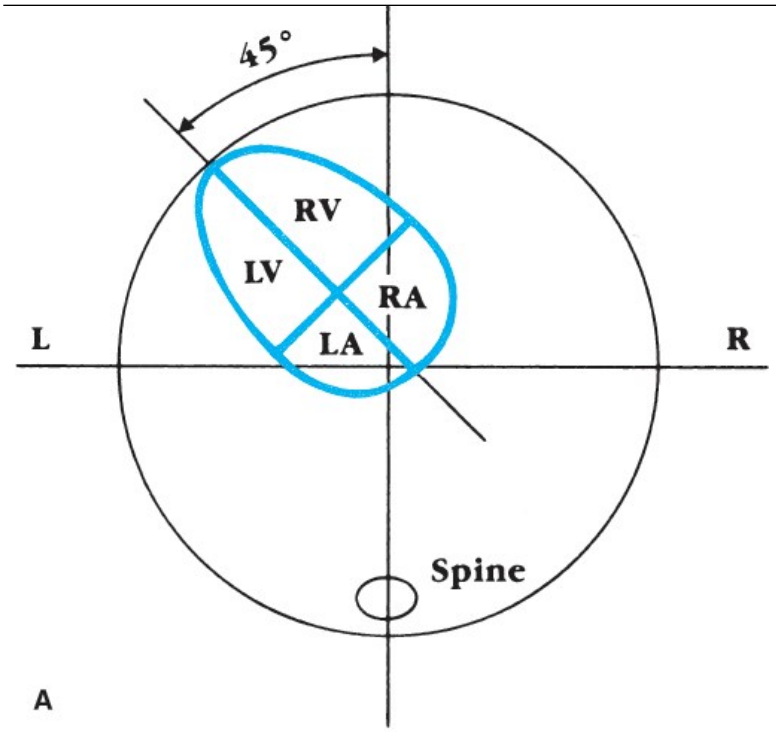

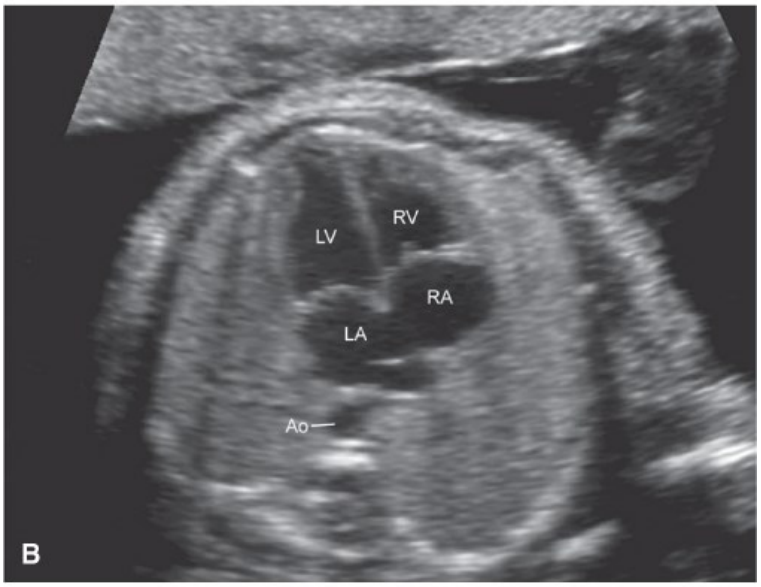

FIGURE 10-28

Fetal echocardiography gray-scale imaging planes. **A.** Four-chamber view. **B.** Left ventricular outflow tract view. The white arrow illustrates the mitral valve becoming the wall of the aorta. The arrow with asterisk marks the interventricular septum becoming the opposing aortic wall. **C.** Right ventricular outflow tract view. **D.** Three vessel and trachea view. **E.** High short-axis view (outflow tracts). **F.** Low short-axis view (ventricles). **G.** Aortic arch view. **H.** Ductal arch view. **I.** Superior and inferior vena cavae views. Ao = aorta; IVC = inferior vena cava; LA = left atrium; LV = left ventricle; PA = pulmonary artery; RA = right atrium; RV = right ventricle; SVC = superior vena cava.

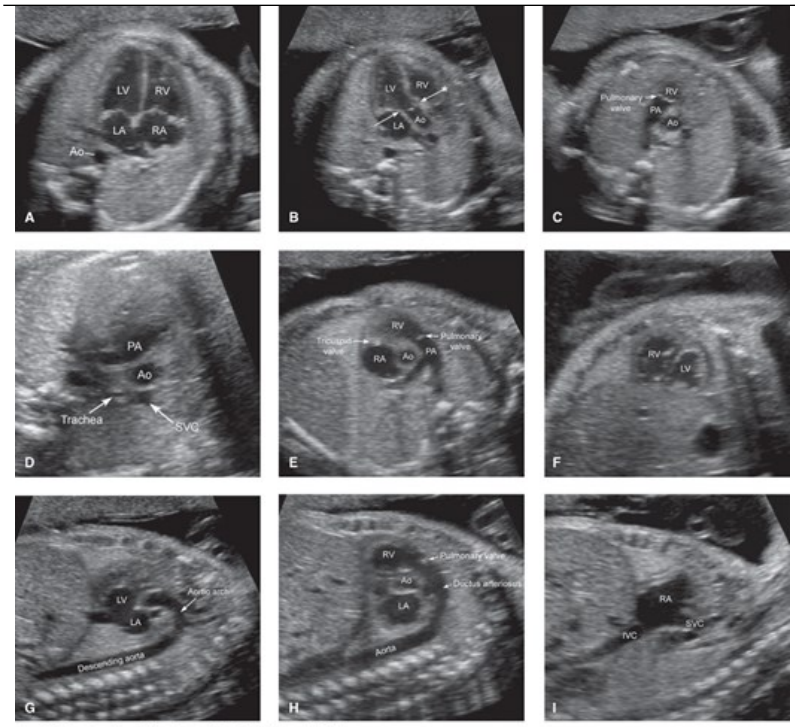

The *four-chamber view* is a transverse image of the fetal thorax at a level immediately above the diaphragm. It allows evaluation of cardiac size, position in the thorax, cardiac axis, atria and ventricles, foramen ovale, atrial septum primum, interventricular septum, and atrioventricular valves (see Fig. 10–27). The atria and ventricles should be similar in size, and the apex of the heart should form a 45-degree angle with the left anterior chest wall. Abnormalities of cardiac axis are frequently encountered with structural cardiac anomalies and occur in more than a third (Shipp, 1995).

The *left ventricular outflow tract view* is a transverse image just above the diaphragm and demonstrates that the ascending aorta arises entirely from the left ventricle. The interventricular septum is shown to be in continuity with the anterior wall of the aorta, and the mitral valve in continuity with the posterior wall of the aorta (see Fig. 10–28B). Ventricular septal defects and outflow tract abnormalities are often visible in this view (Fig. 10–29).

FIGURE 10-29

Ventricular septal defect. **A.** In this four-chamber view of a 22-week fetus, a defect (*arrow*) is noted in the superior (membranous) portion of the interventricular septum. **B.** The left-ventricular outflow tract view of the same fetus demonstrates a break (*arrow*) in continuity between the interventricular septum and the anterior wall of the aorta.

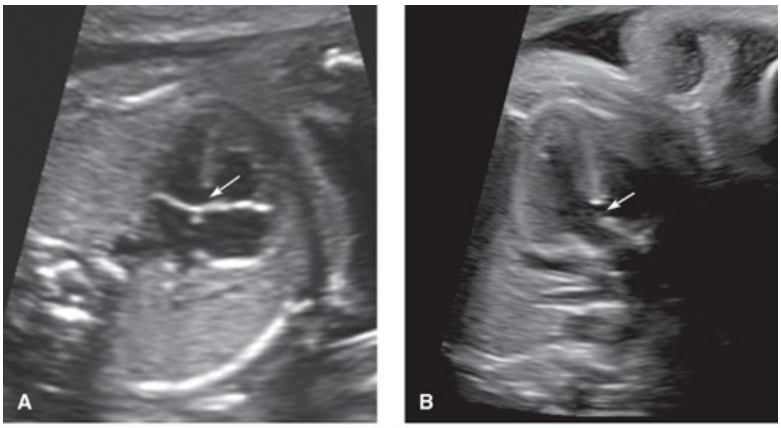

The *right ventricular outflow tract view* shows the right ventricle giving rise to the pulmonary artery (see Fig. 10–28C). Together, the left and right

outflow tract views demonstrate the normal perpendicular orientation of the aorta and pulmonary artery, and the comparable size of these great arteries. Structures visible in the right ventricular outflow tract view include the right ventricle and the main pulmonary artery, which subsequently branches into the right and left pulmonary arteries. These structures are also visible in the short axis view, shown in Figure 10–28E.

Fetal Echocardiography

This is a specialized examination of fetal cardiac structure and function designed to identify and characterize abnormalities. Guidelines for its performance have been developed collaboratively by the American Institute of Ultrasound in Medicine, American College of Obstetricians and Gynecologists, Society for Maternal-Fetal Medicine, American Society of Echocardiography, and American College of Radiology. Echocardiography indications include suspected fetal cardiac anomaly, extracardiac anomaly, or chromosomal abnormality; fetal arrhythmia; hydrops; thick nuchal translucency; monochorionic twin gestation; first-degree relative to the fetus with a congenital cardiac defect; in vitro fertilization; maternal anti-Ro or anti-La antibodies; exposure to a medication associated with cardiac defects; and maternal metabolic disease associated with cardiac defects—such as pregestational diabetes or phenylketonuria (American Institute of Ultrasound in Medicine, 2013a). Components of the examination are listed in Table 10-9, and examples of nine required gray-scale imaging views are shown in Figure 10-28. Examples of selected cardiac anomalies are reviewed below.

TABLE 10-9

Components of Fetal Echocardiography

Basic imaging parameters
Evaluation of atria
Evaluation of ventricles
Evaluation of great vessels
Cardiac and visceral situs
Atrioventricular junctions
Ventriculoarterial junctions
Scanning planes, gray scale
Four-chamber view
Left ventricular outflow tract
Right ventricular outflow tract
Three-vessel and trachea view
Short-axis view, low (ventricles)
Short-axis view, high (outflow tracts)
Aortic arch
Ductal arch
Superior and inferior vena cavae
Color Doppler evaluation
Systemic veins (vena cavae and ductus venosus[a])
Pulmonary veins
Foramen ovale
Atrioventricular valves[a]
Atrial and ventricular septae
Aortic and pulmonary valves[a]
Ductus arteriosus
Aortic arch
Umbilical artery and vein (optional)[a]
Cardiac rate and rhythm assessment

[a]Pulsed-wave Doppler sonography should be used as an adjunct to evaluate these structures.

Cardiac biometry and functional assessment are optional but should be considered for suspected structural/functional abnormalities.

Adapted from the American Institute of Ultrasound in Medicine, 2013b.

Ventricular Septal Defect

This is the most common congenital cardiac anomaly and is found in approximately 1 in 300 births (Cragan, 2009; Dolk, 2010). Even with adequate visualization, the prenatal detection rate of ventricular septal defect (VSD) is low. A defect may be appreciated in the membranous or muscular portion of the interventricular septum in the four-chamber view, and color Doppler demonstrates flow through the defect. Imaging of the left ventricular outflow tract may show discontinuity of the interventricular septum as it becomes the wall of the aorta (see Fig. 10-29). Fetal VSD is associated with other abnormalities and aneuploidy, and chromosomal microarray analysis should be offered. That said, the prognosis for an isolated defect is good.

More than a third of prenatally diagnosed VSDs close in utero, and another third close in the first year of life (Axt-Fliedner, 2006; Paladini, 2002).

Endocardial Cushion Defect

This is also called an *atrioventricular (AV) septal defect* or *AV canal defect*. It has a prevalence of approximately 1 in 2500 births and is associated with trisomy 21 in more than half of cases (Christensen, 2013; Cragan, 2009; Dolk, 2010). The endocardial cushions are the crux of the heart, and defects jointly involve the atrial septum primum, interventricular septum, and medial leaflets of the mitral and tricuspid valves (Fig. 10-30). Approximately 6 percent of cases occur with heterotaxy syndromes, that is, those in which the heart and/or abdominal organs are on the incorrect side. Endocardial cushion defects associated with heterotaxy can have comorbid conduction system abnormalities resulting in third-degree AV block, which confers a poor prognosis (Chap. 16, Tachyarrhythmias).

FIGURE 10-30

Endocardial cushion defect. **A.** During ventricular systole, the lateral leaflets of the mitral and triscuspid valves come together in the midline. But the atrioventricular valve plane is abnormal, a common atrium (*A*) is observed, and there is a visible defect (*arrow*) in the interventricular septum. **B.** During diastolic filling, opening of the atrioventricular valves more clearly demonstrates the absence of their medial leaflets.

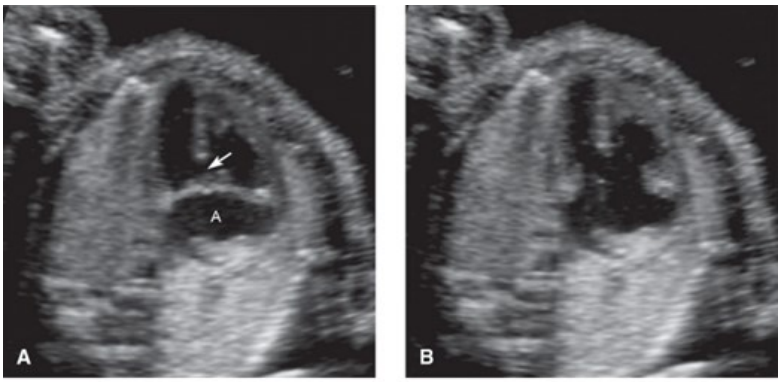

Hypoplastic Left Heart Syndrome

This anomaly is found in approximately 1 in 4000 births (Cragan, 2009; Dolk, 2010). Sonographically, the left side of the heart may appear "filled-in" or the left ventricle may be so small and attenuated that a ventricular chamber is difficult to appreciate (Fig. 10-31). There may be no visible left ventricular inflow or outflow, and reversal of flow may be documented in the aortic arch.

FIGURE 10-31

Hypoplastic left heart syndrome. **A.** In this 4-chamber view at 16 weeks, the left ventricle (*LV*) appears "filled in" and is significantly smaller than the right ventricle (*RV*). The tricuspid valve (*TV*) is open, whereas the mitral valve appears closed (*asterisk*). **B.** Color Doppler depicts flow from the right atrium to the right ventricle only, and left ventricular filling is not visible. **C.** The left ventricular outflow tract view demonstrates marked narrowing of the aorta (Ao). RV = right ventricle; LA = left atrium. **D.** The tiny circle (arrow) in this short axis view is the hypoplastic aortic root. (Reproduced with permission from Rafael Levy, RDMS.)

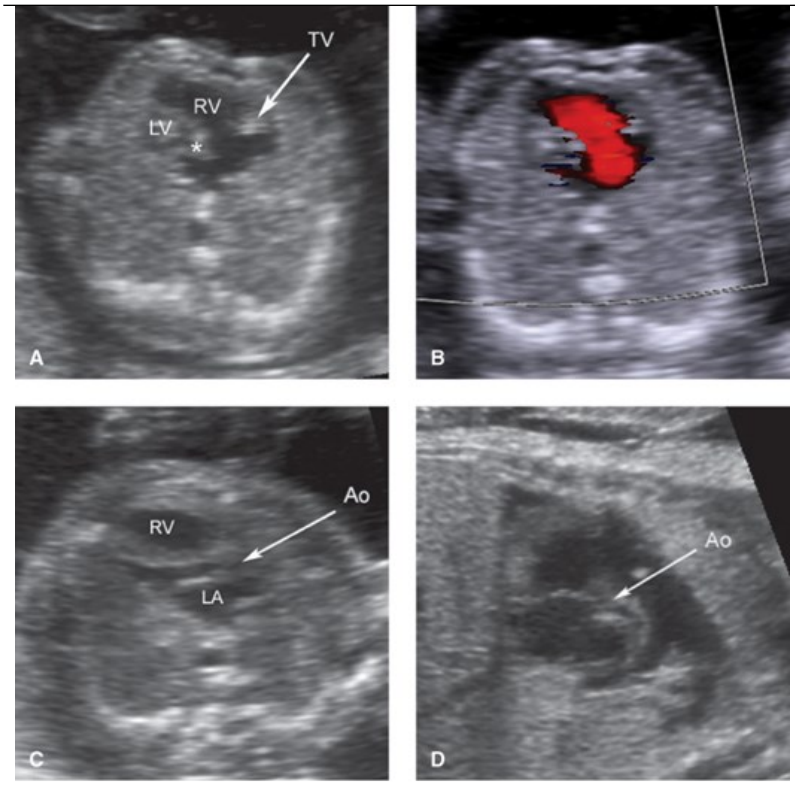

Source: F. Gary Cunningham, Kenneth J. Leveno, Steven L. Bloom, Catherine Y. Spong, Jodi S. Dashe, Barbara L. Hoffman, Brian M. Casey, Jeanne S. Sheffield: *Williams Obstetrics*, 25th Edition

Although this anomaly was once considered a lethal prognosis, 70 percent of affected infants may now survive to adulthood (Feinstein, 2012). Postnatal treatment consists of a three-stage palliative repair or cardiac transplantation. Still, morbidity remains high, and developmental delays are common (Lloyd, 2017; Paladini, 2017). This is a ductal-dependent lesion for which neonatal administration of prostaglandin therapy is essential. Fetal therapy for hypoplastic left heart is discussed in Chapter 16 (Radiofrequency Ablation).

Tetralogy of Fallot

This anomaly occurs in approximately 1 in 3000 births (Cragan, 2009; Dolk, 2010; Nelson, 2016). It includes a ventricular septal defect; an overriding aorta; a pulmonary valve abnormality, typically stenosis; and right ventricular hypertrophy (Fig. 10-32). The last does not present before birth. Due to the location of the ventricular septal defect, the four-chamber view may appear normal.

FIGURE 10-32

Tetralogy of Fallot. This image shows a ventricular septal defect with an overriding aorta in a fetus with tetralogy of Fallot. The arrow points to the aortic valve. The left ventricle (*LV*) and right ventricle (*RV*) are labeled.

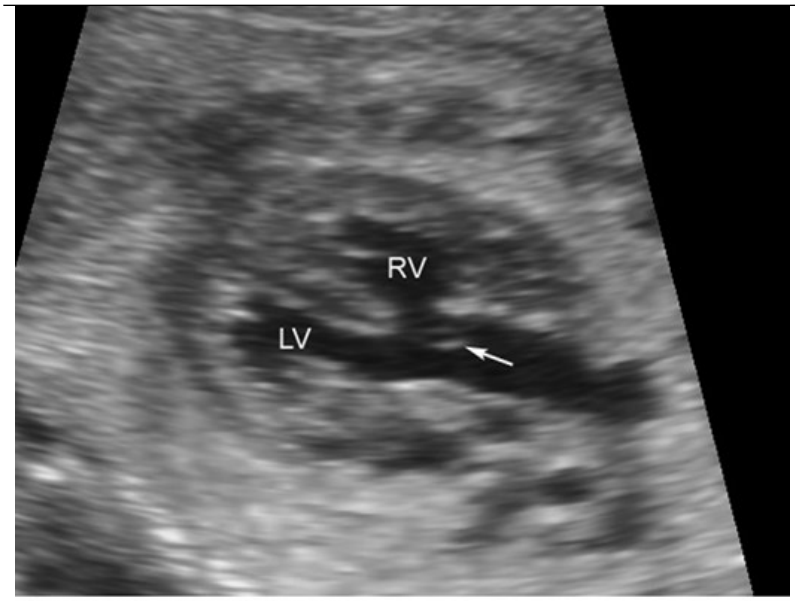

Following postnatal repair, the 20-year survival rates exceed 95 percent (Knott-Craig, 1998). However, cases with *pulmonary atresia* have a more complicated course. There is also a variant in which the pulmonary valve is *absent.* These affected fetuses are at risk for hydrops and for tracheomalacia from compression of the trachea by an enlarged pulmonary artery.

Cardiac Rhabdomyoma

This is the most common cardiac tumor. Approximately 50 percent of cases are associated with tuberous sclerosis, an autosomal dominant disease with multiorgan system manifestations. Tuberous sclerosis is caused by mutations in the hamartin (*TSC1*) and tuberin (*TSC2*) genes.

Cardiac rhabdomyomas appear as well-circumscribed echogenic masses, usually within the ventricles or outflow tracts. They may be single or multiple; may grow in size during gestation; and occasionally, may lead to inflow or outflow obstruction. In cases without obstruction or large tumor size, the prognosis is relatively good from a cardiac standpoint, because the tumors tend to regress after the neonatal period. Because extracardiac findings of tuberous sclerosis may not be apparent with prenatal sonography, MR imaging may be considered to evaluate fetal CNS anatomy (Fetal Anatomical Evaluation).

M-Mode

Motion-mode or M-mode imaging is a linear display of cardiac cycle events, with time on the x-axis and motion on the y-axis. It is often used to measure embryonic or fetal heart rate (Fig. 10-33). If an abnormality of heart rate or rhythm is identified, M-mode imaging permits separate evaluation of atrial and ventricular waveforms. Thus, it is particularly useful for characterizing arrhythmias and their response to treatment (Chap. 16, Tachyarrhythmias). M-mode can also be used to assess ventricular function and atrial and ventricular outputs.

FIGURE 10-33

M-mode, or motion mode, is a linear display of the events of the cardiac cycle, with time on the x-axis and motion on the y-axis. M-mode is used commonly to measure the fetal heart rate, as in this 12-week fetus.

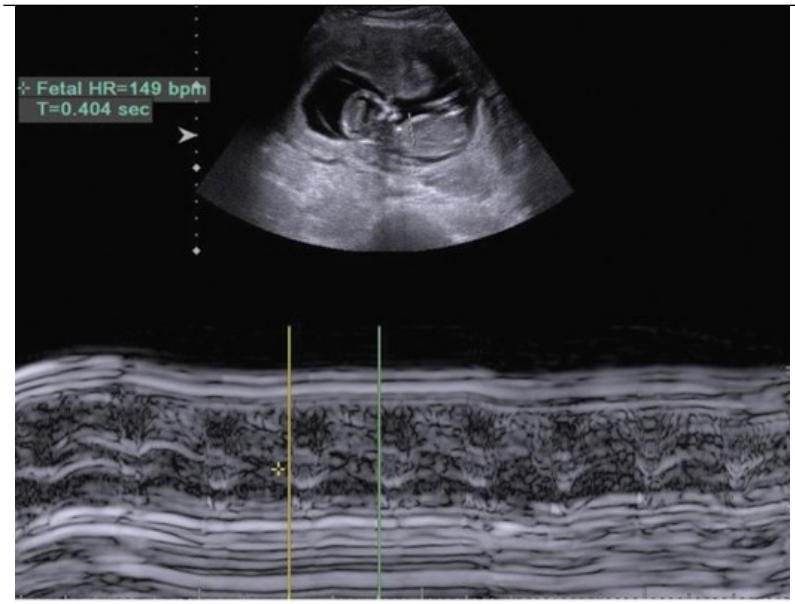

Source: F. Gary Cunningham, Kenneth J. Leveno, Steven L. Bloom, Catherine Y. Spong, Jodi S. Dashe, Barbara L. Hoffman, Brian M. Casey, Jeanne S. Sheffield: *Williams Obstetrics*, 25th Edition

Premature Atrial Contractions

Also called atrial extrasystoles, these are the most common fetal arrhythmia and a frequent finding. They represent cardiac conduction system immaturity and typically resolve later in gestation or in the neonatal period. Premature atrial contractions (PACs) may be conducted and thus sound like an extra beat. However, they are more commonly blocked, and with handheld Doppler they sound like a dropped beat. As shown in Figure 10-34, the dropped beat may be demonstrated with M-mode evaluation as a compensatory pause that follows the premature contraction.

FIGURE 10-34

M-mode. In this image, there is normal concordance between atrial (*A*) and ventricular contractions (*V*). Movement of the tricuspid valve (*T*) is also shown. There is also a premature atrial contraction (*arrow*) and a subsequent early ventricular contraction, followed by a compensatory pause.

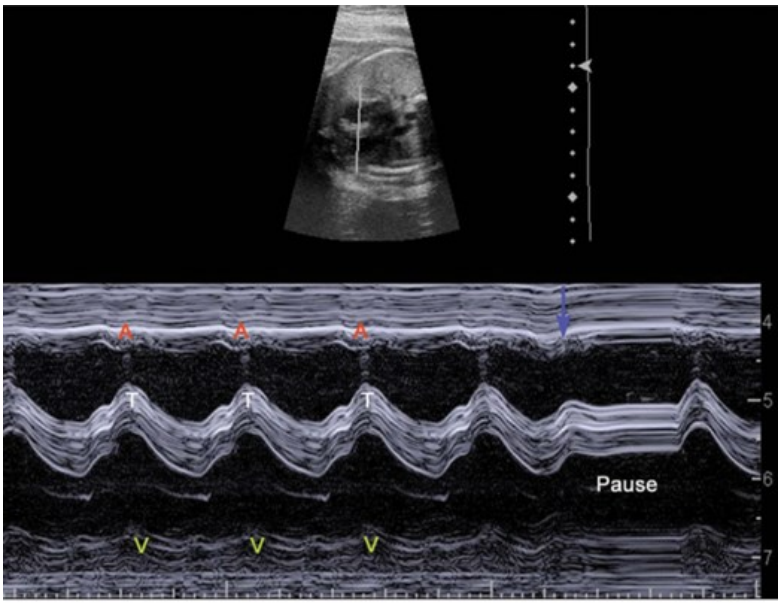

Source: F. Gary Cunningham, Kenneth J. Leveno, Steven L. Bloom, Catherine Y. Spong, Jodi S. Dashe, Barbara L. Hoffman, Brian M. Casey, Jeanne S. Sheffield: *Williams Obstetrics*, 25th Edition

PACs sometimes occur with an atrial septal aneurysm but are not associated with major structural cardiac abnormalities. Older case reports describe

an association with maternal caffeine consumption and with hydralazine (Lodeiro, 1989; Oei, 1989). In approximately 2 percent of cases, affected fetuses are later identified to have a *supraventricular tachycardia* (SVT) that requires urgent treatment (Copel, 2000). Accordingly, pregnancies with fetal PACs are often followed with fetal heart rate assessment as often as every 1 to 2 weeks until ectopy resolves. Treatment of fetal SVT and other arrhythmias is discussed in Chapter 16 (Tachyarrhythmias).

Abdominal Wall

The integrity of the abdominal wall is assessed at the level of the cord insertion during the standard examination (Fig. 10-35). Ventral wall defects include gastroschisis, omphalocele, and body stalk anomaly.

FIGURE 10-35

Normal ventral wall. Transverse view of the abdomen in a second-trimester fetus with an intact anterior abdominal wall and normal cord insertion.

Gastroschisis is a full-thickness abdominal wall defect located to the right of the umbilical cord insertion. Bowel herniates through the defect into the amnionic cavity (Fig. 10-36). The prevalence is approximately 1 in 2000 births (Jones, 2016; Nelson, 2015). Gastroschisis is the one major anomaly more common in fetuses of younger mothers, and the average maternal age is 20 years (Santiago-Muñoz, 2007). Coexisting bowel abnormalities such as *jejunal atresia* are found in approximately 15 percent of cases (Nelson, 2015; Overcash, 2014). Gastroschisis is not associated with aneuploidy, and the survival rate is 90 to 95 percent (Kitchanan, 2000; Nelson, 2015; Nembhard, 2001).

FIGURE 10-36

Gastroschisis. This 18-week fetus has a full-thickness ventral wall defect to the right of the cord insertion (*arrowhead*), through which multiple small bowel loops (*B*) have herniated into the amnionic cavity.

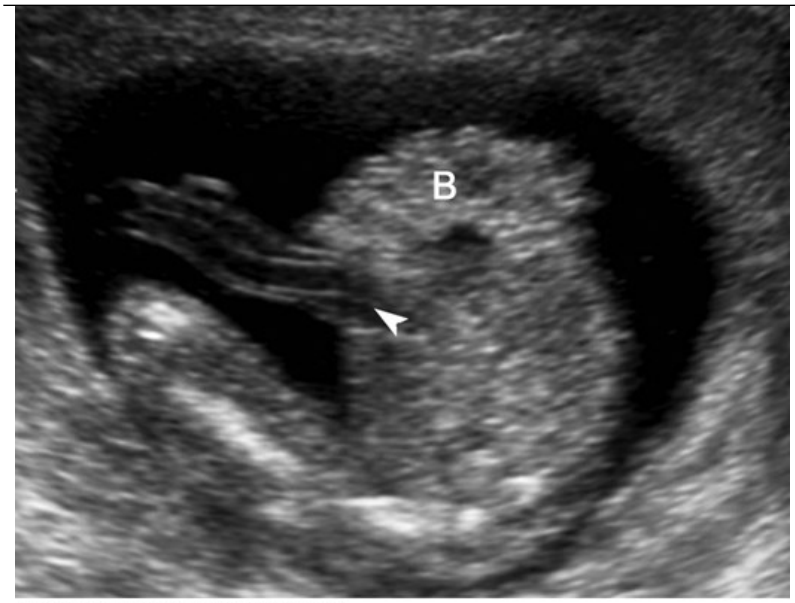

Fetal-growth restriction complicates gastroschisis in 15 to 40 percent of cases (Overcash, 2014; Santiago-Muñoz, 2007). Growth restriction does not appear to be associated with adverse outcomes such as longer hospitalization or higher mortality rate (Nelson, 2015; Overcash, 2014). However, earlier gestational age at delivery does pose a risk for adverse outcome with gastroschisis, and planned delivery at 36 to 37 weeks does not confer neonatal benefit (Al-Kaff, 2016; Overcash, 2014; South, 2013).

Omphalocele complicates 1 in 3000 to 5000 pregnancies (Canfield, 2006; Dolk, 2010). It forms when the lateral ectomesodermal folds fail to meet in the midline. This leaves the abdominal contents covered only by a two-layered sac of amnion and peritoneum into which the umbilical cord inserts (Fig. 10-37). More than half of cases are associated with other major anomalies or aneuploidy. Omphalocele also is a component of syndromes such as *Beckwith–Wiedemann, cloacal exstrophy,* and *pentalogy of Cantrell.* Smaller defects confer greater risk for aneuploidy (De Veciana, 1994). Chromosomal microarray analysis should be offered in all cases of omphalocele.

FIGURE 10-37

Omphalocele. Transverse view of the abdomen showing an omphalocele as a large abdominal wall defect with exteriorized liver covered by a thin membrane.

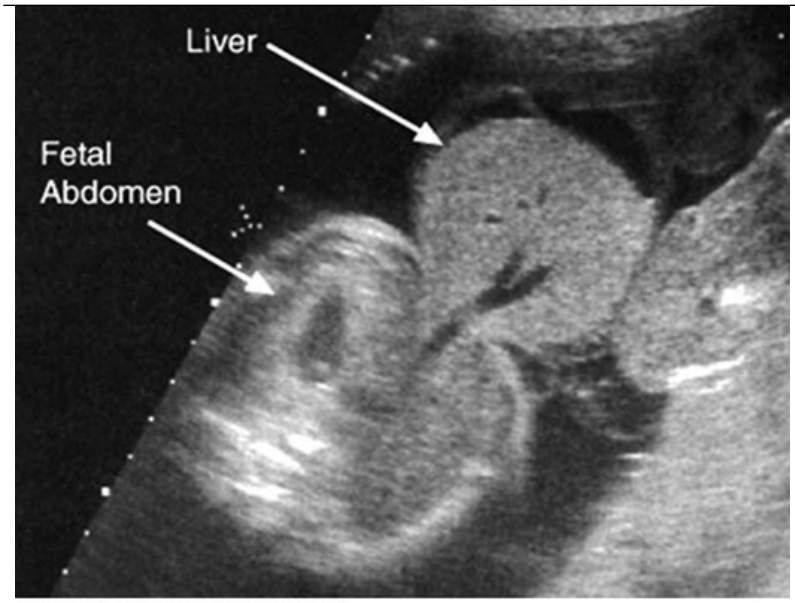

Body stalk anomaly, also known as *limb-body-wall complex* or *cyllosoma*, is a rare, lethal anomaly characterized by abnormal formation of the body wall. Typically, *no* abdominal wall is visible, and the abdominal organs extrude into the extraamnionic coelom. There is close approximation or fusion of the body to the placenta, and the umbilical cord is extremely short. Acute-angle scoliosis is another feature. Amnionic bands are often identified.

Gastrointestinal Tract

The stomach is visible in nearly all fetuses after 14 weeks' gestation. If the stomach is not seen during initial evaluation, the examination is repeated, and targeted sonography should be considered. Nonvisualization of the stomach may be secondary to impaired swallowing in the setting of oligohydramnios or to underlying causes such as esophageal atresia, a craniofacial anomaly, or a CNS or musculoskeletal abnormality. Fetuses with hydrops may also have impaired swallowing.

The bowel, liver, gallbladder, and spleen can be identified in many second- and third-trimester fetuses. Bowel appearance changes with fetal maturation. Occasionally, it may be bright or echogenic, which may indicate small amounts of swallowed intraamnionic blood, especially with comorbid MSAFP elevation. Bowel that appears as bright as fetal bone confers a slightly greater risk for underlying gastrointestinal malformations, for cystic fibrosis, for trisomy 21, and for congenital infection such as cytomegalovirus (Fig. 14-3).

Gastrointestinal Atresia

Bowel atresia is characterized by obstruction and proximal bowel dilation. In general, the more proximal the obstruction, the more likely it is to lead to hydramnios. At times, hydramnios from proximal small-bowel obstruction can be sufficiently severe to result in maternal respiratory compromise or preterm labor and may necessitate amnioreduction (Chap. 11, Oligohydramnios).

Esophageal atresia occurs in approximately 1 in 4000 births (Cragan, 2009; Pedersen, 2012). It may be suspected when the stomach cannot be visualized and hydramnios is present. That said, in up to 90 percent of cases, a concomitant *tracheoesophageal fistula* allows fluid to enter the stomach, such that prenatal detection is problematic. More than half have associated anomalies or genetic syndromes. Multiple malformations are present in 30 percent of cases, and aneuploidy such as trisomy 18 or 21, in 10 percent (Pedersen, 2012). Cardiac, urinary tract, and other gastrointestinal abnormalities are the most frequently associated anomalies. Approximately 10 percent of cases of esophageal atresia occur as part of the VACTERL association, which is vertebral defects, anal atresia, cardiac defects, tracheoesophageal fistula, renal anomalies, and limb abnormalities (Pedersen, 2012).

Duodenal atresia is found in approximately 1 in 10,000 births (Best, 2012; Dolk, 2010). It is characterized by the sonographic *double-bubble sign,* which represents distention of the stomach and the first part of the duodenum (Fig. 10-38). This finding is usually not present before 22 to 24 weeks' gestation. Demonstrating continuity between the stomach and proximal duodenum confirms that the second "bubble" is the proximal duodenum.

Approximately 30 percent of affected fetuses have an associated chromosomal abnormality or genetic syndrome, particularly trisomy 21. Of cases without a genetic abnormality, a third have associated anomalies, most commonly cardiac defects and other gastrointestinal abnormalities (Best, 2012). Obstructions in the more distal small bowel usually result in multiple dilated loops that may have enhanced peristaltic activity.

FIGURE 10-38

Duodenal atresia. The *double-bubble* sign represents distension of the stomach (*S*) and the first part of the duodenum (*D*), as seen on this axial abdominal image. Demonstrating continuity between the stomach and proximal duodenum confirms that the second "bubble" is the proximal duodenum.

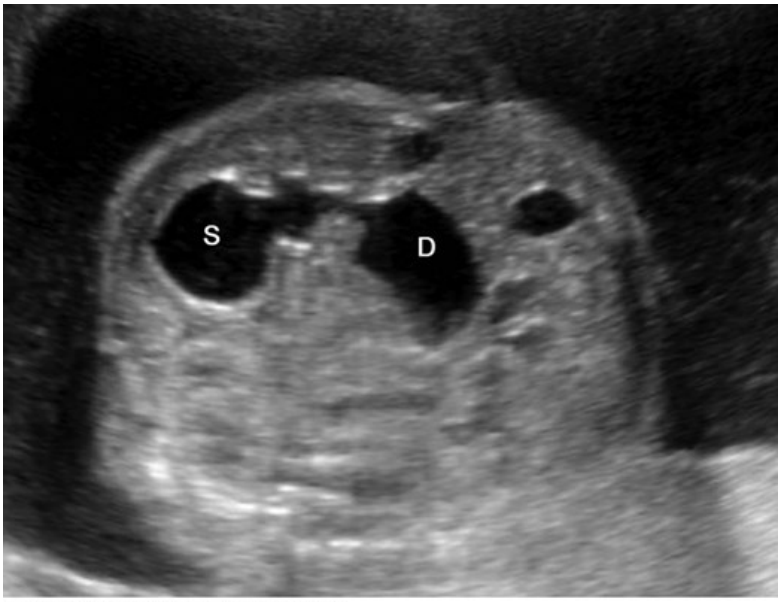

Large-bowel obstructions and anal atresia are less readily diagnosed by sonography, because hydramnios is not a typical feature and the bowel may not be significantly dilated. A transverse view through the pelvis may show an enlarged rectum as an anechoic structure between the bladder and the sacrum.

Kidneys and Urinary Tract

The fetal kidneys are visible adjacent to the spine, frequently in the first trimester and routinely by 18 weeks' gestation (Fig. 10-39). The length of the kidney approximates 20 mm at 20 weeks and grows by about 1.1 mm each week thereafter (Chitty, 2003). With advancing gestation, the kidneys become relatively less echogenic, and a rim of perinephric fat aids visualization of their margins.

FIGURE 10-39

Normal fetal kidneys. The kidneys are visible adjacent to the fetal spine in this 29-week fetus. With advancing gestation, a rim of perinephric fat aids visualization of the kidney margins. A physiological amount of urine is visible in the renal pelves and is marked in one kidney by an arrow.

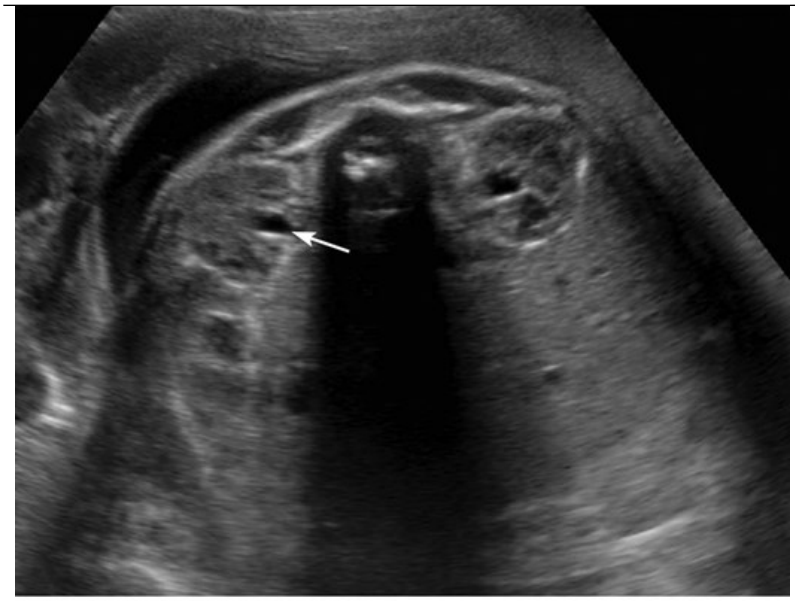

The fetal bladder is readily visible in the second trimester as a round, anechoic structure in the anterior midline of the pelvis. With application of Doppler, the bladder is outlined by the two superior vesical arteries as they become the umbilical arteries of the umbilical cord (Fig. 10-40 and Chap. 6, Umbilical Cord). The fetal ureters and urethra are not visible sonographically unless abnormally dilated.

FIGURE 10-40

Normal fetal bladder. The normal fetal bladder is readily visible as a round, fluid-filled structure in the anterior pelvis, outlined by the two superior vesical arteries as they become the umbilical arteries of the umbilical cord.

The placenta and membranes are the major sources of amnionic fluid early in pregnancy. However, after 18 weeks' gestation, most of the fluid is produced by the kidneys (Chap. 11, Normal Amnionic Fluid Volume). Fetal urine production rises from 5 mL/hr at 20 weeks to approximately 50 mL/hr at term (Rabinowitz, 1989). Normal amnionic fluid volume in the second half of pregnancy suggests urinary tract patency with at least one functioning kidney. But, unexplained oligohydramnios suggests a urinary tract defect or placental perfusion abnormality.

Renal Pelvis Dilatation

This finding is present in 1 to 5 percent of fetuses. It is also called urinary tract dilatation or hydronephrosis. In 40 to 90 percent of cases, it is transient or physiological and does not represent an underlying abnormality (Ismaili, 2003; Nguyen, 2010). In approximately a third of cases, a urinary tract abnormality is confirmed in the neonatal period. Of these, *ureteropelvic junction (UPJ) obstruction* and *vesicoureteral reflux (VUR)* are the most frequent.

The fetal renal pelvis is measured anterior to posterior in a transverse plane, and calipers are placed on the inner border of the fluid collection (Fig. 10-41). Although various thresholds have been defined, the pelvis is typically considered dilated if it exceeds 4 mm in the second trimester or 7 mm at approximately 32 weeks' gestation (Reddy, 2014). Typically, the second-trimester threshold is used to identify pregnancies that warrant subsequent third-trimester evaluation.

FIGURE 10-41

Renal pelvis dilatation. This common finding is identified in 1 to 5 percent of pregnancies. **A.** In this 34-week fetus with mild renal pelvis dilatation, the anterior-posterior diameter of the renal pelvis measured 7 mm in the transverse plane. **B.** Sagittal image of the kidney in a 32-week fetus with severe renal pelvis dilatation secondary to ureteropelvic junction obstruction. The arrow points to one of the rounded calyces.

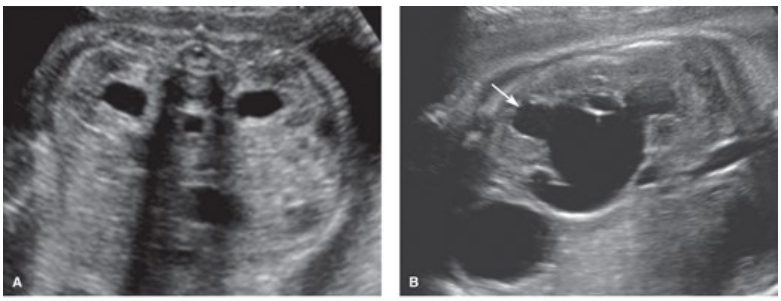

The Society for Fetal Urology categorized renal pelvis dilatation based on a metaanalysis of more than 100,000 screened pregnancies (Table 10-10) (Lee, 2006; Nguyen, 2010). The degree of dilatation correlates with the likelihood of an underlying abnormality. Other suggestive findings of pathology include calyceal dilatation, cortical thinning, or dilatation elsewhere along the urinary tract. Mild pyelectasis in the second trimester is associated with a slightly greater risk for Down syndrome and is considered a soft marker for this (Fig. 14-3).

TABLE 10-10

Risk for Postnatal Urinary Abnormality According to Degree of Renal Pelvis Dilatation[a]

Dilatation	Second Trimester	Third Trimester	Postnatal Abnormality
Mild	4 to <7 mm	7 to <9 mm	12%
Moderate	7 to ≤10 mm	9 to ≤15 mm	45%
Severe	>10 mm	>15 mm	88%

[a]Society for Fetal Urology Classification.

Modified from Lee, 2006; Nguyen, 2010.

Ureteropelvic Junction Obstruction

This condition is the most common abnormality associated with renal pelvis dilatation. The birth prevalence is 1 in 1000 to 2000, and males are

affected three times more often than females (Williams, 2007; Woodward, 2002). Obstruction is generally functional rather than anatomical, and it is bilateral in up to a fourth of cases. The likelihood of ureteropelvic junction obstruction rises from 5 percent with mild renal pelvis dilatation to more than 50 percent with severe dilatation (Lee, 2006).

Duplicated Renal Collecting System

In this anatomical anomaly, the upper and lower poles of the kidney—called moieties—are each drained by a separate ureter (Fig. 10-42). Duplication is found in approximately 1 in 4000 pregnancies, is more common in females, and is bilateral in 15 to 20 percent of cases (James, 1998; Vergani, 1998; Whitten, 2001). Sonographically, an intervening tissue band separates two distinct renal pelves. Development of hydronephrosis or ureteral dilatation may occur due to abnormal implantation of one or both ureters within the bladder—a relationship that reflects the anatomical *Weigert-Meyer* rule. The upper pole ureter may develop obstruction from a ureterocele within the bladder, whereas the lower pole ureter has a shortened intravesical segment that predisposes to vesicoureteral reflux (see Fig. 10-42B). Thus, both moieties may become dilated from different etiologies, and both are at risk for loss of function.

FIGURE 10-42

Duplicated renal collecting system. The upper and lower moieties of the kidney are each drained by a separate ureter. **A.** Renal pelvis dilatation is visible in both the upper (*U*) and lower (*L*) pole moieties, which are separated by an intervening band of renal tissue (*arrowhead*). **B.** The bladder, encircled by the highlighted umbilical arteries, contains a ureterocele (*arrowhead*).

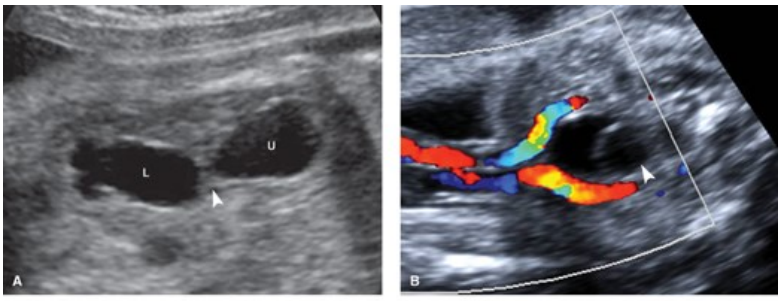

Renal Agenesis

The prevalence of bilateral renal agenesis is approximately 1 in 8000 births, whereas that of unilateral renal agenesis is 1 in 1000 births (Cragan, 2009; Dolk, 2010; Sheih, 1989; Wiesel, 2005). When a kidney is absent, color Doppler imaging of the descending aorta demonstrates absence of the ipsilateral renal artery (Fig. 10-43). In addition, the ipsilateral adrenal gland typically enlarges to fill the renal fossa, termed the *lying down adrenal sign* (Hoffman, 1992). As with other fetal anomalies, amniocentesis for chromosomal microarray analysis should be considered.

FIGURE 10-43

Renal agenesis. **A.** In this coronal image of the fetal abdomen, color Doppler shows the course of the abdominal aorta. The ultrasound beam is perpendicular to the aorta, demonstrating absence of the renal arteries bilaterally. **B.** This coronal image of a fetus with unilateral renal agenesis shows the adrenal gland (*arrowheads*) filling the renal fossa, termed the "lying-down" adrenal sign. The adrenal gland has a hypoechoic cortex and hyperechoic medulla.

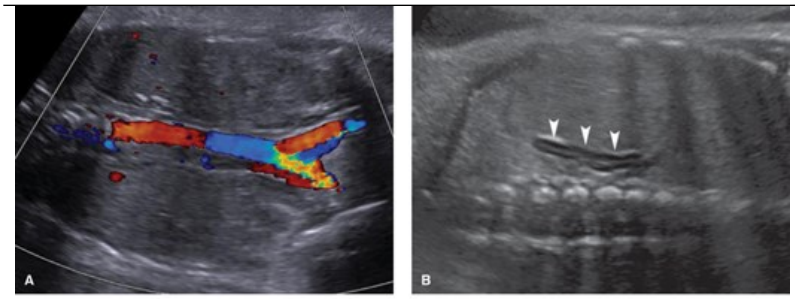

If renal agenesis is bilateral, no urine is produced, and the resulting anhydramnios leads to pulmonary hypoplasia, limb contractures, and a distinctively compressed face. When this combination results from renal agenesis, it is called *Potter syndrome,* after Dr. Edith Potter, who described it in 1946. When these abnormalities result from severely decreased amnionic fluid volume from another etiology, such as bilateral multicystic dysplastic kidney or autosomal recessive polycystic kidney disease, it is called *Potter sequence.* The prognosis for these abnormalities is extremely poor.

Multicystic Dysplastic Kidney

This severe form of renal dysplasia results in a nonfunctioning kidney. The nephrons and collecting ducts do not form normally, such that primitive ducts are surrounded by fibromuscular tissue, and the ureter is atretic (Hains, 2009). Sonographically, the kidney contains numerous smooth-walled cysts of varying size that do not communicate with the renal pelvis and are surrounded by echogenic cortex (Fig. 10-44).

FIGURE 10-44

Multicystic dysplastic kidneys. Coronal view of the fetal abdomen demonstrates markedly enlarged kidneys containing multiple cysts of varying sizes that do not communicate with a renal pelvis.

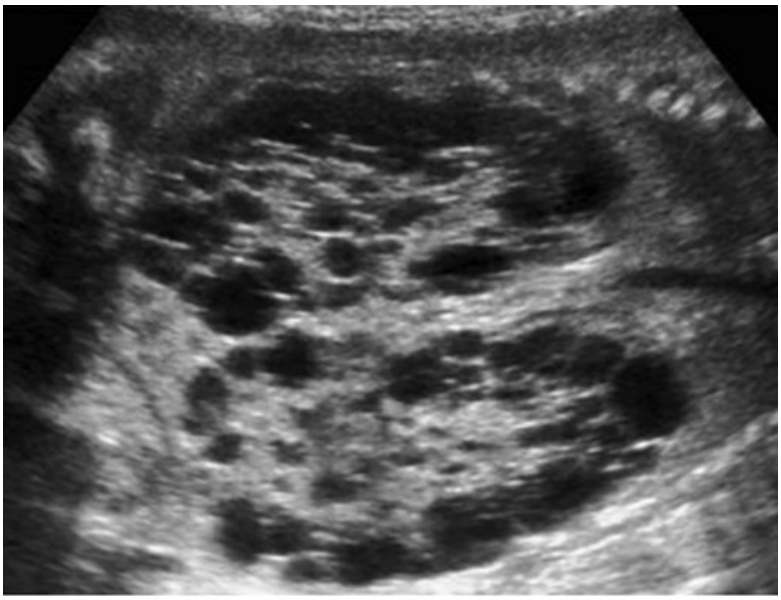

Unilateral multicystic dysplastic kidney (MCDK) has a prevalence of 1 in 4000 births. Contralateral renal abnormalities are present in 30 to 40 percent—most frequently vesicoureteral reflux or ureteropelvic junction obstruction (Schreuder, 2009). Nonrenal anomalies have been reported in 25 percent of cases, and cystic dysplasia may occur as a component of many genetic syndromes (Lazebnik, 1999; Schreuder, 2009). If MCDK is isolated and unilateral, the prognosis is generally good.

Bilateral MCDK is found in approximately 1 in 12,000 births. It is associated with severely decreased amnionic fluid volume starting early in gestation. This leads to Potter sequence and a poor prognosis (Lazebnik, 1999).

Polycystic Kidney Disease

Of the hereditary polycystic diseases, only the infantile form of *autosomal recessive polycystic kidney disease (ARPKD)* may be reliably diagnosed prenatally. ARPKD is a chronic, progressive disease of the kidneys and liver that results in cystic dilatation of the renal collecting ducts and in congenital hepatic fibrosis (Turkbey, 2009). The carrier frequency of a disease-causing mutation in the *PKHD1* gene approximates 1 in 70, and the disease prevalence is 1 in 20,000 (Zerres, 1998). The phenotypic variability of ARPKD ranges from lethal pulmonary hypoplasia at birth to presentation in late childhood or even adulthood with predominantly hepatic manifestations. Sonographically, infantile ARPKD displays abnormally large kidneys that fill and distend the fetal abdomen and have a solid, ground-glass texture. Severe oligohydramnios confers a poor prognosis.

Autosomal dominant polycystic kidney disease (ADPKD), which is far more common, usually does not manifest until adulthood (Chap. 53, Pregnancy Outcomes). Even so, some fetuses with ADPKD have mild renal enlargement and enhanced renal echogenicity in the setting of normal amnionic fluid volume. The differential diagnosis for these findings includes several genetic syndromes, aneuploidy, or normal variant.

Bladder Outlet Obstruction

Distal obstruction of the urinary tract is more frequent in male fetuses, and the most common etiology is *posterior urethral valves*. Characteristically, the bladder and proximal urethra are dilated, termed the “keyhole” sign, and the bladder wall is thick (Fig. 10-45). Oligohydramnios, particularly before midpregnancy, portends a poor prognosis because of pulmonary hypoplasia. Unfortunately, the outcome may be poor even with normal amnionic fluid volume. Evaluation includes a careful search for associated anomalies, which may occur in 40 percent of cases, and for aneuploidy, which has been reported in 5 to 8 percent (Hayden, 1988; Hobbins, 1984; Mann, 2010). If neither are present, affected male fetuses with severe oligohydramnios who have fetal urinary electrolytes suggesting a potentially favorable prognosis may be fetal therapy candidates. Evaluation and treatment of fetal bladder outlet obstruction is discussed in Chapter 16 (Urinary Shunts).

FIGURE 10-45

Posterior urethral valve. In this 19-week fetus with severe bladder outlet obstruction, the bladder is dilated and thick-walled, with dilatation of the proximal urethra that resembles a “keyhole.” Adjacent to the bladder is an enlarged kidney with evidence of cystic dysplasia, conferring a poor prognosis.

Skeletal Abnormalities

The 2015 revision of the Nosology and Classification of Genetic Skeletal Disorders includes an impressive 436 skeletal anomalies in 42 groups,

characterized by genetic abnormalities, phenotypic features, or radiographic criteria (Bonafe, 2015). The two types of skeletal dysplasias are *osteochondrodysplasias*— the generalized abnormal development of bone and/or cartilage, and *dysostoses*—which are abnormalities of individual bones, for example, *polydactyly.* In addition to these *malformations*, skeletal abnormalities include *deformations*, as with some cases of clubfoot, and *disruptions* such as limb-reduction defects.

Skeletal Dysplasias

The prevalence of skeletal dysplasias approximates 3 in 10,000 births. Two groups account for more than half of all cases: the *fibroblast growth factor 3 (FGFR3) chondrodysplasia* group and the *osteogenesis imperfecta* and decreased bone density group. Each occurs in 0.8 in 10,000 births (Stevenson, 2012).

Evaluation of a pregnancy with suspected skeletal dysplasia includes a survey of every long bone, as well as the hands and feet, skull size and shape, clavicles, scapulae, thorax, and spine. Reference tables are used to determine which long bones are affected and ascertain the degree of shortening (Appendix, Fetal Sonographic Measurements). Involvement of all long bones is termed *micromelia,* whereas predominant involvement of only the proximal, intermediate, or distal long bone segments is termed *rhizomelia, mesomelia,* and *acromelia*, respectively. The degree of ossification should be noted, as should presence of bowing or fractures. Each of these may provide clues to narrow the differential diagnosis and occasionally suggest a specific skeletal dysplasia. Many, if not most, skeletal dysplasias have a genetic component, and knowledge of specific mutations has advanced dramatically (Bonafe, 2015).

Although precise characterization may elude prenatal diagnosis, it is frequently possible to determine whether a skeletal dysplasia is lethal. Lethal dysplasias show profound long bone shortening, with measurements <5th percentile, and display femur length-to-abdominal circumference ratios below 16 percent (Nelson, 2014; Rahemtullah, 1997; Ramus, 1998). Generally, other sonographic abnormalities are evident. Pulmonary hypoplasia is suggested by a thoracic circumference <80 percent of the abdominal circumference value, by a thoracic circumference <2.5th percentile, and a cardiac circumference >50 percent of the thoracic circumference value (Appendix, Fetal Sonographic Measurements). Affected pregnancies also may develop hydramnios and/or hydrops (Nelson, 2014).

The FGFR3 chondrodysplasias include *achondroplasia* and *thanatophoric dysplasia.* Achondroplasia, also called *heterozygous achondroplasia*, is the most common nonlethal skeletal dysplasia. An impressive 98 percent of cases are due to a specific point mutation in the *FGFR3* gene. It has an autosomal dominant inheritance, and 80 percent of cases result from a new mutation. Achondroplasia is characterized by long bone shortening that is predominantly *rhizomelic*, an enlarged head with frontal bossing, depressed nasal bridge, exaggerated lumbar lordosis, and a trident configuration of the hands. Intelligence is typically normal. Sonographically, the femur and humerus measurements may not lie below the 5th percentile until the early third trimester. Thus, this condition is usually not diagnosed until late in pregnancy. In homozygotes, which represent 25 percent of the offspring of heterozygous parents, the condition is characterized by greater long bone shortening and is lethal.

The other major class of FGFR3 dysplasias, *thanatophoric dysplasia*, is the most common lethal skeletal disorder. It is characterized by severe micromelia, and affected fetuses—particularly those with type II—may develop a characteristic cloverleaf skull deformity (*Kleeblattschädel*) due to craniosynostosis. More than 99 percent of cases may be confirmed with genetic testing.

Osteogenesis imperfecta represents a group of skeletal dysplasias typified by hypomineralization. There are multiple types, and more than 90 percent of cases are characterized by a mutation in the *COL1A1* or *COL1A2* gene. Type IIa, also called the perinatal form, is lethal. It displays a profound lack of skull ossification, such that gentle pressure on the maternal abdomen from the ultrasound transducer results in visible skull deformation (Fig. 10-46). Other features include multiple in-utero fractures and ribs that appear “beaded.” Inheritance is autosomal dominant, such that all cases result from either new mutations or gonadal mosaicism (Chap. 13, Modes of Inheritance). Another skeletal dysplasia that results in severe hypomineralization is *hypophosphatasia*, which has an autosomal recessive inheritance.

FIGURE 10-46

Osteogenesis imperfecta. Type IIa, which is lethal, is characterized by such profound lack of skull ossification that gentle pressure on the maternal abdomen from the ultrasound transducer results in visible deformation (flattening) of the skull (*arrowheads*).

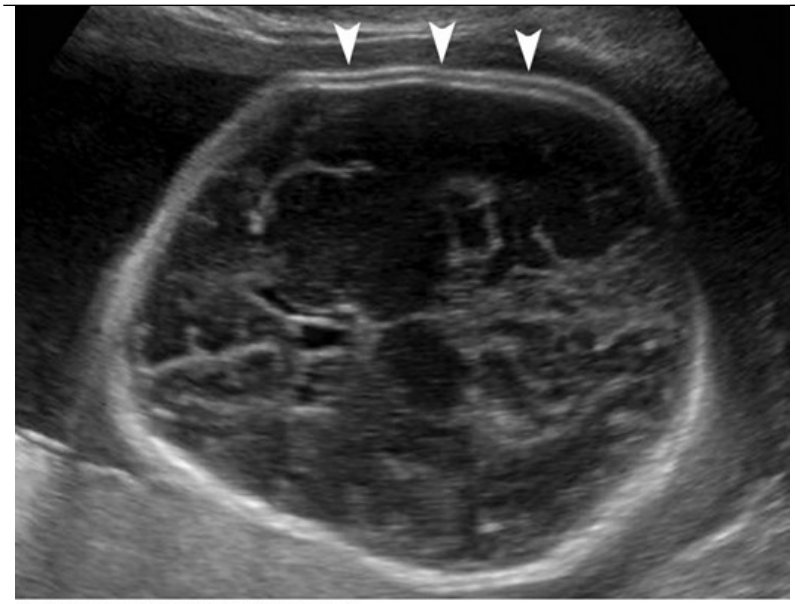

Clubfoot—Talipes Equinovarus

This disorder is notable for a deformed talus and shortened Achilles tendon. The affected foot is abnormally fixed and positioned with *equinus* (downward pointing), *varus* (inward rotation), and forefoot adduction. Most cases are considered malformations, with a multifactorial genetic component. However, an association with environmental factors and with early amniocentesis suggests that deformation also plays a role (Tredwell, 2001). Sonographically, the footprint is visible in the same plane as the tibia and fibula (Fig. 10-47).

FIGURE 10-47

Foot position. **A.** Normal fetal lower leg, demonstrating normal position of the foot. **B.** With talipes equinovarus, the foot "print" is visible in the same plane as the tibia and fibula.

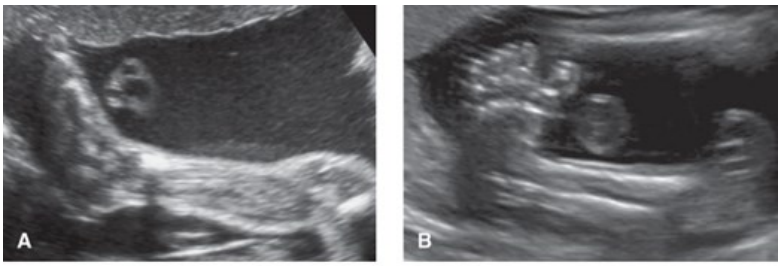

The prevalence of clubfoot approximates 1 in 1000 births, and the male:female ratio is 2:1 (Carey, 2003; Pavone, 2012). Clubfoot is bilateral in approximately 50 percent of affected individuals, and associated anomalies are present in at least 50 percent of all cases (Mammen, 2004; Sharma, 2011). Frequently associated anomalies include neural-tube defects, arthrogryposis, and myotonic dystrophy and other genetic syndromes. In cases with associated anomalies, aneuploidy is found in approximately 30 percent. In contrast, the rate is <4 percent when clubfoot appears isolated (Lauson, 2010; Sharma, 2011). Thus, a careful search for associated structural abnormalities is warranted, and chromosomal microarray analysis may be considered.

Limb-Reduction Defects

Documentation of the arms and legs is a component of the standard examination. The absence or hypoplasia of all or part of one or more extremities is a *limb-reduction defect.* The birth prevalence is 4 to 8 in 10,000 (Kucik, 2012; Stoll, 2010; Vasluian, 2013). Approximately half of these are isolated

defects, up to one third occur as part of a recognized syndrome, and individuals in the remaining cases have other coexisting anomalies (Stoll, 2010; Vasluian, 2013). Upper extremities are affected more frequently than lower ones. Of categories, a terminal *transverse limb defect* lacks part or all of a distal limb to create a stump (Fig. 10-48). This is more common than a *longitudinal defect*, which is complete or partial absence of the long bone(s) on only one side of a given extremity.

FIGURE 10-48

Transverse limb-reduction defect. **A.** At 18 weeks' gestation, only a rudimentary hand was visible. **B.** By 24 weeks, the radius and ulna were normal in size and appearance, and small rudimentary digits were evident.

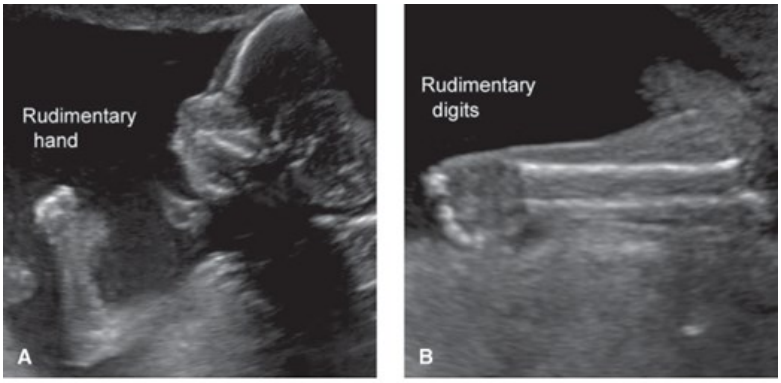

Absence of an entire extremity is termed *amelia. Phocomelia,* associated with thalidomide exposure, is an absence of one or more long bones with the hands or feet attached to the trunk (Chap. 12, Thalidomide and Lenalidomide). Limb-reduction defects are associated with numerous genetic syndromes, such as *Roberts syndrome*, an autosomal recessive condition characterized by *tetraphocomelia.* A *clubhand deformity*, usually from an absent radius, is associated with trisomy 18 and is also a component of the *thrombocytopenia-absent radius syndrome* (Fig. 13-5B). Limb-reduction defects may occur in the setting of a disruption such as amnionic-band sequence (Chap. 6, Amniochorion). They have also been associated with chorionic villus sampling when performed before 10 weeks' gestation (Fig. 14-6).

THREE- AND FOUR-DIMENSIONAL SONOGRAPHY

During the past two decades, three-dimensional (3-D) sonography has gone from a novelty to a standard feature of most modern ultrasound equipment (Fig. 10-49). 3-D sonography is not *routinely* used during a standard examination nor considered a required modality. However, it may be a component of specialized evaluations.

FIGURE 10-49

Fetal face. Surface rendered three-dimensional image of a normal fetal face and hand at 32 weeks.

Source: F. Gary Cunningham, Kenneth J. Leveno, Steven L. Bloom, Catherine Y. Spong, Jodi S. Dashe, Barbara L. Hoffman, Brian M. Casey, Jeanne S. Sheffield: *Williams Obstetrics*, 25th Edition

Most 3-D scanning uses a special transducer developed for this purpose. After a region of interest is identified, a 3-D volume is acquired that can be rendered to display axial, sagittal, coronal, or oblique images. Sequential "slices" may be generated, similar to computed tomographic (CT) or MR images. Unlike two-dimensional (2-D) scanning, which appears to be in "real time," 3-D imaging is static and obtained by processing a volume of stored images. With *four-dimensional (4-D) sonography*, also known as real-time 3-D sonography, rapid reconstruction of the rendered images conveys the impression that the scanning is in real time.

For 4-D imaging, one application known as *spatiotemporal image correlation—STIC* improves visualization of cardiac anatomy. During an automated sweep over the heart, the STIC application acquires a volume that includes thousands of 2D images captured at a rate as high as 150 frames per second (Devore, 2003). These individual images are obtained at different locations in the heart but at the same point in time. These views are subsequently arranged according to their spatial and temporal domains. This permits display of an ordered sequence of volume sets in a continuous cine loop (or video clip) of the cardiac cycle (Yeo, 2016). For example, after obtaining a volume sweep over the cardiac apex, an application such as Fetal Intelligent Navigation Echocardiography (FINE) can be applied to display videos of each of the different cardiac views shown in Fig. 10-28 (Garcia, 2016). It is hoped that such technology may eventually improve detection of fetal cardiac anomalies.

For selected anomalies, such as those of the face and skeleton, for tumors, and for some cases of neural-tube defects, 3-D sonography can add useful information (American College of Obstetricians and Gynecologists, 2016; Goncalves, 2005). That said, comparisons of 3-D and conventional 2-D sonography for the diagnosis of most congenital anomalies have not demonstrated better overall detection rates (Goncalves, 2006; Reddy, 2008). The American College of Obstetricians and Gynecologists (2016) concludes that proof of a clinical advantage of 3-D sonography for prenatal diagnosis is generally lacking.

DOPPLER

When sound waves strike a moving target, the frequency of the waves reflected back is shifted in proportion to the velocity and direction of that moving target—a phenomenon known as the *Doppler shift*. Because the magnitude and direction of the frequency shift depend on the relative motion of the moving target, Doppler can help evaluate flow within blood vessels. The Doppler equation is shown in Figure 10-50.

FIGURE 10-50

Doppler equation. Ultrasound emanating from the transducer with initial frequency f_o strikes blood moving at velocity v. Reflected frequency f_d is dependent on angle θ between beam of sound and vessel.

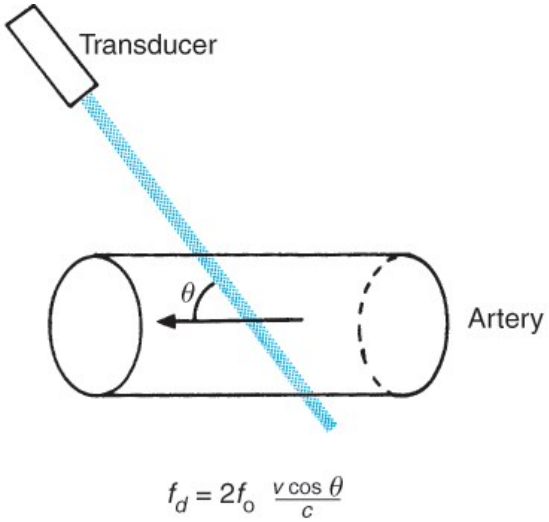

Source: F. Gary Cunningham, Kenneth J. Leveno, Steven L. Bloom, Catherine Y. Spong, Jodi S. Dashe, Barbara L. Hoffman, Brian M. Casey, Jeanne S. Sheffield: *Williams Obstetrics*, 25th Edition

An important component of the equation is the angle of insonation, abbreviated as theta (θ). This is the angle between the sound waves from the transducer and flow within the vessel. Measurement error becomes large when θ is not close to zero, in other words, when blood flow is not coming *directly* toward or away from the transducer. For this reason, ratios are often used to compare different waveform components, allowing cosine θ to cancel out of the equation. Figure 10-51 is a schematic of the Doppler waveform and describes the three ratios commonly used. The simplest is the *systolic-diastolic ratio (S/D ratio),* which compares the maximal (or peak) systolic flow with end-diastolic flow to evaluate downstream impedance to flow. Currently, two types of Doppler modalities are available for clinical use.

FIGURE 10-51

Doppler systolic–diastolic waveform indices of blood flow velocity. S represents the peak systolic flow or velocity, and D indicates the end-diastolic flow or velocity. The mean, which is the time-average mean velocity, is calculated from computer-digitized waveforms.

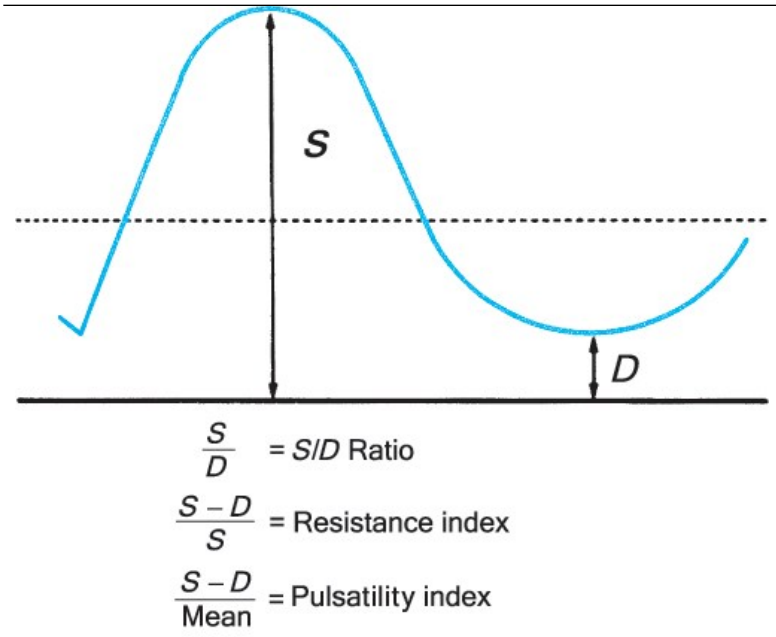

Source: F. Gary Cunningham, Kenneth J. Leveno, Steven L. Bloom, Catherine Y. Spong, Jodi S. Dashe, Barbara L. Hoffman, Brian M. Casey, Jeanne S. Sheffield: *Williams Obstetrics*, 25th Edition

Continuous-wave Doppler equipment has two separate types of crystals—one transmits high-frequency sound waves, and another continuously captures signals. In M-mode imaging, continuous-wave Doppler is used to evaluate motion through time, however, it cannot image individual vessels.

Pulsed-wave Doppler uses only one crystal, which transmits the signal and then waits until the returning signal is received before transmitting another one. It allows precise targeting and visualization of the vessel of interest. Pulsed-wave Doppler can be configured to allow color-flow mapping—such that blood flowing toward the transducer is displayed in red and that flowing away from the transducer appears in blue. Various combinations of pulsed-wave Doppler, color-flow Doppler, and real-time sonography are commercially available.

Umbilical Artery

Umbilical artery Doppler has been subjected to more rigorous assessment than any previous test of fetal health. The umbilical artery differs from other vessels in that it normally has forward flow throughout the cardiac cycle. Moreover, the amount of flow during diastole increases as gestation advances, and this reflects decreasing placental impedance. *As a result, the S/D ratio normally declines from approximately 4.0 at 20 weeks' gestation, to generally less than 3.0 after 30 weeks' and finally to 2.0 at term.* Because of downstream impedance to flow, *more* end-diastolic flow is observed at the placental cord insertion than at the fetal ventral wall. Thus, abnormalities such as absent or reversed end-diastolic flow will appear first at the fetal cord insertion site. The International Society of Ultrasound in Obstetrics and Gynecology recommends that umbilical artery Doppler measurements be made in a free loop of cord (Bhide, 2013). However, assessment close to the ventral wall insertion may optimize measurement reproducibility when flow is diminished (Berkley, 2012).

The waveform is considered abnormal if the S/D ratio is >95th percentile for gestational age. In extreme cases of growth restriction, end-diastolic flow can become absent or even reversed (Fig. 44-8). Such reversal of end-diastolic flow has been associated with greater than 70-percent obliteration of the small muscular arteries in placental tertiary stem villi (Kingdom, 1997; Morrow, 1989).

As described in Chapter 44 (Prevention), umbilical artery Doppler aids management of fetal-growth restriction and has been associated with improved outcome in these cases (American College of Obstetricians and Gynecologists, 2015). It is not recommended for complications other than growth restriction. Similarly, its use for growth-restriction screening is not advised (Berkley, 2012). Abnormal umbilical artery Doppler findings should prompt a complete fetal evaluation, if not already done, because abnormal measurements are associated with major fetal anomalies and aneuploidy (Wenstrom, 1991).

Ductus Arteriosus

Doppler evaluation of the ductus arteriosus has been used primarily to monitor fetuses exposed to indomethacin and other nonsteroidal antiinflammatory agents (NSAIDs). Indomethacin, which is used by some for tocolysis, may cause ductal constriction or closure, particularly when used in the third trimester (Huhta, 1987). The resulting increased pulmonary flow can cause reactive hypertrophy of the pulmonary arterioles and eventual development of pulmonary hypertension. In a review of 12 randomized controlled trials involving more than 200 exposed pregnancies, Koren and coworkers (2006) reported that NSAIDs raised the odds of ductal constriction 15-fold. When these agents are indicated, their duration is typically limited to less than 72 hours. And, women taking NSAIDs are closely monitored so that these can be discontinued if ductal constriction is identified. Fortunately, ductal constriction is often reversible after NSAID discontinuation.

Uterine Artery

Uterine blood flow is estimated to rise from 50 mL/min early in gestation to 500 to 750 mL/min by term. The uterine artery Doppler waveform is characterized by high diastolic flow velocities and markedly turbulent flow. Greater resistance to flow and development of a *diastolic notch* are associated with later development of gestational hypertension, preeclampsia, and fetal-growth restriction. Zeeman and coworkers (2003) also found that women with chronic hypertension who had elevated uterine artery impedance at 16 to 20 weeks' gestation were at greater risk to develop superimposed preeclampsia. However, the technique, best testing interval, and defining criteria for this indication have not been standardized. As the predictive value of uterine artery Doppler testing is considered to be low, its use for screening or for clinical decision-making is not recommended in either high-risk or low-risk pregnancies (Sciscione, 2009).

Middle Cerebral Artery

Doppler interrogation of the middle cerebral artery (MCA) has been investigated and applied clinically for fetal anemia detection and fetal-growth restriction evaluation. Anatomically, the path of the MCA is such that flow often approaches the transducer "head-on," allowing for accurate determination of flow velocity (Fig. 10-52). The MCA is imaged in an axial view of the head at the base of the skull, ideally within 2 mm of the internal carotid artery origin. Velocity measurement is optimal when the insonating angle is close to zero, and no more than 30 degrees of angle correction should be used. In general, velocity assessment is not performed in other fetal vessels, because a larger insonating angle is needed and confers significant measurement error.

FIGURE 10-52

Middle cerebral artery (MCA) Doppler. **A.** Color Doppler of the circle of Willis, demonstrating the correct location to sample the MCA. **B.** The waveform demonstrates a peak systolic velocity exceeding 70 cm/sec in a 32-week fetus with severe fetal anemia secondary to Rh alloimmunization.

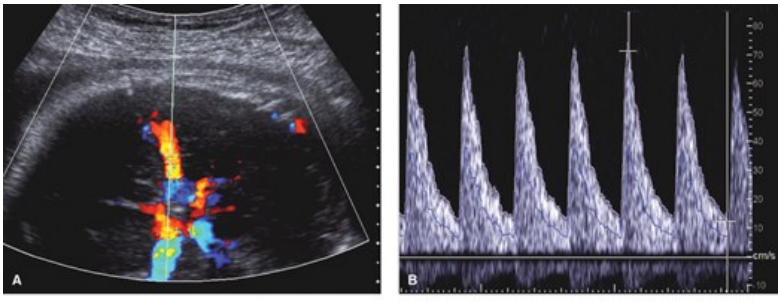

When fetal anemia is present, the *peak systolic velocity* is enhanced due to greater cardiac output and decreased blood viscosity (Segata, 2004). This has permitted the reliable, noninvasive detection of fetal anemia in cases of blood-group alloimmunization. Mari and colleagues (2000) demonstrated that an MCA peak systolic velocity threshold of 1.50 MoM could reliably identify fetuses with moderate or severe anemia. As discussed in Chapter 15 (Management of the Alloimmunized Pregnancy), MCA peak systolic velocity has replaced invasive testing with amniocentesis as the preferred test for fetal anemia detection (Society for Maternal-Fetal Medicine, 2015).

MCA Doppler has also been studied as an adjunct in evaluation of fetal-growth restriction. Fetal hypoxemia is believed to result in increased blood flow to the brain, heart, and adrenal glands, leading to greater end-diastolic flow in the MCA. This phenomenon, "brain-sparing," is actually a misnomer, as it is not protective for the fetus but rather is associated with perinatal morbidity and mortality (Bahado-Singh, 1999; Cruz-Martinez, 2011). The utility of MCA Doppler to aid the timing of delivery is uncertain. It has *not* been evaluated in randomized trials or adopted as standard practice in the

management of growth restriction (American College of Obstetricians and Gynecologists, 2015; Berkley, 2012).

Ductus Venosus

The ductus venosus is imaged as it branches from the umbilical vein at approximately the level of the diaphragm. Fetal position poses more of a challenge in imaging the ductus venosus than it does with either the umbilical artery or the middle cerebral artery. The waveform is biphasic and normally has forward flow throughout the cardiac cycle. The first peak reflects ventricular systole, and the second is ventricular diastolic filling. These are followed by a nadir during atrial contraction—termed the *a-wave*.

It is believed that Doppler findings in preterm fetuses with growth restriction show a progression in which umbilical artery Doppler abnormalities are followed by ones in the middle cerebral artery and then in the ductus venosus. However, manifestations of these abnormalities vary widely (Berkley, 2012). With severe fetal-growth restriction, cardiac dysfunction may lead to flow in the a-wave that is decreased, absent, and eventually reversed, along with pulsatile flow in the umbilical vein (Fig. 10-53).

FIGURE 10-53

Venous Doppler abnormalities. **A.** Reversal of a-wave flow in the ductus venosus. Arrows depict a-waves below the baseline. This finding may be identified with cardiac dysfunction in the setting of severe fetal-growth restriction. **B.** Pulsatile flow in the umbilical vein. The undulating umbilical venous waveform below the baseline indicates tricuspid regurgitation. Above the baseline is the umbilical artery waveform, in which there is no visible end-diastolic flow. Because the venous waveform is below the baseline in this image, it is not possible to determine whether the umbilical artery end-diastolic flow is reversed.

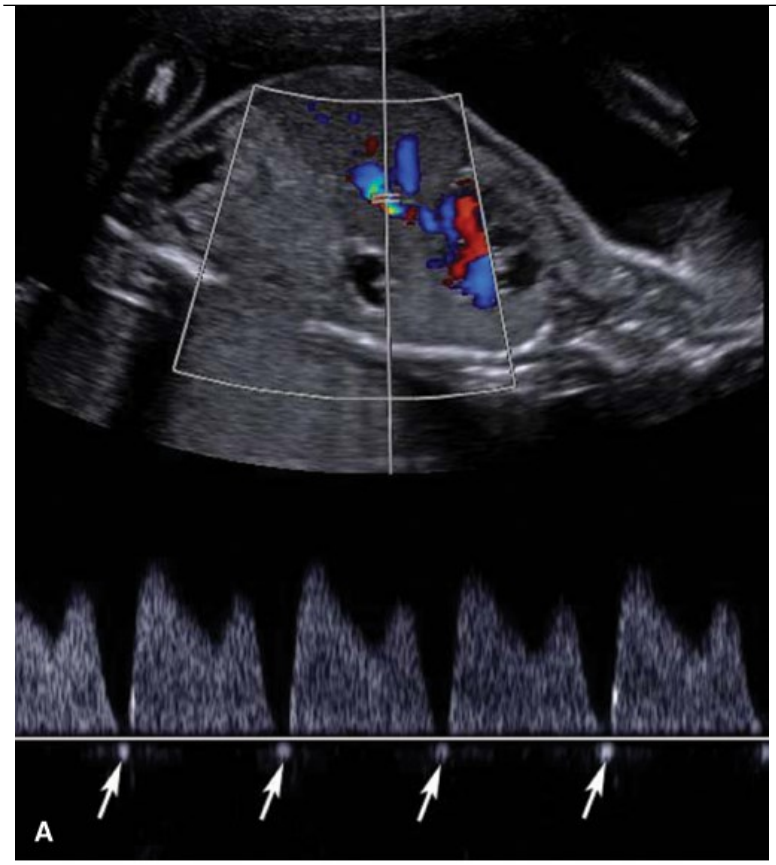

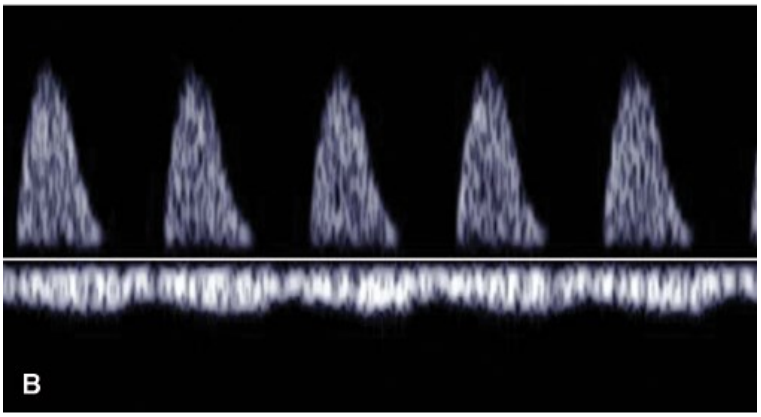

Source: F. Gary Cunningham, Kenneth J. Leveno, Steven L. Bloom, Catherine Y. Spong, Jodi S. Dashe, Barbara L. Hoffman, Brian M. Casey, Jeanne S. Sheffield: *Williams Obstetrics*, 25th Edition

Ductus venosus abnormalities have potential to identify preterm growth-restricted fetuses that are at greatest risk for adverse outcomes (Baschat, 2003, 2004; Bilardo, 2004; Figueras, 2009). As noted by the Society for Maternal-Fetal Medicine, however, they have not been sufficiently evaluated in randomized trials (Berkley, 2012). In sum, Doppler assessment of vessels other than the umbilical artery has not been shown to improve perinatal outcome, and thus their role in clinical practice remains uncertain (American College of Obstetricians and Gynecologists, 2015).

MAGNETIC RESONANCE IMAGING

Image resolution with MR is often superior to that with sonography because it is not as hindered by bony interfaces, maternal obesity, oligohydramnios, or an engaged fetal head. Thus, it can serve as an adjunct to sonography in evaluating suspected fetal abnormalities. Examples include complex abnormalities of the fetal CNS, thorax, gastrointestinal system, genitourinary system, and musculoskeletal system. MR has also been used in the evaluation of maternal pelvic masses and placental invasion. MR imaging, however, is not portable, it is time-consuming, and its use is

generally limited to referral centers with expertise in fetal imaging.

To guide clinical use, the American College of Radiology and Society for Pediatric Radiology (2015) have developed a practice guideline for fetal MR imaging. This document acknowledges primacy of sonography as the preferred screening modality. Moreover, it recommends that fetal MR imaging be used for problem solving to ideally contribute to prenatal diagnosis, counseling, treatment, and delivery planning. Specific indications for fetal MR imaging are listed in Table 10-11 and are discussed subsequently.

TABLE 10-11

Fetal Conditions for Which Magnetic Resonance Imaging May Be Indicated[a]

Brain and spine
Ventriculomegaly
Agenesis of the corpus callosum
Cavum septum pellucidum abnormalities
Holoprosencephaly
Posterior fossa abnormalities
Cerebral cortical malformation or migrational abnormalities
Cephalocele
Solid or cystic masses
Vascular malformations
Hydranencephaly
Infarctions
Hemorrhage
Monochorionic twin pregnancy complications
Neural-tube defects
Sacrococcygeal teratoma
Sacral agenesis (caudal regression)
Sirenomelia
Vertebral anomalies
Family history conferring a risk for brain anomaly
Skull, face, and neck
Venolymphatic malformations
Hemangiomas
Goiter
Teratomas
Facial clefts
Other abnormalities with potential airway obstruction
Thorax
Congenital cystic adenomatoid malformation
Extralobar pulmonary sequestration
Bronchogenic cyst or congenital lobar overinflation
Diaphragmatic hernia
Effusions
Mediastinal masses
Assessment for esophageal atresia
Evaluation of pulmonary hypoplasia secondary to diaphragmatic hernia, oligohydramnios, chest mass, or skeletal dysplasia

Abdomen, pelvis, and retroperitoneum
Abdominopelvic cystic mass evaluation
Tumor evaluation (sacrococcygeal teratoma, neuroblastoma, hemangioma, suprarenal or renal masses)
Complex genitourinary anomalies (bladder outlet obstruction syndromes, bladder exstrophy, cloacal exstrophy)
Assess renal anomalies with oligohydramnios
Diagnose bowel anomalies (anorectal malformations, complex obstructions)
Complications of monochorionic twins
Determine vascular anatomy prior to laser treatment
Assess morbidity after death of a monochorionic co-twin
Evaluate conjoined twins
Fetal surgery assessment
Fetal brain anatomy before and after surgical intervention
Anomalies for which fetal surgery is planned

[a]In some cases, magnetic resonance (MR) imaging is indicated only if the anomaly is suspected but cannot be adequately characterized sonographically, which is assessed on a case-by-case basis.

Data from American College of Radiology, 2015.

Safety

MR imaging uses no ionizing radiation, but theoretical concerns include the effects of fluctuating electromagnetic fields and high sound-intensity levels. The strength of the magnetic field is measured in *tesla (T),* and most imaging studies during pregnancy are performed using 1.5 T. A few preliminary studies advocate the use of 3 T for fetal imaging to potentially improve signal-to-noise ratios and thus image clarity (Victoria, 2016). For safety, all clinical examinations must adhere to the specific absorption rate, which is regulated by the Food and Drug Administration, and the ALARA principle should be followed. Thus, for routine clinical examinations, the lower field strength of 1.5 T is recommended (Prayer, 2017).

Human and tissue studies support the safety of fetal MR imaging. Repetitive exposure of human lung fibroblasts to a static 1.5-T magnetic field does not affect cellular proliferation (Wiskirchen, 1999). Fetal heart rate patterns have been evaluated before and during MR imaging, and no significant differences were observed (Vadeyar, 2000). Children exposed to MR as fetuses do not show a greater incidence of disease or disability when tested at age 9 months or 3 years (Baker, 1994; Clements, 2000).

Glover and associates (1995) attempted to mimic the sound level experienced by the fetal ear by having an adult volunteer swallow a microphone while the stomach was filled with a liter of fluid to represent the amnionic sac. Sound intensity was attenuated at least 30-dB from the body surface to the fluid-filled stomach and reduced the sound pressure from 120 dB to below 90 dB. This level is considerably less than the 135 dB experienced from vibroacoustic stimulation used in antepartum well-being assessments (Chap. 17, Acoustic Stimulation Tests). Cochlear function testing in infants exposed to 1.5-T MR imaging as fetuses showed no hearing impairment (Reeves, 2010).

The American College of Radiology (2013) concludes that based on available evidence, MR imaging has no documented deleterious effects on the developing fetus. Therefore, MR imaging can be performed in pregnancy if data are needed to care for the fetus or mother. Health-care providers who are pregnant may work in and around an MR unit, but it is recommended that they not remain in the MR scanner magnet room—known as Zone IV—while an examination is in progress.

Gadolinium-based MR contrast agents are gadolinium (Gd^{3+}) chelates. These contrast agents readily enter the fetal circulation and are excreted via fetal urination into amnionic fluid, where they may remain for an indeterminate period before being ingested and reabsorbed. The longer the gadolinium-chelate molecule remains in a protected space such as the amnionic sac, the greater the potential for dissociation of the toxic Gd^{3+} ion. Accordingly, gadolinium contrast should be avoided during pregnancy because of this potential for dissociation. Routine use of gadolinium is not recommended unless there are overwhelming potential benefits (American College of Radiology, 2013). In adults with renal disease, this contrast agent

has been associated with development of nephrogenic systemic fibrosis, a potentially severe complication.

Technique

Before MR examination, all women complete a written safety questionnaire that includes information about metallic implants, pacemakers, or other metal- or iron-containing devices that may alter the study (American College of Radiology, 2013). Iron supplementation may cause artifact in the colon but does not usually affect the resolution of fetal images. In more than 4000 MR procedures performed at Parkland Hospital in pregnancy during the past 15 years, maternal anxiety secondary to claustrophobia and/or fear of MR equipment has developed in less than 1 percent of our patients. To reduce maternal anxiety in this small group, a single oral dose of diazepam, 5 to 10 mg, or lorazepam, 1 to 2 mg, may be given.

To begin an MR examination, women are placed in a supine or left lateral decubitus position. A torso coil is used in most circumstances to send and receive the radiofrequency pulses, but a body coil can be used alone to accommodate large maternal habitus. A series of three-plane localizers, or scout views, are obtained relative to the maternal coronal, sagittal, and axial planes. The gravid uterus is imaged in the maternal axial plane (7-mm slices, 0 gap) with a T2-weighted fast acquisition. Typically, these may be a single-shot fast spin echo sequence (SSFSE), half-Fourier acquisition single-shot turbo spin echo (HASTE), or rapid acquisition with relaxation enhancement (RARE), depending on the brand of machine. Next, a fast T1-weighted acquisition such as spoiled gradient echo (SPGR) is performed (7-mm thickness, 0 gap). These large-field-of-view acquisitions through the maternal abdomen and pelvis are particularly good for identifying fetal and maternal anatomy.

Orthogonal images of targeted fetal or maternal structures are then obtained. In these cases, 3- to 5-mm slice thickness, 0 gap T2-weighted acquisitions are performed in the coronal, sagittal, and axial planes. Depending on the anatomy and underlying suspected abnormality, T1-weighted images can be performed to evaluate for subacute hemorrhage, fat, or location of normal structures that appear bright on these sequences, such as liver and meconium in the colon (Brugger, 2006; Zaretsky, 2003b).

Short T1 inversion recovery (STIR) and frequency-selective fat-saturated T2-weighted images may provide differentiation in cases in which the water content of the abnormality is similar to that of the normal structure. An example is a thoracic mass compared with normal lung. Diffusion-weighted imaging may be employed to evaluate for restricted diffusion, which can be seen in ischemia, cellular tumors, or clotted blood (Brugger, 2006; Zaretsky, 2003b). Our series also includes an axial brain 3- to 5-mm T2-weighted sequence to obtain head biometry for gestational age estimation using the biparietal diameter and head circumference (Reichel, 2003).

Fetal Anatomical Evaluation

Whenever a fetal abnormality is identified, findings from the affected organ and other organ systems should be thoroughly characterized. Accordingly, a fetal anatomical survey is generally completed during each MR examination. In a recent prospective study, nearly 95 percent of the anatomical components recommended by the International Society of Ultrasound in Obstetrics and Gynecology were visible at 30 weeks' gestation (Millischer, 2013). The aorta and pulmonary artery were the most difficult to evaluate. Zaretsky and coworkers (2003a) similarly found that with the exclusion of cardiac structures, fetal anatomical evaluation was possible in 99 percent of cases.

Central Nervous System

For intracranial anomalies, very fast T2-weighted images produce excellent tissue contrast, and CSF-containing structures are hyperintense or bright. This allows exquisite detail of the posterior fossa, midline structures, and cerebral cortex. T1-weighted images are used to identify hemorrhage.

CNS biometry obtained with MR imaging is comparable with that obtained using sonography (Twickler, 2002). Nomograms have been published for multiple intracranial structures, including corpus callosum and cerebellar vermis lengths (Garel, 2004; Tilea, 2009).

MR imaging provides valuable added information for cerebral abnormalities suspected sonographically (Benacerraf, 2007; Li, 2012). In early studies, MR imaging changed the diagnosis in 40 to 50 percent of cases and affected management in 15 to 50 percent (Levine, 1999b; Simon, 2000; Twickler, 2003). Additional information is more likely to be gained when the examination is performed beyond 24 weeks' gestation. More recently, Griffiths and associates (2017) reported that MR evaluation of suspected fetal brain anomalies identified additional findings in nearly 50 percent and changed prognosis in 20 percent.

Fetuses with a cerebral abnormality may have a significant lag in cortical development. Levine and colleagues (1999a) demonstrated that MR imaging

accurately portrays cerebral gyration and sulcation patterns (Fig. 10-54). Sonography permits limited evaluation of subtle migrational abnormalities, and MR imaging provides greater accuracy, particularly later in gestation.

FIGURE 10-54

Axial images of the fetal brain at 23 weeks' gestation **(A)** and at 33 weeks **(B)** demonstrate the normal gyration and sulcation progression during fetal development. These images were obtained using a Half Fourier Acquisition Single Shot Turbo Spin Echo (HASTE) sequence because it is relatively motion insensitive.

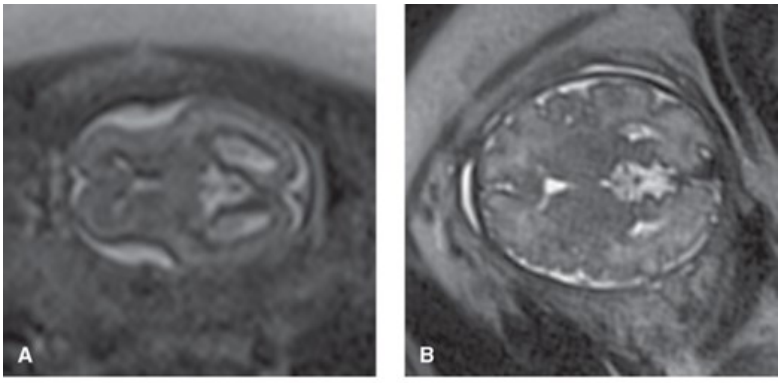

For ventriculomegaly, fetal MR imaging is selected to help identify associated underlying CNS dysmorphology (Ventriculomegaly). In cases of septo-optic dysplasia, MR imaging may confirm absence of the septum pellucidum and display hypoplastic optic tracts (Fig. 10-55). In other fetuses, MR imaging can also assist with identifying agenesis or dysgenesis of the corpus callosum and characterizing migrational abnormalities (Benacerraf, 2007; Li, 2012; Twickler, 2003).

FIGURE 10-55

Septo-optic dysplasia. Axial **(A)** and coronal **(B)** images at 30 weeks' gestation confirm absence of the cavum septum pellucidum (*arrowheads*) in both. There is also associated mild ventriculomegaly (*arrow*).

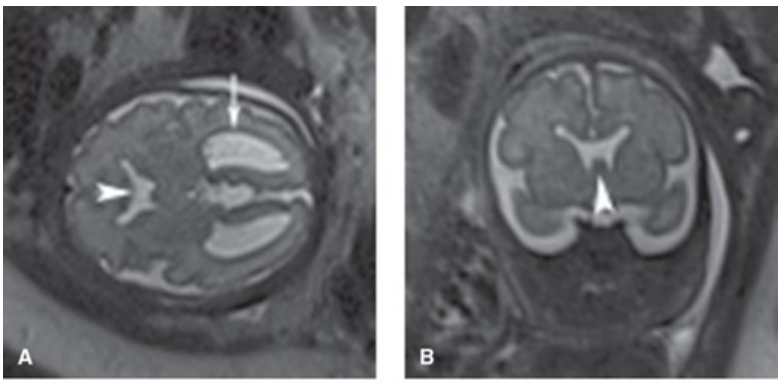

Another fetal MR imaging indication is evaluation of suspected intraventricular hemorrhage (IVH). Fetal IVH risk factors include atypical-appearing ventriculomegaly, neonatal alloimmune thrombocytopenia, and a monochorionic multifetal gestation complicated by demise of one fetus or by severe twin-twin transfusion syndrome (Hu, 2006). If hemorrhage is seen, MR imaging characteristics may indicate which structures are involved and approximately when bleeding occurred. In the setting of congenital fetal infections, MR imaging can delineate the variable degrees of neural parenchymal abnormality and subsequent maldevelopment (Soares de Oliveira-Szejnfeld, 2016).

Aside from cerebral structure, suspected spinal dysraphisms, including neural-tube defects, can also be further characterized for surgical planning. Figure 10-56 demonstrates a complex skin-covered dysraphism with associated tethering of the spinal cord. This terminal myelocystocele will benefit

from early intervention following delivery.

FIGURE 10-56

Terminal myelocystocele, 36 weeks' gestation. **A.** In this sagittal T2-weighted image, the spinal cord is tethered, expanding into the terminal cyst (*arrow*). **B.** Seen in this T1-weighted image, the meningocele and terminal cyst are covered by subcutaneous fat (*arrows*) and skin.

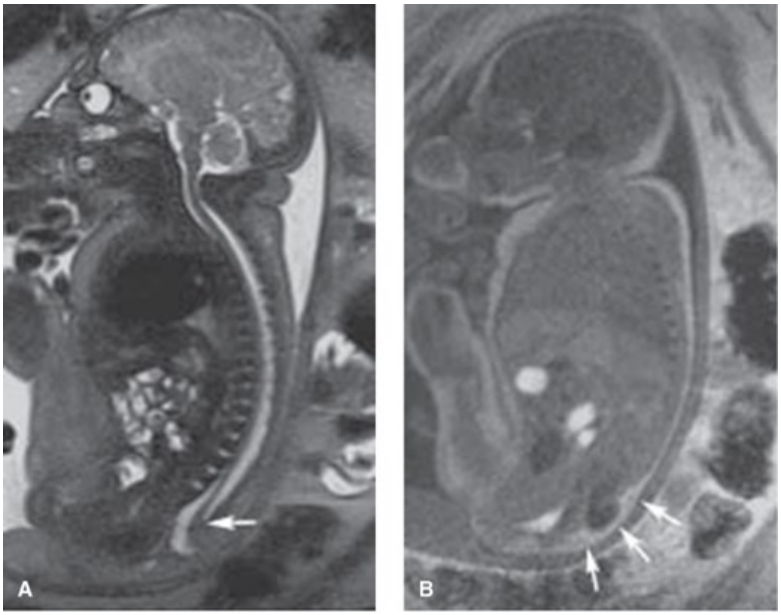

Thorax

Many thoracic abnormalities are readily seen with targeted sonography. MR imaging, however, may help delineate the location and size of space-occupying thoracic lesions and quantify remaining lung tissue volumes. MR imaging can aid in characterizing the type of congenital cystic adenomatoid malformation and in visualizing the blood supply of pulmonary sequestration (Heart). With congenital diaphragmatic hernia, MR imaging can help verify and quantify the abdominal organs within the thorax. This includes the volume of herniated liver and compressed lung tissue volumes (Fig. 10-57) (Debus, 2013; Lee, 2011; Mehollin-Ray, 2012). Also in fetuses with diaphragmatic hernia, MR imaging can assist in identifying other organ-system abnormalities, which may greatly affect fetal prognosis (Kul, 2012). MR imaging similarly is used for chest evaluation in skeletal dysplasia and to measure lung volumes in pregnancies with prolonged oligohydramnios secondary to renal disease or ruptured membranes (Messerschmidt, 2011; Zaretsky, 2005).

FIGURE 10-57

A. Coronal image of normal lungs on a balanced sequence at 29 weeks' gestation. The liver (*L*) and stomach (*S*) lie below the diaphragm. **B.** Left-sided congenital diaphragmatic hernia (CDH) (*dotted ellipse*) seen on balanced sequence at 33 weeks. **C.** The T1-weighted sequence confirms the subdiaphragmatic position of the liver and better delineates the small bowel (*arrow*) and meconium-containing colon (*arrowhead*) that have herniated into the chest. **D.** Another image of a left-sided CDH at 22 weeks demonstrates no normal lung, the heart (*H*) displaced into the right chest, and an elevated liver (*dotted ellipse*).

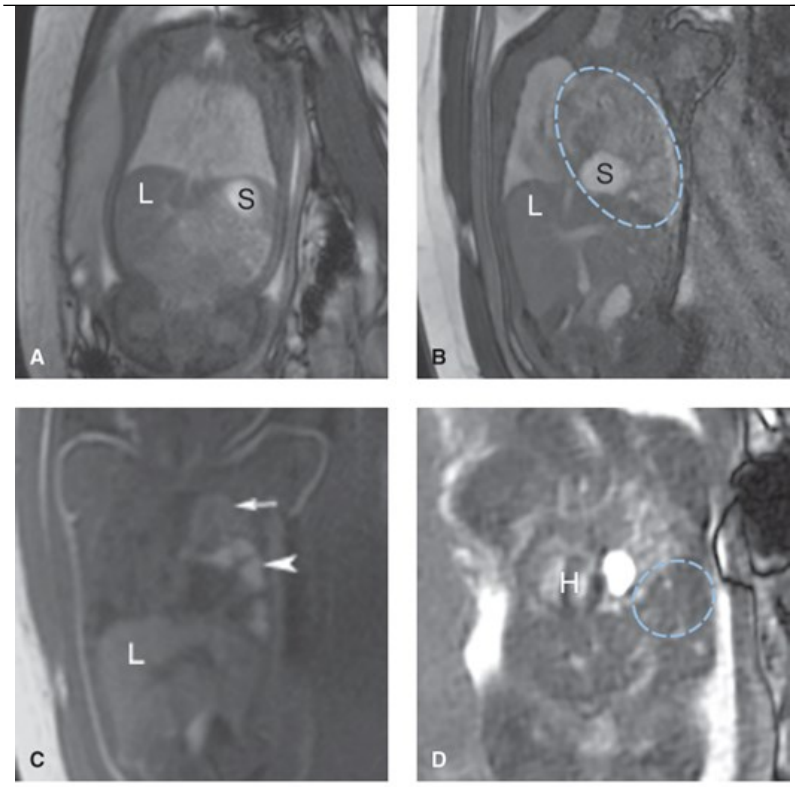

Source: F. Gary Cunningham, Kenneth J. Leveno, Steven L. Bloom, Catherine Y. Spong, Jodi S. Dashe, Barbara L. Hoffman, Brian M. Casey, Jeanne S. Sheffield: *Williams Obstetrics*, 25th Edition

Abdomen

When sonographic viewing of fetal abdominal abnormalities is limited by oligohydramnios or maternal obesity, MR imaging may add value (Caire, 2003). Hawkins and coworkers (2008) found that lack of signal in a contracted fetal bladder on T2-weighted sequences was associated with lethal renal abnormalities (Fig. 10-58). Differences in signal characteristics between meconium in the fetal colon and urine in the bladder may permit definition of cystic abdominal abnormalities (Farhataziz, 2005). Given the predictable pattern of meconium accumulation within the gastrointestinal tract and high signal intensity on T1-weighted sequences, MR imaging is a complementary tool in diagnosing gastrointestinal abnormalities and complex cloacal malformations (Furey, 2016). Peritoneal calcifications related to meconium peritonitis are more readily apparent sonographically, whereas pseudocysts and resultant abnormalities of meconium migration are better delineated with MR imaging.

FIGURE 10-58

A. Sagittal short T1 inversion recovery (STIR) image through a fetus with posterior urethral valve at 23 weeks' gestation. Notice the characteristic dilation of the posterior urethra (*arrowhead*). **B.** At 31 weeks, a coronal image shows progression of severe hydronephrosis, cystic changes in the parenchyma, hydroureter, and anhydramnios. The lungs (*L*) show a decreased signal and are small. **C.** An axial balanced sequence shows a distended bladder (*B*) with thickened wall (*arrows*).

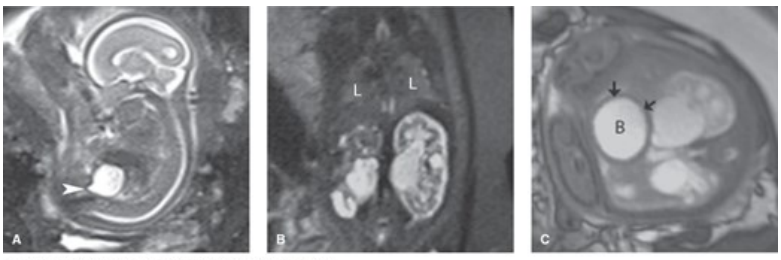

Adjunct to Fetal Therapy

As indications for fetal therapy have grown, MR imaging is used preoperatively to outline abnormalities. At some centers, before laser ablation of placental anastomoses for twin-twin transfusion syndrome, MR imaging is performed to assess the fetal brain for IVH or periventricular leukomalacia (Chap. 45, Twin-Twin Transfusion Syndrome) (Hu, 2006; Kline-Fath, 2007). Because of its precision in visualizing brain and spine findings in cases of myelomeningocele, it is often used preoperatively. For sacrococcygeal teratomas, if fetal surgery is considered, MR imaging may identify tumor extension into the fetal pelvis (Avni, 2002; Neubert, 2004; Perrone, 2017). With a fetal neck mass for which an EXIT is considered, MR imaging may help delineate the lesion extent and its effect on the oral cavity, hypopharynx, and trachea (Hirose, 2003; Lazar, 2012; Ogamo, 2005; Shiraishi, 2000). Finally, MR imaging can also calculate a jaw index when an EXIT procedure may be needed for severe micrognathia (MacArthur, 2012; Morris, 2009). Fetal therapy is discussed in Chapter 16 (Ex-Utero Intrapartum Treatment).

Placenta

The clinical importance of identifying women with placenta accreta is discussed in Chapter 41 (Morbidly Adherent Placenta). Sonography is generally used to identify placental invasion into the myometrium, however, MR evaluation is an adjunct for indeterminate cases. Findings concerning for invasion include dark intraplacental bands on T2-weighted images, focal bulging, and placental heterogeneity (Leyendecker, 2012). When used in a complementary role, MR imaging sensitivity is high for detection of placental invasion, although the depth of invasion is difficult to predict. Clinical risk factors and sonographic findings should be taken into account when interpreting MR placental images.

Emerging Concepts

Of these, MR diffusion tensor imaging and tractography may allow further understanding of neural development and more precise definition of abnormality and pathology (Kasprian, 2008; Mitter, 2015). Automatic and semiautomated extraction of quantitative data from MR imaging volumetric acquisitions of fetal brain and placenta may enable subanalyses of massive datasets not previously possible with laborious manual segmentation (Tourbier, 2017; Wang, 2016). Using multiparametric MR of the placenta in vivo will expand our understanding of function and pathology without risk to mother or fetus. Last, although echocardiography will always be paramount in fetal heart assessment, MR imaging may contribute to volumetric cardiac analysis and will further evaluation of the aorta, which is often difficult to completely examine sonographically (Lloyd, 2017).

REFERENCES

Adzick NS, Harrison MR, Glick PL, et al: Fetal cystic adenomatoid malformation: prenatal diagnosis and natural history. J Pediatr Surg 20:483, 1985

Al-Kaff A, MacDonald SC, Kent N, et al: Delivery planning for pregnancies with gastroschisis: findings from a prospective national registry. Am J Obstet Gynecol 213(4):557.e1, 2015

Altman RP, Randolph JG, Lilly JR: Sacrococcygeal teratoma: American Academy of Pediatrics Surgical Section survey—1973. J Pediatr Surg 9:389, 1974

American College of Obstetricians and Gynecologists: Fetal growth restriction. Practice Bulletin No. 134, May 2013, Reaffirmed 2015

American College of Obstetricians and Gynecologists: Ultrasound in pregnancy. Practice Bulletin No. 175, December 2016

American College of Obstetricians and Gynecologists: Management of suboptimally dated pregnancies. Committee Opinion No. 688, March 2017a

American College of Obstetricians and Gynecologists: Methods for estimating the due date. Committee Opinion No. 700, May 2017b

American College of Radiology: Expert Panel on MR Safety: ACR guidance document on MR safe practices. J Magn Reson Imaging 37:501, 2013

American College of Radiology and Society for Pediatric Radiology: ACR-SPR practice guideline for the safe and optimal performance of fetal magnetic resonance imaging. Resolution No. 11, 2015. Available at: https://www.acr.org/-/media/ACR/Files/Practice-Parameters/mr-fetal.pdf. Accessed July 10, 2017

American Institute of Ultrasound in Medicine (AIUM): Official statements. Prudent use in pregnancy. 2012. Available at: http://www.aium.org/officialStatements/33. Accessed July 10, 2017

American Institute of Ultrasound in Medicine (AIUM): Official statements. Statement on the safe use of Doppler ultrasound during 11–14 weeks scans (or earlier in pregnancy). 2016. Available at: http://www.aium.org/officialStatements/42. Accessed September 16, 2017

American Institute of Ultrasound in Medicine (AIUM): Practice guideline for the performance of fetal echocardiography. J Ultrasound Med 32(6):1067, 2013a

American Institute of Ultrasound in Medicine (AIUM): Practice guideline for the performance of obstetric ultrasound examinations. J Ultrasound Med 32(6):1083, 2013b

Avni FE, Guibaus L, Robert Y, et al: MR imaging of fetal sacrococcygeal teratoma: diagnosis and assessment. AJR Am J Roentgenol 178(1):179, 2002

Axt-Fliedner R, Schwarze A, Smrcek J, et al: Isolated ventricular septal defects dated by color Doppler imaging: evolution during fetal and first year of postnatal life. Ultrasound Obstet Gynecol 27:266, 2006

Azizkhan RG, Crombleholme TM: Congenital cystic lung disease: contemporary antenatal and postnatal management. Pediatric Surg Int 24:643, 2008

Bahado-Singh RO, Kovanci E, Jeffres A, et al: The Doppler cerebroplacental ratio and perinatal outcome in intrauterine growth restriction. Am J Obstet Gynecol 180(3):750, 1999

Baker PN, Johnson IR, Harvey PR, et al: A three-year follow-up of children imaged in utero with echo-planar magnetic resonance. Am J Obstet Gynecol 170:32, 1994

Baschat AA: Doppler application in the delivery timing of the preterm growth-restricted fetus: another step in the right direction. Ultrasound Obstet Gynecol 23:111, 2004

Baschat AA: Relationship between placental blood flow resistance and precordial venous Doppler indices. Ultrasound Obstet Gynecol 22:561, 2003

Benacerraf BR, Shipp TD, Bromley B, et al: What does magnetic resonance imaging add to the prenatal sonographic diagnosis of ventriculomegaly? J Ultrasound Med 26:1513, 2007

Berkley E, Chauhan SP, Abuhamad A: Society for Maternal-Fetal Medicine Clinical Guideline: Doppler assessment of the fetus with intrauterine growth restriction. Am J Obstet Gynecol 206(4):300, 2012

Best KE, Tennant PWG, Addor M, et al: Epidemiology of small intestinal atresia in Europe: a register-based study. Arch Dis Child Fetal Neonatal Ed 97(5):F353, 2012

Bhide A, Acharya G, Bilardo CM, et al: ISUOG Practice Guidelines: use of Doppler ultrasonography in obstetrics. Ultrasound Obstet Gynecol 41(2):233, 2013

Bilardo CM, Wolf H, Stigter RH, et al: Relationship between monitoring parameters and perinatal outcome in severe, early intrauterine growth restriction. Ultrasound Obstet Gynecol 23:119, 2004

Bonafe L, Cormier-Daire V, Hall C, et al: Nosology and classification of genetic skeletal disorders: 2015 revision. Am J Med Genet 167A(12):2869, 2015

Bromley B, Shipp TD, Lyons J, et al: Detection of fetal structural anomalies in a basic first-trimester screening program for aneuploidy. J Ultrasound Med 33(10):1737, 2014

Bronshtein M, Ornoy A: Acrania: anencephaly resulting from secondary degeneration of a closed neural tube: two cases in the same family. J Clin Ultrasound 19(4):230, 1991

Brugger PC, Stuhr F, Lindner C, et al: Methods of fetal MR: beyond T2-weighted imaging. Euro J Radiol 57(2):172, 2006

Burge D, Wheeler R: Increasing incidence of detection of congenital lung lesions. Pediatr Pulmonol 45(1):103, 2010

Caire JT, Ramus RM, Magee KP, et al: MRI of fetal genitourinary anomalies. AJR Am J Roentgenol 181:1381, 2003

Canfield MA, Honein MA, Yuskiv N, et al: National estimates and race/ethnic-specific variation of selected birth defects in the United States, 1999–2001. Birth Defects Res A Clin Mol Teratol 76(11):747, 2006

Carey M, Bower C, Mylvaganam A, et al: Talipes equinovarus in Western Australia. Paediatr Perinat Epidemiol 17:187, 2003

Cavoretto P, Molina F, Poggi S, et al: Prenatal diagnosis and outcome of echogenic fetal lung lesions. Ultrasound Obstet Gynecol 32:769, 2008

Centers for Disease Control and Prevention: Workplace solutions. Preventing work-related musculoskeletal disorders in sonography. DHHS (NIOSH) Publication No. 2006–148, 2006

Chitty LS, Altman DG: Charts of fetal size: kidney and renal pelvis measurements. Prenat Diagn 23:891, 2003

Christensen N, Andersen H, Garne E, et al: Atrioventricular septal defects among infants in Europe: a population-based study of prevalence, associated anomalies, and survival. Cardiol Young 23(4):560, 2013

Clements H, Duncan KR, Fielding K, et al: Infants exposed to MRI in utero have a normal paediatric assessment at 9 months of age. B J Radiol 73(866):190, 2000

Colvin J, Bower C, Dickinson JE, et al: Outcomes of congenital diaphragmatic hernia: a population-based study in Western Australia. Pediatr 116:e356, 2005

Copel JA, Liang R, Demasio K, et al: The clinical significance of the irregular fetal heart rhythm. Am J Obstet Gynecol 182:813, 2000

Cragan JD, Gilboa SM: Including prenatal diagnoses in birth defects monitoring: experience of the Metropolitan Atlanta Congenital Defects Program. Birth Defects Res A Clin Mol Teratol 85:20, 2009

Cruz-Martinez R, Figueras F, Hernandez-Andrade E, et al: Fetal brain Doppler to predict cesarean delivery for nonreassuring fetal status in term small-for-gestational-age fetuses. Obstet Gynecol 117:618, 2011

Curran PF, Jelin EB, Rand L, et al: Prenatal steroids for microcystic congenital adenomatoid malformations. J Pediatr Surg 45:145, 2010

Dashe JS, McIntire DD, Twickler DM: Effect of maternal obesity on the ultrasound detection of anomalous fetuses. Obstet Gynecol 113(5):1001, 2009

De Biasio P, Ginocchio G, Aicardi G, et al: Ossification timing of sacral vertebrae by ultrasound in the mid-second trimester of pregnancy. Prenat Diagn 23:1056, 2003

Debus A, Hagelstein C, Kilian A, et al: Fetal lung volume in congenital diaphragmatic hernia: association of prenatal MR imaging findings with postnatal chronic lung disease. Radiology 266(3):887, 2013

Derikx JP, De Backer A, Van De Schoot L, et al: Factors associated with recurrence and metastasis in sacrococcygeal teratoma. Br J Surg 93:1543, 2006

Devaseelan P, Cardwell C, Bell B, et al: Prognosis of isolated mild to moderate fetal cerebral ventriculomegaly: a systematic review. J Perinat Med 38:401, 2010

De Veciana M, Major CA, Porto M: Prediction of an abnormal karyotype in fetuses with omphalocele. Prenat Diagn 14:487, 1994

DeVore GR, Falkensammer P, Sklansky MS, et al: Spatio-temporal image correlation (STIC): new technology for evaluation of the fetal heart. Ultrasound Obstet Gynecol 22:380, 2003

Dolk H, Loane M, Garne E: The prevalence of congenital anomalies in Europe. Adv Exp Med Biol 686:349, 2010

Duncombe GJ, Dickinson JE, Kikiros CS: Prenatal diagnosis and management of congenital cystic adenomatoid malformation of the lung. Am J Obstet Gynecol 187(4): 950, 2002

Ecker JL, Shipp TD, Bromley B, et al: The sonographic diagnosis of Dandy-Walker and Dandy-Walker variant: associated findings and outcomes. Prenat Diagn 20:328, 2000

EUROCAT: Prenatal Detection Rates. Available at: http://www.eurocat-network.eu/prenatalscreeninganddiagnosis/prenataldetection(pd)rates. Accessed July 10, 2017

Farhataziz N, Engels JE, Ramus RM, et al: Fetal MRI of urine and meconium by gestational age for the diagnosis of genitourinary and gastrointestinal abnormalities. AJR Am J Roentgenol 184:1891, 2005

Feinstein JA, Benson DW, Dubin AM, et al: Hypoplastic left heart syndrome: current considerations and expectations. J Am Coll Cardiol 59(1 Suppl):S1, 2012

Figueras F, Benavides A, Del Rio M, et al: Monitoring of fetuses with intrauterine growth restriction: longitudinal changes in ductus venosus and aortic isthmus flow. Ultrasound Obstet Gynecol 33(1):39, 2009

Food and Drug Administration: Avoid fetal “keepsake” images, heartbeat monitors. 2014. Available at: https://www.fda.gov/ForConsumers/ConsumerUpdates/ucm095508.htm. Accessed July 10, 2017

Franklin O, Burch M, Manning N, et al: Prenatal diagnosis of coarctation of the aorta improves survival and reduces morbidity. Heart 87:67, 2002

Furey EA, Bailey AA, Twickler DM: Fetal MR imaging of gastrointestinal abnormalities. Radiographics 36(3):904, 2016

Gaglioti P, Oberto M, Todros T: The significance of fetal ventriculomegaly: etiology, short-and long-term outcomes. Prenat Diagn 29(4):381, 2009

Gallot D, Boda C, Ughetto S, et al: Prenatal detection and outcome of congenital diaphragmatic hernia: a French registry-based study. Ultrasound Obstet Gynecol 29:276, 2007

Garcia M, Yeo L, Romero R, et al: Prospective evaluation of the fetal heart using Fetal Intelligent Navigation Echocardiography (FINE). Ultrasound Obstet Gynecol 47(4):450, 2016

Garel C (ed): Development of the fetal brain. In MRI of the Fetal Brain: Normal Development and Cerebral Pathologies. New York, Springer, 2004

Garne E, Loane M, Dolk H, et al: Spectrum of congenital anomalies in pregnancies with pregestational diabetes. Birth Defects Res A Clin Mol Teratol 94(3):134, 2012

Glass HC, Shaw GM, Ma C, et al: Agenesis of the corpus callosum in California 1983–2003: a population-based study. Am J Med Genet A 146A:2495, 2008

Glover P, Hykin J, Gowland P, et al: An assessment of the intrauterine sound intensity level during obstetric echo-planar magnetic resonance imaging. Br J Radiol 68:1090, 1995

Goldstein I, Reece EA, Pilu G, et al: Cerebellar measurements with ultrasonography in the evaluation of fetal growth and development. Am J Obstet Gynecol 156:1065, 1987

Goncalves LF, Lee W, Espinoza J, et al: Three- and 4-dimensional ultrasound in obstetric practice: does it help? J Ultrasound Med 24:1599, 2005

Goncalves LF, Nien JK, Espinoza J, et al: What does 2-dimensional imaging add to 3- and 4-dimensional obstetric ultrasonography? J Ultrasound Med 25:691, 2006

Griffiths PD, Bradburn M, Campbell MJ, et al: Use of MRI in the diagnosis of fetal brain abnormalities in utero (MERIDIAN): a multicenter, prospective cohort study. Lancet 389(10068):538, 2017

Gucciardo L, Uyttebroek A, de Wever I, et al: Prenatal assessment and management of sacrococcygeal teratoma. Prenat Diagn 31:678, 2011

Hains DS, Bates CM, Ingraham S, et al: Management and etiology of the unilateral multicystic dysplastic kidney: a review. Pediatr Nephrol 24:233, 2009

Hartman RJ, Rasmussen SJ, Botto LD, et al: The contribution of chromosomal abnormalities to congenital heart defects: a population-based study. Pediatr Cardiol 32:1147, 2011

Hawkins JS, Dashe JS, Twickler DM: Magnetic resonance imaging diagnosis of severe fetal renal anomalies. Am J Obstet Gynecol 198:328.e1, 2008

Hayden SA, Russ PD, Pretorius DH, et al: Posterior urethral obstruction. Prenatal sonographic findings and clinical outcome in fourteen cases. J Ultrasound Med 7:371, 1988

Hirose S, Sydorak RM, Tsao K, et al: Spectrum of intrapartum management strategies for giant fetal cervical teratoma. J Pediatr Surg 38(3):446, 2003

Hobbins JC, Robero R, Grannum P, et al: Antenatal diagnosis of renal anomalies with ultrasound: I. Obstructive uropathy. Am J Obstet Gynecol 148:868, 1984

Hoffman CK, Filly RA, Callen PW: The “lying down” adrenal sign: a sonographic indicator of renal agenesis or ectopia in fetuses and neonates. J Ultrasound Med 11:533, 1992

Howe DT, Rankin J, Draper ES: Schizencephaly prevalence, prenatal diagnosis and clues to etiology: a register-based study. Ultrasound Obstet Gynecol 39(1):75, 2012

Hu LS, Caire J, Twickler DM: MR findings of complicated multifetal gestations. Obstet Gynecol 36(1): 76, 2006

Huhta JC, Moise KJ, Fisher DJ, et al: Detection and quantitation of construction of the fetal ductus arteriosus by Doppler echocardiography. Circulation 75:406, 1987

Iams JD, Grobman WA, Lozitska A, et al: Adherence to criteria for transvaginal ultrasound imaging and measurement of cervical length. Am J Obstet Gynecol 209(4):365.e1, 2013

International Society of Ultrasound in Obstetrics and Gynecology: Sonographic examination of the fetal central nervous system: guidelines for performing the “basic examination” and the “fetal neurosonogram.” Ultrasound Obstet Gynecol 29:109, 2007

International Society of Ultrasound in Obstetrics and Gynecology: ISUOG statement on ultrasound exposure in the first trimester and autism spectrum disorders. 2016. Available at: https://www.isuog.org/uploads/assets/uploaded/89d1db1a-551c-49cf-b5754882032e47f0.pdf. Accessed July 28, 2017

Ismaili K, Hall M, Donner C, et al: Results of systematic screening for minor degrees of fetal renal pelvis dilatation in an unselected population. Am J Obstet Gynecol 188:242, 2003

James CA, Watson AR, Twining P, et al: Antenatally detected urinary tract abnormalities: changing incidence and management. Eur J Pediatr 157:508, 1998

Janga D, Akinfenwa O: Work-related repetitive strain injuries amongst practitioners of obstetric and gynecologic ultrasound worldwide. Arch Gynecol Obstet 286(2):353, 2012

Jani JC, Peralta CFA, Nicolaides KH: Lung-to-head ratio: a need to unify the technique. Ultrasound Obstet Gynecol 39:2, 2012

Johnson MP, Johnson A, Holzgreve W, et al: First-trimester simple hygroma: cause and outcome. Am J Obstet Gynecol 168:156, 1993

Jones AM, Isenburg J, Salemi JL, et al: Increasing prevalence of gastroschisis—14 states, 1995–2012. MMWR 65(2):23, 2016

Joó JG, Tóth Z, Beke A, et al: Etiology, prenatal diagnoses and outcome of ventriculomegaly in 230 cases. Fetal Diagn Ther 24(3):254, 2008

Karim JN, Roberts NW, Salomon LJ, et al: Systematic review of first trimester ultrasound screening in detecting fetal structural anomalies and factors affecting screening performance. Ultrasound Obstet Gynecol 50(4):429, 2017

Kasprian G, Brugger PC, Weber M, et al: In utero tractography of fetal white matter development. Neuroimage 43:213, 2008

Kharrat R, Yamamoto M, Roume J, et al: Karyotype and outcome of fetuses diagnosed with cystic hygroma in the first trimester in relation to nuchal translucency thickness. Prenat Diagn 26:369, 2006

Kingdom JC, Burrell SJ, Kaufmann P: Pathology and clinical implications of abnormal umbilical artery Doppler waveforms. Ultrasound Obstet Gynecol 9:271, 1997

Kitchanan S, Patole SK, Muller R, et al: Neonatal outcome of gastroschisis and exomphalos: a 10-year review. J Paediatric Child Health 36:428, 2000

Kline-Fath BM, Calvo-Garcia MA, O'Hara SM, et al: Twin-twin transfusion syndrome: cerebral ischemia is not the only fetal MR imaging finding. Pediatr Radiol 37(1):47, 2007

Knott-Craig CJ, Elkins RC, Lane MM, et al: A 26-year experience with surgical management of tetralogy of Fallot: risk analysis for mortality or late reintervention. Ann Thorac Surg 66:506, 1998

Koren G, Florescu A, Costei AM, et al: Nonsteroidal antiinflammatory drugs during third trimester and the risk of premature closure of the ductus arteriosus: a meta-analysis. Ann Pharmacother 40(5):824, 2006

Kucik JE, Alverson CJ, Gliboa SM, et al: Racial/ethnic variations in the prevalence of selected major birth defects, Metropolitan Atlanta, 1994–2005. Public Health Reports 127(1):52, 2012

Kul S, Korkmaz HA, Cansu A, et al: Contribution of MRI to ultrasound in the diagnosis of fetal anomalies. J Magn Reson Imaging 35:882, 2012

Lauson S, Alvarez C, Patel MS, et al: Outcome of prenatally diagnosed isolated clubfoot. Ultrasound Obstet Gynecol 35:708, 2010

Lazar DA, Cassady CI, Olutoye OO, et al: Tracheoesophageal displacement index on predictors of airway obstruction for fetuses with neck masses. J Pediatr Surg 47:46, 2012

Lazebnik N, Bellinger MF, Ferguson JE, et al: Insights into the pathogenesis and natural history of fetuses with multicystic dysplastic kidney disease. Prenat Diagn 19:418, 1999

Lee RS, Cendron M, Kinnamon DD, et al: Antenatal hydronephrosis as a predictor of postnatal outcome: a meta-analysis. Pediatrics 118:586, 2006

Lee TC, Lim FY, Keswani SG, et al: Late gestation fetal magnetic resonance imaging-derived total lung volume predicts postnatal survival and need for

extracorporeal membrane oxygenation support in isolated congenital diaphragmatic hernia. J Pediatr Surg 46(6):1165, 2011

Levine D, Barnes PD: Cortical maturation in normal and abnormal fetuses as assessed with prenatal MR imaging. Radiology 210:751, 1999a

Levine D, Barnes PD, Madsen JR, et al: Central nervous system abnormalities assessed with prenatal magnetic resonance imaging. Obstet Gynecol 94:1011, 1999b

Leyendecker JR, DuBose M, Hosseinzadeh K, et al: MRI of pregnancy-related issues: abnormal placentation. AJR Am J Roentgenol 198(2):311, 2012

Li Y, Estroff JA, Khwaja O, et al: Callosal dysgenesis in fetuses with ventriculomegaly: levels of agreement between imaging modalities and postnatal outcome. Ultra Obstet Gynecol 40(5): 522, 2012

Lloyd DF, Rutherford MA, Simpson JM, et al: The neurodevelopmental implications of hypoplastic left heart syndrome in the fetus. Cardiol Young 27(2):217, 2017

Lodeiro JG, Feinstein SJ, Lodeiro SB: Fetal premature atrial contractions associated with hydralazine. Am J Obstet Gynecol 160:105, 1989

Long A, Moran P, Robson S: Outcome of fetal cerebral posterior fossa anomalies. Prenat Diagn 26:707, 2006

Maarse W, Berge SJ, Pistorius L, et al: Diagnostic accuracy of transabdominal ultrasound in detecting prenatal cleft lip and palate: a systematic review. Ultrasound Obstet Gynecol 35:495, 2010

Maarse W, Pistorius LR, Van Eeten WK, et al: Prenatal ultrasound screening for orofacial clefts. Ultrasound Obstet Gynecol 38:434, 2011

MacArthur CJ: Prenatal diagnosis of fetal cervicofacial anomalies. Curr Opin Otolaryngol Head Neck Surg 20(6):482, 2012

Mahle WT, Clancy RR, McGaurn SP, et al: Impact of prenatal diagnosis on survival and early neurologic morbidity in neonates with the hypoplastic left heart syndrome. Pediatrics 107:1277, 2001

Malone FD, Ball RH, Nyberg DA, et al: First-trimester septated cystic hygroma: prevalence, natural history, and pediatric outcome. Obstet Gynecol 106:288, 2005

Mammen L, Benson CB: Outcome of fetuses with clubfeet diagnosed by prenatal sonography. J Ultrasound Med 23:497, 2004

Mann S, Johnson MP, Wilson RD: Fetal thoracic and bladder shunts. Semin Fetal Neonatal Med 15:28, 2010

Mari G, Deter RL, Carpenter RL, et al: Noninvasive diagnosis by Doppler ultrasonography of fetal anemia due to maternal red-cell alloimmunization. Collaborative group for Doppler assessment of the blood velocity in anemic fetuses. N Engl J Med 342:9, 2000

Mehollin-Ray AR, Cassady CI, Cass DL, et al: Fetal MR imaging of congenital diaphragmatic hernia. Radiographics 32(4):1067, 2012

Messerschmidt A, Pataraia A, Helber H, et al: Fetal MRI for prediction of neonatal mortality following preterm premature rupture of the fetal membranes. Pediatr Radiol 41:1416, 2011

Millischer AE, Sonigo P, Ville Y, et al: Standardized anatomical examination of the fetus at MRI. A feasibility study. Ultrasound Obstet Gynecol 42(5):553, 2013

Mitter C, Jakab A, Brugger PC, et al: Validation of in utero tractography of human fetal commissural and internal capsule fibers with histological structure tensor analysis. Front Neuroanat 24:164, 2015

Morris LM, Lim F-Y, Elluru RG, et al: Severe micrognathia: indications for EXIT-to-Airway. Fetal Diagn Ther 26(30):162, 2009

Morrow RJ, Abramson SL, Bull SB, et al: Effect of placental embolization of the umbilical artery velocity waveform in fetal sheep. Am J Obstet Gynecol 151:1055, 1989

Mullassery D, Ba'ath ME, Jesudason EC, et al: Value of liver herniation in prediction of outcome in fetal congenital diaphragmatic hernia: a systematic review and meta-analysis. Ultrasound Obstet Gynecol 35:609, 2010

Nelson DB, Dashe JS, McIntire DD, et al: Fetal skeletal dysplasias: sonographic indices associated with adverse outcomes. J Ultrasound Med 33(6):1085, 2014

Nelson DB, Martin R, Twickler DM, et al: Sonographic detection and clinical importance of growth restriction in pregnancies with gastroschisis. J Ultrasound Med 34(12):2217, 2015

Nelson JS, Stebbins RC, Strassle PD, et al: Geographic distribution of live births with tetralogy of Fallot in North Carolina 2003 to 2012. Birth Defect Res A Clin Mol Teratol 106(11):881, 2016

Nembhard WN, Waller DK, Sever LE, et al: Patterns of first-year survival among infants with selected congenital anomalies in Texas, 1995–1997. Teratology 64:267, 2001

Neubert S, Trautmann K, Tanner B, et al: Sonographic prognostic factors in prenatal diagnosis of SCT. Fetal Diagn Ther 19(4): 319, 2004

Nguyen HT, Herndon CDA, Cooper C, et al: The Society for Fetal Urology consensus statement on the evaluation and management of antenatal hydronephrosis. J Pediatr Urol 6:212, 2010

Nicolaides KH, Campbell S, Gabbe SG, et al: Ultrasound screening for spina bifida: cranial and cerebellar signs. Lancet 2:72, 1986

Oei SG, Vosters RP, van der Hagen NL: Fetal arrhythmia caused by excessive intake of caffeine by pregnant women. BMJ 298:568, 1989

Offerdal K, Jebens N, Swertsen T, et al: Prenatal ultrasound detection of facial cleft: a prospective study of 49,314 deliveries in a non-selected population in Norway. Ultrasound Obstet Gynecol 31:639, 2008

Ogamo M, Sugiyama T, Maeda T, et al: The ex utero intrapartum treatment (EXIT) procedure in giant fetal neck masses. Fetal Diagn Ther 20(3):214, 2005

Oluyomi-Obi T, Kuret V, Puligandla P, et al: Antenatal predictors of outcome in prenatally diagnosed congenital diaphragmatic hernia (CDH). J Pediatr Surg 52(5):881, 2017

Orioli IM, Catilla EE: Epidemiology of holoprosencephaly: prevalence and risk factors. Am J Med Genet Part C Semin Med Genet 154C:13, 2010

Overcash RT, DeUgarte DA, Stephenson ML, et al: Factors associated with gastroschisis outcomes. Obstet Gynecol 124(3):551, 2014

Paladini D, Alfirevic Z, Carvalho JS, et al: ISUOG consensus statement on current understanding of the association of neurodevelopmental delay and congenital heart disease: impact on prenatal counseling. Ultrasound Obstet Gynecol 49(2):287, 2017

Paladini D, Russo M, Teodoro A, et al: Prenatal diagnosis of congenital heart disease in the Naples area during the years 1994–1999—the experience of a joint fetal-pediatric cardiology unit. Prenatal Diagn 22(7):545, 2002

Pavone V, Bianca S, Grosso G, et al: Congenital talipes equinovarus: an epidemiological study in Sicily. Acta Orthop 83(3):294, 2012

Pedersen RN, Calzolari E, Husby S, et al: Oesophageal atresia: prevalence, prenatal diagnosis and associated anomalies in 23 European regions. Arch Dis Child 97:227, 2012

Peranteau WH, Boelig MM, Khalek N, et al: Effect of single and multiple courses of maternal betamethasone on prenatal congenital lung lesion growth and fetal survival. J Pediatr Surg 51(1):28, 2016

Perrone EE, Jarboe MD, Maher CO, et al: Early delivery of sacrococcygeal teratoma with intraspinal extension. Fetal Diagn Ther May 3, 2017 [Epub ahead of print]

Phelan JP, Ahn MO, Smith CV, et al: Amnionic fluid index measurements during pregnancy. J Reprod Med 32:601, 1987

Pilu G: Prenatal diagnosis of cerebrospinal anomalies. In: Fleischer AC, Toy EC, Lee W, et al (eds): Sonography in Obstetrics and Gynecology: Principles and Practice, 7th ed. New York, McGraw-Hill, 2011

Prayer D, Malinger G, Brugger PC, et al: ISUOG Practice Guidelines: performance of fetal magnetic resonance imaging. Ultrasound Obstet Gynecol 49(5):671, 2017

Rabinowitz R, Peters MT, Vyas S, et al: Measurement of fetal urine production in normal pregnancy by real-time ultrasonography. Am J Obstet Gynecol 161:1264, 1989

Rahemtullah A, McGillivray B, Wilson RD: Suspected skeletal dysplasias: femur length to abdominal circumference ratio can be used in ultrasonographic prediction of fetal outcome. Am J Obstet Gynecol 177:864, 1997

Ramos GA, Romine LE, Gindes L, et al: Evaluation of the fetal secondary palate by 3-dimensional sonography. J Ultrasound Med 29:357, 2010

Ramus RM, Martin LB, Twickler DM: Ultrasonographic prediction of fetal outcome in suspected skeletal dysplasias with use of the femur length-to-abdominal circumference ratio. Am J Obstet Gynecol 179(5):1348, 1998

Reddy UM, Abuhamad AZ, Levine D, et al: Fetal imaging: executive summary of a joint Eunice Kennedy Shriver National Institute of Child Health and Human Development, Society for Maternal-Fetal Medicine, American Institute of Ultrasound in Medicine, American College of Obstetricians and Gynecologists, American College of Radiology, Society for Pediatric Radiology, and Society of Radiologists in Ultrasound Fetal Imaging workshop. Obstet Gynecol 123(5):1070, 2014

Reddy UM, Filly RA, Copel JA: Prenatal imaging: ultrasonography and magnetic resonance imaging. Obstet Gynecol 112:145, 2008

Reeves MJ, Brandreth M, Whitby EH, et al: Neonatal cochlear function: measurement after exposure to acoustic noise during in utero MR imaging. Radiology 257(3):802, 2010

Reichel TF, Ramus RM, Caire JT, et al: Fetal central nervous system biometry on MR imaging. Am J Roentgenol 180(4): 1155, 2003

Roll SC, Evans KD, Hutmire CD, et al: An analysis of occupational factors related to shoulder discomfort in diagnostic medical sonographers and vascular technologists. Work 42(3):355, 2012

Romosan G, Henriksson E, Rylander A, et al: Diagnostic performance of routine ultrasound screening for fetal malformations in an unselected Swedish population 2000–2005. Ultrasound Obstet Gynecol 34:526, 2009

Rydberg C, Tunon K: Detection of fetal abnormalities by second-trimester ultrasound screening in a non-selected population. Acta Obstet Gynecol Scand 96(2):176, 2017

Salomon LJ, Alfirevic Z, Berghella V, et al: Practice guidelines for performance of the routine mid-trimester fetal ultrasound scan. Ultrasound Obstet Gynecol 37(1):116, 2011

Sanford A, Saadai P, Lee H, et al: Congenital high airway obstruction sequence (CHAOS): a new case and a review of phenotypic features. Am J Med Genet 158A(12):3126, 2012

Santiago-Munoz PC, McIntire DD, Barber RG, et al: Outcomes of pregnancies with fetal gastroschisis. Obstet Gynecol 110:663, 2007

Schreuder MF, Westland R, van Wijk JA: Unilateral multicystic dysplastic kidney: a meta-analysis of observational studies on the incidence, associated urinary tract malformations and the contralateral kidney. Nephrol Dial Transplant 24:1810, 2009

Sciscione AC, Hayes EJ, Society for Maternal-Fetal Medicine: Uterine artery Doppler flow studies in obstetric practice. Am J Obstet Gynecol 201(2):121, 2009

Segata M, Mari G: Fetal anemia: new technologies. Curr Opin Obstet Gynecol 16:153, 2004

Sharma R, Stone S, Alzouebi A, et al: Perinatal outcome of prenatally diagnosed congenital talipes equinovarus. Prenat Diagn 31:142, 2011

Sheih CP, Liu MB, Hung CS, et al: Renal abnormalities in schoolchildren. Pediatrics 84:1086, 1989

Shipp TD, Bromley B, Hornberger LK, et al: Levorotation of the fetal cardiac axis: a clue for the presence of congenital heart disease. Obstet Gynecol 85:97, 1995

Shiraishi H, Nakamura M, Ichihashi K, et al: Prenatal MRI in a fetus with a giant neck hemangioma: a case report. Prenat Diagn 20(12):1004, 2000

Shulman LP, Emerson DS, Felker RE, et al: High frequency of cytogenetic abnormalities in fetuses with cystic hygroma diagnosed in the first trimester. Obstet Gynecol 80:80, 1992

Simon EM, Goldstein RB, Coakley FV, et al: Fast MR imaging of fetal CNS anomalies in utero. Am J Neuroradiol 21:1688, 2000

Soares de Oliveira-Szejnfeld P, Levine D, Melo AS, et al: Congenital brain abnormalities and Zika virus: what the radiologist can expect to see prenatally and postnatally. Radiology 281:203, 2016

Society for Maternal-Fetal Medicine, Mari G, Norton ME, et al: SMFM Clinical Guideline No. 8: The fetus at risk for anemia—diagnosis and management. Am J Obstet Gynecol 212(6):697, 2015

Society for Maternal-Fetal Medicine: SMFM resolution on ultrasound practice accreditation. 2013. Available at: https://www.smfm.org/publications/150-smfm-resolution-on-ultrasound-practice-accreditation. Accessed July 28, 2017

Solomon BD, Rosenbaum KN, Meck JM, et al: Holoprosencephaly due to numeric chromosome abnormalities. Am J Med Genet Part C Semin Med Genet 154C:146, 2010

Sotiriadis A, Makrydimas G: Neurodevelopment after prenatal diagnosis of isolated agenesis of the corpus callosum: an integrative review. Am J Obstet Gynecol 206(4):337.e1, 2012

South AP, Stutey KM, Meinzen-Derr J, et al: Metaanalysis of the prevalence of intrauterine fetal death in gastroschisis. Am J Obstet Gynecol 209(2):114.e.1, 2013

Stege G, Fenton A, Jaffray B: Nihilism in the 1990s: the true mortality of congenital diaphragmatic hernia. Pediatr 112:532, 2003

Stevenson DA, Carey JC, Byrne JL, et al: Analysis of skeletal dysplasias in the Utah population. Am J Med Genet 158A:1046, 2012

Stocker JT: Congenital pulmonary airway malformation: a new name and expanded classification of congenital cystic adenomatoid malformation of the lung. Histopathology 41(Suppl):424, 2002

Stocker JT, Madewell JE, Drake RM: Congenital cystic adenomatoid malformation of the lung: classification and morphologic spectrum. Hum Pathol 8:155, 1977

Stoll C, Alembik Y, Dott B, et al: Associated malformations in patients with limb reduction deficiencies. Eur J Med Genet 53(5):286, 2010

Swamy R, Embleton N, Hale J, et al: Sacrococcygeal teratoma over two decades: birth prevalence, prenatal diagnosis and clinical outcomes. Prenat Diagn 28:1048, 2008

Syngelaki A, Chelemen T, Dagklis T, et al: Challenges in the diagnosis of fetal non-chromosomal abnormalities at 11–13 weeks. Prenat Diagn 31:90, 2011

Szabo N, Gergev G, Kobor J, et al: Corpus callosum abnormalities: birth prevalence and clinical spectrum in Hungary. Pediatr Neurol 44:420, 2011

Tilea B, Alberti C, Adamsbaum C, et al: Cerebral biometry in fetal magnetic resonance imaging: new reference data. Ultrasound Obstet Gynecol 33(2):173, 2009

Tourbier S, Velasco-Annis C, Taimouri V, et al: Automated template-based brain localization and extraction for fetal brain MRI reconstruction. Neuroimage 155:460, 2017

Tredwell SJ, Wilson D, Wilmink MA, et al: Review of the effect of early amniocentesis on foot deformity in the neonate. J Pediatr Orthol 21:636, 2001

Trivedi N, Levy D, Tarsa M, et al: Congenital cardiac anomalies: prenatal readings versus neonatal outcomes. J Ultrasound Med 31:389, 2012

Turkbey B, Ocak I, Daryanani K, et al: Autosomal recessive polycystic kidney disease and congenital hepatic fibrosis. Pediatr Radiol 39:100, 2009

Twickler DM, Magee KP, Caire J, et al: Second-opinion magnetic resonance imaging for suspected fetal central nervous system abnormalities. Am J Obstet Gynecol 188:492, 2003

Twickler DM, Reichel T, McIntire DD, et al: Fetal central nervous system ventricle and cisterna magna measurements by magnetic resonance imaging. Am J Obstet Gynecol 187:927, 2002

Tworetzky W, McElhinney DB, Reddy VM, et al: Improved surgical outcome after fetal diagnosis of hypoplastic left heart syndrome. Circulation 103:1269, 2001

Vadeyar SH, Moore RJ, Strachan BK, et al: Effect of fetal magnetic resonance imaging on fetal heart rate patterns. Am J Obstet Gynecol 182:666, 2000

Vasluian E, van der Sluis CK, van Essen AJ, et al: Birth prevalence for congenital limb defects in the northern Netherlands: a 30-year population-based study. BMC Musculoskel Disord 14:323, 2013

Vergani P, Ceruti P, Locatelli A, et al: Accuracy of prenatal ultrasonographic diagnosis of duplex renal system. J Ultrasound Med 18:463, 1998

Victoria T, Johnson AM, Edgar JC, et al: Comparison between 1.5-T and 3-T MRI for fetal imaging: is there an advantage to imaging with a higher field strength? AJR Am J Roentgenol 206:195, 2016

Walker SJ, Ball RH, Babcook CJ, et al: Prevalence of aneuploidy and additional anatomic abnormalities in fetuses and neonates with cleft lip with or without cleft palate. A population-based study in Utah. J Ultrasound Med 20(11):1175, 2001

Wang G, Zuluaga MA, Pratt R, et al: Slic-Seg: a minimally interactive segmentation of the placenta from sparse and motion-corrupted fetal MRI in multiple views. Med Image Anal 24:137, 2016

Wax JR, Benacerraf BR, Copel J, et al: Consensus report on the 76811 scan: modification. J Ultrasound Med 34(10):1915

Wax J, Minkoff H, Johnson A, et al: Consensus report on the detailed fetal anatomic ultrasound examination: indications, components, and qualifications. J Ultrasound Med 33(2):189, 2014

Wenstrom KD, Weiner CP, Williamson RA: Diverse maternal and fetal pathology associated with absent diastolic flow in the umbilical artery of high-risk fetuses. Obstet Gynecol 77:374, 1991

Whitten SM, Wilcox DT: Duplex systems. Prenat Diagn 21:952, 2001

Wiesel A, Queisser-Luft A, Clementi M, et al: Prenatal detection of congenital renal malformations by fetal ultrasonographic examination: an analysis of 709,030 births in 12 European countries. Euro J Med Genet 48:131, 2005

Wilhelm L, Borgers H: The “equals sign”: a novel marker in the diagnosis of fetal isolated soft palate. Ultrasound Obstet Gynecol 36:439, 2010

Williams B, Tareen B, Resnick M: Pathophysiology and treatment of ureteropelvic junction obstruction. Curr Urol Rep 8:111, 2007

Wiskirchen J, Groenewaeller EF, Kehlbach R, et al: Long-term effects of repetitive exposure to a static magnetic field 1.5 T on proliferation of human fetal lung fibroblasts. Magn Reson Med 41:464, 1999

Woodward M, Frank D: Postnatal management of antenatal hydronephrosis. BJU Int 89:149, 2002

Worley KC, Dashe JS, Barber RG, et al: Fetal magnetic resonance imaging in isolated diaphragmatic hernia: volume of herniated liver and neonatal outcome. Am J Obstet Gynecol 200(3):318.e1, 2009

Yamada S, Uwabe C, Fujii S, et al: Phenotypic variability in human embryonic holoprosencephaly in the Kyoto collection. Birth Defects Res Part A Clin Mol Teratol 70:495, 2004

Yeo L, Romero R: How to acquire cardiac volumes for sonographic examination of the fetal heart, part I. J Ultrasound Med 35(5):1021, 2016

Yildirim G, Gungorduk K, Aslan H, et al: Prenatal diagnosis of extralobar pulmonary sequestration. Arch Gynecol Obstet 278:181, 2008

Zaretsky M, Ramus R, McIntire D, et al: MRI calculation of lung volumes to predict outcome in fetuses with genitourinary abnormalities. AJR Am J Roentgenol 185:1328, 2005

Zaretsky MV, McIntire DD, Twickler DM: Feasibility of the fetal anatomic and maternal pelvic survey by magnetic resonance imaging at term. Am J Obstet Gynecol 189:997, 2003a

Zaretsky MV, Twickler DM: Magnetic imaging in obstetrics. Clin Obstet Gynecol 46:868, 2003b

Zeeman GG, McIntire DD, Twickler DM: Maternal and fetal artery Doppler findings in women with chronic hypertension who subsequently develop superimposed pre-eclampsia. J Matern Fetal Neonatal Med 14:318, 2003

Zerres K, Mucher G, Becker J, et al: Prenatal diagnosis of autosomal recessive polycystic kidney disease: molecular genetics, clinical experience, and fetal morphology. Am J Med Genet 6:137, 1998